Max-Planck-Institut für Extraterrestrische Physik

The Formation of Brown Dwarfs

Fundamental properties of very young objects near and below the substellar limit

Dissertation der Fakultät für Physik
an der Ludwigs-Maximilians-Universität München

vorgelegt am
7. August 2002
von

Viki Joergens
aus München

Erstgutachter: Prof. Dr. Gregor Morfill

Zweitgutachter: Prof. Dr. Ralf Bender

Tag der mündlichen Prüfung: 24.1.2003

Contents

Kurzfassung auf deutsch **1**

Abstract **3**

1 Brown dwarfs – an introduction **5**

1.1 Brown dwarfs: objects between stars and planets 5

1.2 Formation models 8

1.2.1 Planet-like formation 8

1.2.2 Star-like formation 10

1.3 Substellar evolution 13

1.3.1 Principles 13

1.3.2 Evolutionary models 16

1.4 Atmospheres, spectra and weather phenomena 18

1.4.1 Atmospheres and spectra 18

1.4.2 Condensation, clouds and weather 19

1.5 Magnetic activity 21

1.6 Substellar tests 24

1.6.1 The lithium test 24

1.6.2 Methane test 26

1.6.3 Substellar test by mass determination 26

1.7 Multiplicity and circumstellar material 26

1.7.1 Brown dwarf companions to stars 27

1.7.2 Brown dwarf binaries 28

1.7.3 Planets around brown dwarfs 29

1.7.4 Circumstellar disks 30

2 The brown dwarfs in Cha I **33**

3 High-resolution spectroscopy (UVES/VLT) **37**

3.1 Data acquisition and analysis 38

3.2 Radial velocities 40

3.3 Kinematics of brown dwarfs in Cha I 43

3.3.1 Velocity dispersion of brown dwarfs 43

3.3.2 Velocity dispersion of the molecular gas 44

3.3.3 Velocity dispersion of T Tauri stars in Cha I 44

3.3.4 Constraints for formation theories 47

3.4 Projected rotational velocities $v \sin i$ 48

3.5 Lithium equivalent width 49

3.6 Radial velocity survey for substellar companions 50

4 High-resolution imaging (HST/VLT/NTT) **55**

4.1 HST observations and data reduction 55

4.2 Ground-based imaging with VLT and NTT 61

4.3 Colors of companion candidates 64

4.4 The companion candidate near Cha Hα 5 66

4.5 Hints of binarity of Cha Hα 2 68

5 Photometric monitoring **71**

5.1 Hitherto known periods for brown dwarfs 72

5.2 Data acquisition 73

5.3 Time series analysis 74

5.4 Rotational periods 75

5.4.1 B 34 ($\sim 0.12\,M_\odot$) 76

5.4.2 CHXR 78C ($\sim 0.09\,M_\odot$) 76

5.4.3 Cha Hα 2 ($\sim 0.07\,M_\odot$) 80

5.4.4 Cha Hα 3 ($\sim 0.06\,M_\odot$) 81

5.4.5 Cha Hα 6 ($\sim 0.05\,M_\odot$) 81

5.5 Discussion 82

5.5.1 Rotational modulation due to spots 82

5.5.2 Comparison with spectroscopic velocities $v \sin i$ 83

5.5.3 Radii of brown dwarfs 84

5.5.4 Evolution of angular momentum 84

5.6 Summary 86

6 Summary and outlook **89**

6.1 Kinematics of brown dwarfs in Cha I – constraints for their formation 90

6.2 Multiplicity of brown dwarfs and very low-mass stars in Cha I 91

6.3 Rotation rates, surface spots and substellar angular momentum evolution 93

6.4 Outlook 95

Appendix **97**

References **101**

List of Figures

1.1 Scheme of the star formation out of cloud cores 11
1.2 Evolution of the central temperature 13
1.3 Cooling curves – Evolution of the luminosity 14
1.4 Evolution of the radius 15
1.5 Spectra of late-M and L-dwarfs 19
1.6 Spectra of L- and T-dwarfs 20
1.7 Lithium depletion 25
1.8 Mass distribution of planetary and stellar companions to stars . . 27
1.9 Observed and modeled spectral energy distribution of Cha Hα 1 . 30

2.1 HRD with bona fide and candidate brown dwarfs in Cha I 35

3.1 UVES spectrum 40
3.2 RV distribution of brown dwarfs in Cha I 44
3.3 Distribution of $v \sin i$ for brown dwarfs and T Tauri stars in Cha I 48
3.4 Illustration of the Dopplershift caused by an unseen planet 50
3.5 Radial velocity vs. time for Cha Hα 1, 2, 3, 5, 6, 7, 8 and 12 . . . 52
3.6 Radial velocity vs. time for Cha Hα 4 53
3.7 Radial velocity vs. time for Cha Hα 4 54

4.1 HST I band image of Cha Hα 4, 10, and 11 57
4.2 HST R and I band images of Cha Hα 5 59
4.3 NTT H and K_s band images of Cha Hα 5 62

4.4 Color-magnitude diagram: R_V vs. (R_V−I_V) 64
4.5 Color-color diagram: (J−H) vs. (H−K_s) 65
4.6 V and J band images of Cha Hα 5 67
4.7 Apparent elongation of the point-spread-functions (PSF) 68
4.8 HST R and Hα images of Cha Hα 2 69

5.1 Modulation of the brightness due to a spot 71
5.2 (R-i) curve of B 34 76
5.3 Light curves of B 34 77
5.4 Light curves of CHXR 78C and Cha Hα 2 78
5.5 Light curves of Cha Hα 3 and Cha Hα 6 79
5.6 Evolution of angular momentum 85

List of Tables

1.1 Compilation of known brown dwarf companions to stars 28

1.2 Compilation of known brown dwarf binaries 29

2.1 Parameters of brown dwarfs and very low-mass stars in Cha I . . . 34

3.1 Radial velocities for bona fide and candidate brown dwarfs in Cha I 41

3.2 Radial velocities for very low-mass T Tauri stars in Cha I 42

3.3 Mean radial and rotational velocities for brown dwarfs and very low-mass stars in Cha I 45

3.4 List of T Tauri stars in Cha I with known precise radial velocities 46

3.5 Upper mass limits for companions around brown dwarfs and very low-mass stars in Cha I 51

4.1 Observing log of HST observations 56

4.2 List of wide companion candidates found in HST images 60

4.3 Observing log of ground-based VLT and NTT images 61

4.4 Space- and ground-based VRI and JHK magnitudes for all companion candidates 63

5.1 Compilation of brown dwarfs with known photometric periods . . 72

5.2 Rotational periods and photometric amplitudes for brown dwarfs and very low-mass stars in Cha I 80

6.1 Observing log: UVES spectroscopy of brown dwarfs and very low-mass stars in Cha I 98

6.2 Table 6.1 continued 99

Kurzfassung

In der vorliegenden Arbeit wurden zwölf sehr junge Braune Zwerge und Kandidaten für Braune Zwerge (Cha Hα 1–12) in der Cha I Sternentstehungswolke im Hinblick auf ihre kinematischen und Rotationseigenschaften, sowie auf das Vorkommen von Mehrfachsystemen hin untersucht. Hochaufgelöste Spektren aufgenommen mit UVES am VLT von neun der zwölf Objekte, erlaubten die Messung von Radial- und Rotationsgeschwindigkeiten mit hoher Genauigkeit. Eine kinematische Studie des Samples zeigte, dass ihre Radialgeschwindigkeitsdispersion relativ gering ist ($2.2\,\mathrm{km\,s^{-1}}$). Sie ist deutlich geringer als die von T Tauri Sternen im gleichen Feld ($3.6\,\mathrm{km\,s^{-1}}$) und etwas höher als die des sie umgebenden Gases ($1.2\,\mathrm{km\,s^{-1}}$). Dieses Ergebnis deutet darauf hin, dass die untersuchten Braunen Zwerge während ihrer Entstehung nicht herausgeschleudert wurden, jedenfalls nicht mit Geschwindigkeiten grösser als $\sim$2 km s^{-1}, wie kürzlich vorgeschlagen wurde. Sie könnten eine grössere 3D Geschwindigkeit haben. Allerdings hätten Braune Zwerge, die in ihrer frühen Akkretionsphase in Richtungen mit einem signifikanten Anteil senkrecht zur Sehline geschleudert wurden, das Feld schon lange verlassen.

Mittels zeitaufgelöster UVES Spektren wurde eine Radialgeschwindigkeitssuche nach engen Begleitern durchgeführt. Zusätzlich wurde mittels hochaufgelösten Bildern nach Begleitern in weiten Orbits gesucht, basierend auf Aufnahmen mit der WFPC Kamera an Bord des HST, mit FORS am VLT sowie mit SofI am NTT. Mit diesen beiden, sich ergänzenden Suchprogrammen konnte ein grosser Bereich möglicher Begleiterabstände erfasst werden. Für Braune Zwerg Begleiter ($> 13\,\mathrm{M_{Jup}}$) wurde der Bereich < 3 AU und 50–1000 AU abgedeckt. In einem stärker eingeschränkten Bereich (< 0.1 AU und 300–1000 AU) sind die Surveys in der Lage Begleitermassen bis zu $1\,\mathrm{M_{Jup}}$ zu detektieren. HST Bilder von Cha Hα 2 deuten auf ein Doppelsystem mit zwei etwa gleichschweren Komponenten im Abstand von $\sim$30 AU hin. Es wurden keine weiteren Hinweise auf Begleiter in den Bildern gefunden. Die Radialgeschwindigkeiten der untersuchten Objekte sind zudem relativ konstant und setzen obere Grenzen für die Masse $\mathrm{M_2} \sin i$ möglicher Begleiter von $0.1\,\mathrm{M_{Jup}}$ bis $2\,\mathrm{M_{Jup}}$. Diese Ergebnisse deuten auf eine eher kleine Rate von Mehrfachsystemen ($\leq 10\%$) unter den untersuchten Braunen Zwerge hin.

Desweiteren wurden basierend auf photometrischen Beobachtungen Rotationsperioden für Cha Hα 2, 3 und 6 im Bereich von 2.2 bis 3.4 Tagen bestimmt. Dies sind die ersten Rotationsperioden für sehr junge Braune Zwerge und eine der ersten für Braune Zwerge überhaupt. Sie werden ergänzt durch die Messung von Rotationsgeschwindigkeiten $v \sin i$ in UVES Spektren. Die Beobachtungen zeigen, dass Braune Zwerge in einem Alter von 1–5 Myr Flecken auf ihrer Oberfläche haben, ähnlich wie T Tauri Sterne und dass sie mit mittleren Geschwindigkeiten rotieren im Gegensatz zu schnell rotierenden alten Braunen Zwergen. Ein Vergleich mit bisher veröffentlichten Rotationsperioden von älteren Braunen Zwergen, weist darauf hin, dass ein Grossteil der Beschleunigung Brauner Zwerge in ihren ersten 30 Millionen Lebensjahren stattfindet.

Abstract

In the presented work, a population of twelve very young bona fide and candidate brown dwarfs in the Cha I star forming cloud (Cha Hα 1–12) was studied observationally in terms of their kinematic properties, the occurrence of multiple systems among them as well as their rotational characteristics. Based on high-resolution spectra taken for nine out of the twelve objects with UVES at the VLT, radial and rotational velocities have been measured with high accuracy. A kinematic study of the sample showed that their radial velocity dispersion is relatively small ($2.2\,\mathrm{km\,s^{-1}}$). It is significantly smaller than the radial velocity dispersion of the T Tauri stars in the field ($3.6\,\mathrm{km\,s^{-1}}$) and slightly larger than that one of the surrounding molecular gas ($1.2\,\mathrm{km\,s^{-1}}$). This result indicates that the studied brown dwarfs are not ejected during their formation with velocities large than $\sim$$2\,\mathrm{km\,s^{-1}}$ as proposed in recent formation scenarios.The brown dwarfs may have larger 3D velocities. However, brown dwarfs ejected during the early accretion phase in directions with a significant fraction perpendicular to the line-of-sight, would have flown out of the field a long time ago.

By means of time-resolved UVES spectra, a radial velocity survey for close companions to the targets was conducted. In addition, a direct imaging survey for wide companions was carried out with the WFPC camera on board the HST, with FORS at the VLT as well as with SofI at the NTT. With these two complementary search methods, a wide range of possible companion separations has been covered. For brown dwarf companions ($> 13\,\mathrm{M_{Jup}}$) to the targets, separations $< 3\,\mathrm{AU}$ and between 50 and 1000 AU were covered. With more restricted separations ($< 0.1\,\mathrm{AU}$ and 300–1000 AU) the surveys were sensitive also to companion masses down to $1\,\mathrm{M_{Jup}}$. HST images of Cha Hα 2 hint at a binary system comprised of two approximately equal-mass companions with a separation of $\sim$30 AU. No further indications for companions have been found in the images. Furthermore, the radial velocities of the targets turned out to be rather constant setting upper limits for the mass $\mathrm{M_2} \sin i$ of possible companions to $0.1\,\mathrm{M_{Jup}}$ to $2\,\mathrm{M_{Jup}}$. These findings hint at a rather low ($\leq 10\%$) multiplicity fraction of the studied brown dwarfs.

Furthermore, a photometric monitoring campaign of the targets yielded the determination of rotational periods for Cha Hα 2, Cha Hα 3 and Cha Hα 6 in the range of 2.2 to 3.4 days. These are the first rotational periods for very young brown dwarfs and among the first for brown dwarfs at all. They are complemented by measurements of rotational velocities $v \sin i$ from UVES spectra. The observations show that brown dwarfs at an age of 1–5 Myr display surface spots like T Tauri stars and are moderately fast rotators in contrast to rapidly rotating old brown dwarfs consistent with them being in an early contracting stage. A comparison with rotational periods from the literature indicates that most of the acceleration of brown dwarfs takes place in the first 30 million years or less of their lifetime.

Chapter 1

Brown dwarfs – an introduction

1.1 Brown dwarfs: objects between stars and planets

Brown dwarfs fill the gap between low-mass stars and giant planets in the mass range of about 0.08 solar masses ($M_\odot$) and about 13 Jupiter masses (M_{Jup})[1], depending on metallicity. They can never fully stabilize their luminosity by hydrogen burning in contrast to stars but are able to fuse deuterium in contrast to planets. Their existence was first suggested by Kumar (1962, 1963), who predicted the existence of a large number of objects, which cannot reach the main-sequence stage because the temperature and density at the center are too low for the fusion of hydrogen at a rate sufficient to balance gravitational pressure. These objects contract until the gas of electrons in their interiors is completely degenerate. The term *brown dwarf* goes back to Tarter (1975).

The prediction of the existence of brown dwarfs in the early sixties was followed by a 30 year search for such faint objects until in 1995 almost at the same time three brown dwarfs were discovered independently: the Methane dwarf Gl 229 B, a faint companion to a nearby M-dwarf, as cool as 1000 K (Nakajima et al. 1995, Oppenheimer et al. 1995) as well as two brown dwarfs in the Pleiades, Teide 1 (Rebolo et al. 1995) and PPl 15 (Stauffer et al. 1994a). The latter object turned out to be in fact a pair of two gravitationally bound brown dwarfs (Basri & Martín 1999) (cf. also Sect. 1.7). Up to now, more than 300 brown dwarfs have been detected in star forming regions (e.g. Beǰar et al. 2000, Comerón et al. 2000), in young cluster (Pleiades, Martín et al. 2000a) and in the field. The first detected field brown dwarf was Kelu-1 (Ruiz et al. 1997). Most of the known field brown dwarfs have been discovered by two large infrared surveys, DENIS (Delfosse et

[1] $1\,M_\odot = 1047\,M_{Jup}$

al. 1997) and 2MASS (Kirkpatrick et al. 2000), and the optical SLOAN survey (Hawley et al. 2002).

The year 1995 saw another spectacular discovery: the detection of the first extrasolar planet candidate with minimum mass around $\sim$1 M_{Jup} orbiting the sun-like star 51 Peg (Mayor & Queloz 1995)[2]. Since 1995, high-precision radial velocity surveys have detected more than a hundred planetary candidates in orbit around stars (e.g. Marcy et al. 2000). Like the planet around 51 Peg, most of the detected extrasolar planets are giant, close-in planets. It was suggested to call them *Pegasi-planets* (or *51 Peg-type planets*) after the prototype 51 Peg by T. Guillot. These discoveries came as a surprise and they have changed our view of planets radically. The observed orbital parameters (high eccentricities, small semi major axes) as well as the masses (hot gas planets in small orbits) display a rather different situation for the extrasolar systems than for our solar system and raise many new questions concerning the formation of planets. For example, it has to be specified how such massive planets can be formed in-situ or, if they are formed at larger distance from the star as they are found, how they can migrate inwards. The preponderant detection of massive planets in close orbits is a bias of the search methods since this very constellation produces the largest radial velocity amplitudes. It should be noted, that radial velocity measurements alone allow in general only the determination of minimum masses $M \sin i$ since the inclination i of the orbit remains unknown. Therefore, the radial velocity technique alone can detect only planet *candidates*. However, based on statistical arguments most of the found planet candidates are real planets. In addition, Charbonneau et al. (2000) were able to photometrically monitor the transit of a radial velocity extrasolar planet candidate in front of its parent star and to determine the inclination and therefore the true mass (0.6 M_{Jup}) of the orbiting object and hence, to prove that it is an extrasolar planet.

The lower mass limit of brown dwarfs, which is the upper mass limit of planets, is strongly correlated with the definition of *planets*, which is currently a matter of debate. The historical definition of planets and stars was strongly led by the configuration in our own solar system and is based on a discrimination by different formation scenarios: Stars form by the collapse of molecular clouds to self-luminous, hydrogen burning objects, whereas planets form in circumstellar disks. Thus, a planet is an object in a hierarchical orbit around a star, which is not driving nuclear reactions. The latter criterion sets an upper mass limit for planets at the deuterium burning minimum mass at about 0.013 $M_\odot$ (Saumon et al. 1996), depending on metallicity. All three conventional criterions for the definition of a planet, the formation-based one, the requirement that the planet

[2] Six years earlier, Latham et al. (1989) detected a companion with a minimum mass of 11 M_{Jup} around the solar-type star HD114762. However, because the inclination of the orbit to the line of sight is unknown, the mass of the companion may be considerably larger than this lower limit ranking it more likely a brown dwarf than a planet.

resides in a hierarchical orbit around a star as well as that it has to have a mass below $\sim$0.013 $M_\odot$ have come into discussion in the last few years. Firstly, there seems to be a continuum from giant planets to brown dwarfs. The discovered extrasolar planets have masses up to $\sim$10 M_{Jup} and have therefore more in common with brown dwarfs than with terrestrial planets. The formation mechanisms of giant planets and brown dwarfs are not finally specified. Boss (1997) claims that also giant planets might be formed in a 'star-like' manner by direct collapse out of a cloud. A solely formation-based definition seems therefore to be no longer applicable. There may even be a continuum of formation scenarios from planets to low-mass stars. Secondly, recent observations hint at the existence of free-floating planetary mass objects (Zapatero Osorio et al. 2000, 2002c) raising the question, if we shall call them also *planets*, i.e. waive the requirement, that a planet has to necessarily orbit a star (or brown dwarf). And thirdly, the deuterium burning minimum mass is a model dependent value. The onset of deuterium burning might as well occur for slightly lower or higher mass than $\sim$0.013 $M_\odot$. Therefore also the mass-dependent discrimination does not (yet) provide a fixed boundary between brown dwarfs and planets. Given this complex situation, an IAU working group agreed recently on a working definition setting the borderline between brown dwarfs and planets by definition at the limiting mass for the fusion of deuterium, regardless how the object was formed. Furthermore, they agreed that free-floating planetary mass objects should not be called planet. A concise definition including these aspects is: *A planet is a spherical non-fusor in direct orbit around a fusor*. The present work conforms to this definition, but it should be stressed that the brown dwarf/giant planet boundary might be artificial.

In the following sections of chapter 1, the physics of brown dwarfs are outlined including current ideas on formation scenarios and substellar evolutionary models. Also summarized are theoretical as well as observational constraints on atmospheres and spectra of brown dwarfs, how to test that the target of your observations is really a brown dwarf and last but not least, observational results on multiplicity and circumstellar disks of brown dwarfs. Recent reviews on observations and the theory of brown dwarfs have been published by Basri (2000), Chabrier & Baraffe (2000), Burrows et al. (2001).

Brown dwarfs are an extremely young, rapidly developing field in astronomy, linked to our basic visions of the origins of solar systems. Most of the observational results on brown dwarfs and extrasolar planets come from the last two or three years. The present work is intended to add a piece of information to our understanding of the physics of brown dwarfs, planets and stars.

1.2 Formation models

In the traditional picture of (low-mass) star and planet formation we assume that stars form by fragmentation and collapse of molecular clouds (Shu et al. 1987), a process which involves the formation of a circumstellar disk due to conservation of angular momentum. The disk in turn is the birth place for planets, which form by condensation of dust and further growth by accretion of disk material. These ideas are substantially based on the situation in our own solar system. However, observations of extrasolar planets challenge current theories of planet formation and indicate that our solar system may be rather the exception than the rule. It is still an open question how brown dwarfs form, but it is clear that a better knowledge of the mechanisms producing these transition objects between stars and planets will also clarify some open questions in the context of star and planet formation.

Important observational constraints, which have to be taken into account by brown dwarf formation theories, are described in Sect. 1.7 and are listed here very briefly for convenience: The number of brown dwarfs is at least equal to the number of stars or may even outnumber them by a factor of two (Reid et al. 1999a), therefore any formation scenario for brown dwarfs has to be able to produce brown dwarfs efficiently. Brown dwarfs are common as free-floating objects. A lack of brown dwarfs in close (<3 AU), short-period orbits around solar-mass stars (brown dwarf desert) indicates that there is no continuity from planets to stars and that planets and stars form most certainly two crucially different populations. Several brown dwarfs have been found in wide (>1000 AU) orbit around stars and a few brown dwarf binaries (brown dwarf – brown dwarf pairs) with separations of a few AU (0.03–14 AU) have been detected. Furthermore, significant infrared excess emission hints to close-in circumstellar material around many brown dwarfs. The disk sizes would be a valuable information for theorists, however, they can hardly be infered by infrared excess and are therefore still unknown.

Brown dwarfs may form like planets in a disk around a star or like stars by collapsing clouds. The current ideas about brown dwarf formation are outlined in this chapter and organized within these two major mechanisms, planet-like and star-like formation. However, it should be noted that we may very well also find that there is rather a continuum of formation scenarios from giant planets to brown dwarfs and low-mass stars than two distinct ways.

1.2.1 Planet-like formation

Giant planets are thought to form by either core accretion or disk instabilities (see Wuchterl et al. 2000 for a recent review). Giant planet formation in the core

accretion model is thought to be initiated by the condensation of ice and dust particles in a circumstellar disk, which settle down to mid-plane and accrete to larger (km-size) bodies, called *planetesimals*. Further growth yields to a rock/ice core. When this core reaches the critical mass for the accretion of a gas envelope ($\sim$10-15 $M_\oplus$) a so called *runaway gas accretion* is triggered, which is only slowed down when the surrounding gas reservoir is depleted by the accreting protoplanet. Alternatively to this core accretion model, it has been suggested that planets may also form by gravitational instabilities in the disk on dynamical time scales (DeCampli & Cameron 1979, Bodenheimer 1985, Boss 1997, 1998, 2001, Pickett et al. 2000). It has been demonstrated that disk instabilities can produce planetary mass clumps, however, it has not been finally clarified if they can produce *long-living* clumps and therefore protoplanets. In this scenario, the giant planet forms without a core, thus a posteriori formation of a core is necessary since at least the giant planets in our solar system, Jupiter and Saturn, are believed to have massive cores.

If brown dwarfs are formed like giant planets, the question arises, why giant planets apparently remain in orbit around their host star (detection of more than hundred extrasolar close-in giant planets around stars, e.g. Mayor & Queloz 1995, Marcy et al. 2000), while brown dwarfs apparently do not (brown dwarf desert).

Armitage & Bonnell (2001) propose that the brown dwarf desert might be the consequence of inward orbital migration and merging with the star. This is the same mechanism that has been suggested to explain the close orbits of giant extrasolar planets (e.g. Lin et al. 2000, Ward & Hahn 2000 and references therein) with the difference that the planet has to be stopped before plunging into the star: giant planets might have been formed beyond the ice boundary at about $\sim$5 AU in agreement with the core accretion model. Planet-disk interactions then cause an inward migration, which somehow stops at about 0.05 AU (by tidal interactions with the star or by clearing off the inner disk). The orbital migration is caused by angular momentum exchange between the disk and an orbiting object. The mass of the disk has to be comparable to the mass of the object to drive migration. In order to explain how interaction with the disk can lead brown dwarfs to become mergers with the star, whereas planets are stopped at a finite distance from the star, it has to be assumed that the brown dwarfs form contemporaneously with the star, and thus become embedded within a relatively massive disk. In contrast, the planets are formed later, when the disk is close to being dispersed. However, brown dwarfs formed in a planet-like manner are not formed at the same time as the star but later. Therefore it is very unlikely that the disk is still massive enough to drive orbital migration through to merger with the star. And if so, planets should suffer the same fate. In addition, the large number of free-floating brown dwarfs is hardly explained in a planet-like formation scenario.

Boss (1997) showed that even planetary mass clumps (with a mass below 13 $M_{\rm Jup}$)

might be formed by direct collapse of molecular gas. If this would prove true, there may be no discrimination between giant planets and stars concerning their formation history.

1.2.2 Star-like formation

The somewhat more popular idea is that brown dwarfs form similar to stars. Stars form by fragmentation and gravitational collapse of Jeans-unstable interstellar molecular cloud cores (Fig. 1.1). Preservation of angular momentum leads to the formation of a circumstellar disk. The observed high multiplicity fraction of very young pre-main-sequence stars, in some star forming regions close to 100% (e.g. Leinert et al. 1993, Ghez et al. 1993, 1997 Köhler et al. 2000) suggests that multiple systems are the typical outcome of low-mass star formation. The stellar companions may thereby form by disk fragmentation or filament fragmentation, i.e. involving the formation in a disk.

There are two main possibilities how brown dwarfs may form in a star-like manner but do not become stars: They may form by collapse of relatively small, dense cloud cores. The Jeans-criterion for gravitational collapse requires that the mass of a cloud core has to be larger than the Jeans-mass

$$M_{\mathrm{Jeans}} = 5.46 \left(\frac{kT}{\mu} m_u G \right)^{3/2} \rho^{-1/2} \tag{1.1}$$

(k: Boltzmann constant, T: temperature of the cloud, μ: molecular weight of cloud species, m_u atomic mass unit, ρ: density of the cloud) in order to collapse. In particular, the smallest mass that can collapse under self gravity depends on the temperature and the density in the center of the cloud. During the collapse, the density increases and therefore the Jeans-mass decreases. Thus, progressive compression allows for progressive smaller masses to collapse under self gravity. The initial cloud may collapse and fragment in several Jeans-unstable cloud cores (*hierarchical fragmentation*). It is not clear if cloud cores exist, which are cold enough and dense enough to have a Jeans-mass of about $0.1\,\mathrm{M}_\odot$ or less and would therefore be able to produce brown dwarfs. This formation mechanism is the only currently discussed one, which does not involve a stellar companion at any stage. It should produce brown dwarf binaries or multiples with a wide range of separations.

Another idea is that brown dwarfs formed initially exactly like stars and would have become stars if the accretion process was not stopped at an early stage by an external process. Such an external process can be a strong wind from a nearby hot A or B star, which evaporates the surrounding gas, or the ejection of the protostar out of the dense gaseous environment due to dynamical interactions (Reipurth &

Clarke 2001). If the cut-off from the gas reservoir takes place before the object has accreted to stellar mass then a brown dwarf is formed. The ejection-scenario will be elaborated in the following paragraphs.

Early studies of the chaotic dynamics of gravitationally interacting systems of three or more bodies (see review by Valtonen & Mikkola (1991) and references therein) showed that the dynamical evolution leads to frequent close two-body encounters, often to the formation of one or more close binaries formed out of the most massive objects in the system as well as to the throw-out of the lighter bodies into extended orbits (ejection) or out of the system (escape). The escape of the lightest body is an expected outcome since the escape probability scales approximately as the inverse third power of the mass. Dynamical decay models by Sterzik & Durisen (1995, 1998, 1999) and Durisen et al. (2001) also show that a typical result of gravitational interactions among multiple systems is the formation of a close binary pair and the ejection of lower mass members of the initial cluster. The ejection velocity $v_{\rm eject}$ scales with the inverse of the square root of the distance $R_{\rm peri}$ of the closest approach in the encounter that led to the ejection (Armitage & Clarke 1997):

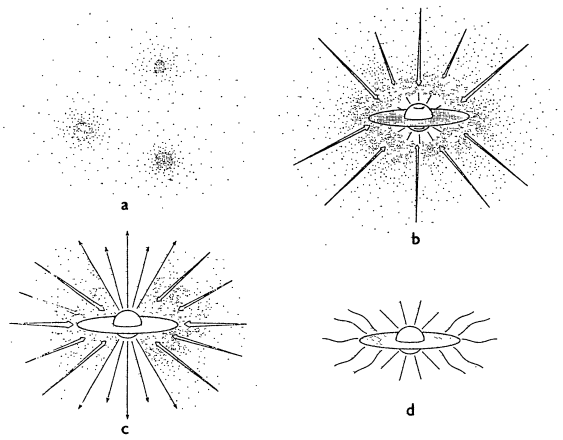

Figure 1.1: **Scheme of the star formation out of cloud cores.** From Shu et al. (1987). (a) Cores form within a molecular cloud. (b) Collapse of cloud core results in the formation of a protostar with a surrounding nebular disk. (c) Bipolar outflow along the rotational axis. (d) The infall terminates, revealing a newly formed star with a circumstellar disk.

$$v_{\rm eject} \approx 15\,{\rm km\,s^{-1}}\ (R_{\rm peri}\,[{\rm AU}])^{-1/2} \quad . \tag{1.2}$$

Assuming a separation of 100 AU the ejection velocity for a single T Tauri star in the models by Sterzik & Durisen would be 3–4 $\rm km\,s^{-1}$.

Reipurth & Clarke (2001) propose that dynamical interactions during the early accretion phase in a star formation process lead to the ejection of protostars in highly eccentric orbits or out of the system with escape velocity. These objects are thenceforth cut off from the dense gas cloud and are therefore prevented from accreting more mass. If the ejection/escape has occured before the object has

accreted to stellar mass it will become a brown dwarf. For brown dwarfs to be formed by this mechanism at a high rate the accretion time scale has to be smaller than the ejection time scale.

Recently Delgado-Donate et al. (2002) and Bate et al. (2002) presented the first theoretical calculations in order to further investigate the ejection hypothesis. Hydrodynamical calculations of the collapse of a star forming cloud with Jeans-mass of $1\,M_\odot$ by Bate et al. (2002) show that roughly equal numbers of brown dwarfs and stars are produced, when an initial turbulent velocity field is imposed on the cloud. In these calculations three quarter of the outcoming brown dwarfs are formed via disk fragmentation, whereas the fragments destined to become brown dwarfs interact with the stars and brown dwarfs to which they are bound until they are ejected. The remaining brown dwarfs originate by filament fragmentation, initially forming on their own, but are then captured into unstable orbits within multiple systems and are ejected before accreting to stellar mass.

The predictions of the ejection-theory are that brown dwarfs are common as free-floating objects, but rare as companions to stars. Furthermore, the violent dynamical interactions should leave the brown dwarf single and diskless, thereby *close* brown dwarf binaries may survive as well as *close-in* disks. In the particular calculations of Bate et al. (2002), only one close (6 AU) brown dwarf binary survives the dynamical interactions in comparison to the formation of about 20 single brown dwarfs (binary frequency of less than 5%). Furthermore, one brown dwarf is orbiting a close stellar binary in a 90 AU highly eccentric, unstable orbit, which will decay in the further evolution. Only about 5% of the young brown dwarfs have circumstellar disks larger than 10 AU. The (ejected) brown dwarfs in the Bate model have a velocity dispersion of $2.1\,\mathrm{km\,s^{-1}}$ in 3D and $1.2\,\mathrm{km\,s^{-1}}$ in 1D, the dispersion of the gas is $1.2\,\mathrm{km\,s^{-1}}$,

Most observed brown dwarfs are indeed apparently free-floating, whereas they are rare or even absent as close companions to stars (brown dwarf desert) in agreement with the ejection-scenario for the formation of brown dwarfs. On the other hand, observations indicate that brown dwarfs are not uncommon as wide (>1000 AU) companions to stars (cf. also Sect. 1.7), these could be the brown dwarfs ejected 'only' into highly eccentric orbits in the ejection-scenario. However, the hierarchical systems are likely supposed to have also decayed. The observed binary frequency of late M (14%–24%, Close et al. 2002) and of L-dwarfs (20%, Reid et al. 2001) are significantly higher than the predictions of Bate et al. (2002).

Decay calculations for brown dwarfs by Sterzik & Durisen (2002) result in one brown dwarf binary (5% binary fraction), two brown dwarfs as companions to stars and 15 single brown dwarfs. The separation distribution shows that 90% of the brown dwarfs with companions have separations smaller than 10 AU, the median is 4 AU compared to 30 AU for G-type stars. The median velocity of the

brown dwarfs is $2\,\mathrm{km\,s^{-1}}$, whereas 10% of the brown dwarfs have a larger velocity than $5\,\mathrm{km\,s^{-1}}$.

The clarification of the formation mechanism for brown dwarfs by observations is additionally complicated by the fact that at least two proposed processes, the orbital migration as well as the ejection due to dynamical interactions would leave the brown dwarf in an entirely different configuration as it was born.

1.3 Substellar evolution

1.3.1 Principles

The principles of the substellar evolution have been outlined already by Shiv Kumar in the early sixties (Kumar 1963). Brown dwarfs never reach the central temperatures required to stabilize their luminosity by hydrogen fusion, therefore they contract and cool as they age until the electron gas in their interior is completely degenerate and they have reached a final radius. Thermonuclear processes

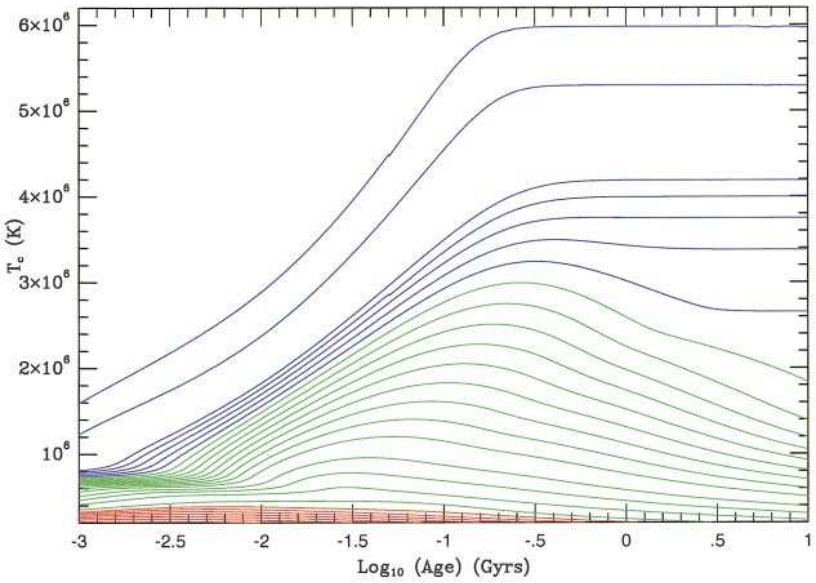

Figure 1.2: **Evolution of the central temperature** for isolated solar-metallicity objects from $0.3\,\mathrm{M_{Jup}}$ ($\sim$ Saturn) to $0.2\,\mathrm{M_\odot}$ ($211\,\mathrm{M_{Jup}}$) versus age. From Burrows et al. (2001). The different colors mark stars (blue), brown dwarfs with masses $> 13\,\mathrm{M_{Jup}}$ (green) and brown dwarfs/giant planets with masses $\leq 13\,\mathrm{M_{Jup}}$ (red). Note the increase (classical plasma), maximum and decrease (quantum plasma) of the central temperature for brown dwarfs.

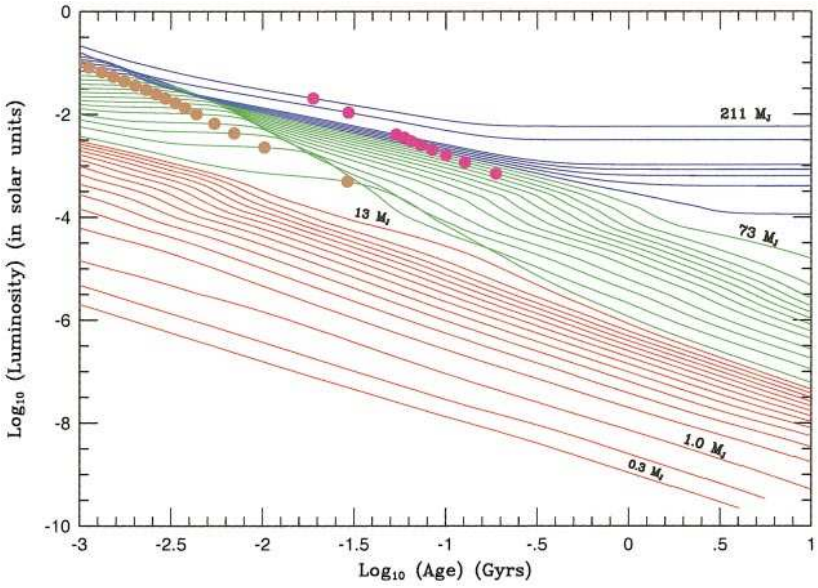

Figure 1.3: **Cooling curves – Evolution of the luminosity** for low-mass stars, brown dwarfs and giant planets. From Burrows et al. (2001). The same color scheme as in Fig. 1.2 was used. For a given object, the gold dots mark when 50% of the deuterium has been burned and the magenta dots mark when 50% of the lithium has been burned.

do not dominate the evolution of brown dwarfs, even though they do burn deuterium, the more massive ones (masses above $0.065\,M_\odot$) burn lithium and may even burn hydrogen for a while. However, they do not burn hydrogen *at a rate sufficient to fully compensate radiative losses.*

The interior of brown dwarfs essentially consists of ionized hydrogen and helium plasma. At the initial contraction stage, brown dwarfs are still relatively hot and extended and the free electrons in the interior plasma obey therefore the Maxwell-Boltzmann statistics for an ideal gas. Energy released due to gravitational contraction is transformed into thermal energy yielding to an increase of the central temperature. As the density in the interior increases part of the electron gas becomes degenerate. Electrons are fermions and obey the *Pauli exclusion principle*, allowing one quantum state to be occupied by only one electron. For the compression of partly degenerate gas, energy is *needed* in order to bring the degenerate electrons closer. Therefore with onwardly contraction the temperature remains constant for a while and then starts to decrease. Fig. 1.2 shows the evolution of the central temperature T_c of isolated solar-metallicity objects from $0.3\,M_{\rm Jup}$ ($\sim$ Saturn) to $0.2\,M_\odot$ ($211\,M_{\rm Jup}$) (from a recent review of Burrows et al. 2001). When the electron gas is completely degenerate, no further contraction is possible, the brown dwarf has reached its final radius (cf. Fig. 1.4) and cools

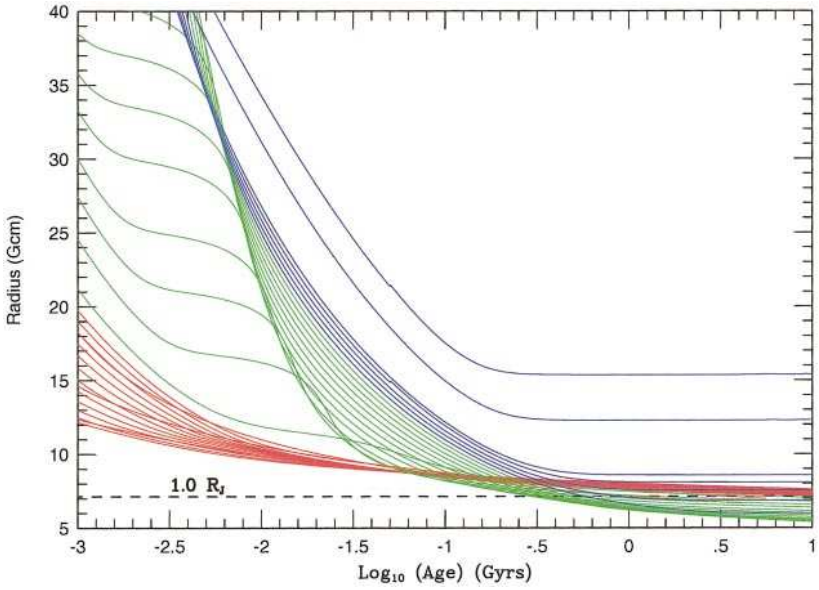

Figure 1.4: **Evolution of the radius** for low-mass stars, brown dwarfs and giant planets. From Burrows et al. (2001). The same color scheme as in Fig. 1.2 was used. Note that the radii are not monotonic and that they cluster near the radius of Jupiter (dashed line) at late times. The plateau in the radius evolution for brown dwarfs is caused by the ignition of deuterium. It is expected to be an observable effect in a rotational period–age diagram.

without compensation by compressional heating.

Fig. 1.3 illustrates the evolution of the luminosity of low-mass stars, brown dwarfs and giant planets. Stars (blue) contract and cool until they stabilize at a luminosity for which the hydrogen-burning compensates for the radiative losses from the surface. They have then reached the hydrogen-burning main-sequence[3]. The contraction and cooling of brown dwarfs (green) is hold up by the fusion of deuterium in the first 10 to 30 Myr for a while (bump in green curves) – gold dots in Fig. 1.3 mark when 50% of the deuterium has been burned – but the cooling essentially progresses during their whole lifetime, whereas the contraction is stopped at some point as soon as it is balanced by the pressure of the completely Fermi-degenerate electron gas.

[3] The point of time when an object arrives on the main-sequence (named zero-age-main-sequence: ZAMS) is not a clearly defined concept in evolutionary models as pointed out recently by Torres & Ribas (2002). While one group defines the ZAMS to be the point where the luminosity released through gravitational contraction falls to 3% of the total, another group defines it as the point when 0.1% of the central hydrogen mass fraction has been burnt. There may be also other definitions.

1.3.2 Evolutionary models

Evolutionary models for low-mass objects have been published by several groups: D'Antona & Mazzitelli (1994, 1997), Burrows et al. (1993, 1997) Baraffe et al. (1995, 1997, 1998), Chabrier et al. (2000), Wuchterl (2000) and Wuchterl & Tscharnuter (2002) (the latter two for the early evolution until 1 Myr). Models of the evolution of (sub)stellar objects require calculations of (a) the equation of state describing the interior pressure and temperature profile, (b) the energy transport in the interior as well as (c) the atmosphere defining the transition between inner optically thick region and the flux radiating photosphere. Evolutionary models predict fundamental (sub)stellar properties as effective temperature and luminosity (some also colors and magnitudes) for a given mass, age and chemical composition, which can be compared with observed properties in order to test the models.

(a) **Equation of state**
The relatively high density of very low-mass objects demands a description of strongly correlated, polarizable, partially degenerate classical and quantum plasmas. It is refered to Saumon (1994) and Saumon et al. (1995) for a review on equation of states for low-mass objects.

(b) **Convective energy transport**
Objects with masses below $\sim 0.4\,M_\odot$ are supposed to be fully convective, i.e. the energy in the interior of very low-mass stars, brown dwarfs and giant planets is dominantly transported by convection. Convection is treated in a parameterized form, the mixing-length-theory (MLT) (Böhm-Vitense 1958). The main hypothesis of the MLT is that rising convective elements dissolve after a characteristic length, the so called mixing length l and emit their energy. Evolutionary tracks are usually calculated for different *mixing length parameters* $\alpha = l/H_P$, which give the mixing length in units of the local pressure scale height H_P.

(c) **Atmospheric models**
Atmospheric models describe the radiative surface layer, where energy from the optically thick interior emerges as light into space. They provide atmospheric temperature and pressure profiles and set therefore the boundary conditions for evolutionary calculations of the interior temperature and pressure profiles. Stellar atmosphere models have developed in the last years from grey models, which integrate the photons across all wavelength, to more realistic non-grey models, which calculate the number of photons for each frequency. Non-grey models need comprehensive scattering and absorption opacities for the relevant chemical species. The spectra of M-dwarfs and cooler objects are dominated by molecular line absorption, which is

crucially wavelength dependent and are therefore better described by non-grey models. Non-grey models allow the calculation of colors enabling the observer to directly compare observed colors and magnitudes with theoretical tracks in color-magnitude-diagrams. See Sect. 1.4 for more details on atmospheres of brown dwarfs.

Most current pre-main-sequence and substellar evolutionary models start from arbitrary initial conditions, ignoring the history of origins of the objects. These models start with the calculation of the contraction of a fully convective object at a sufficiently large radius. Baraffe et al. (2002) show that their models depend crucially on these initial conditions for ages of 1 Myr and younger. However, after $\sim$1 Myr the tracks for different initial radii converge, indicating that the initial radius is forgotten at that time. A different approach is made by Wuchterl & Klessen (2001), who calculate coherently the cloud fragmentation, collapse as well as early evolution of a solar mass star. Similar calculations for brown dwarfs (Wuchterl 2002) hint that the classical initial radii are too large by about 25%. Wuchterl (2001) point out that the time scale for the forgetting of the initial conditions might be significantly larger than 1 Myr if no fully convective interior is assumed. The Wuchterl models are based on a spherically-symmetric collapse and grey atmospheres, surely an oversimplification. However, multi-dimensional protostar collapse calculations accounting for the complex physical processes involved have not yet been performed.

1.4 Atmospheres, spectra and weather phenomena

1.4.1 Atmospheres and spectra

Stellar atmospheres are the radiative surface layers where the light emerges from the optically thick interior[4]. Its knowledge is of crucial importance for a realistic description of (sub)stellar physics and hence, a realistic prediction of (sub)stellar properties. Atmospheric models set the surface conditions of model interiors and provide transformations to the various observational planes (spectra, colors). The atmospheres of brown dwarfs are dominated by the presence of molecules and for cooler brown dwarfs of condensed species (see Burrows & Liebert 1993, Allard et al. 1997, Burrows et al. 2001 for reviews on the subject). Modeling of atmospheres of brown dwarfs/giant planets is complicated by the wide variety of molecular absorbers, each with innumerable line transitions (*molecular opacities*) as well as the variety of condensed species, which can have tremendous effect on the opacity (*grain opacities*).

In brown dwarfs/giant planet atmospheres most of the hydrogen is locked in H_2, and most of the carbon in CO or CH_4. Excess oxygen can be found as TiO, VO and H_2O and nitrogen appears in molecular form of either N_2 or ammonia NH_3, depending on the temperature. Above a temperature of 1600-2000 K, silicates, most metals, TiO and VO are found. Above $\sim$ 1000 K neutral alkali metals are found.

Brown dwarfs cover the spectral types from M over L to T (Fig. 1.5 and 1.6 display spectra of M-, L- and T-dwarfs as an example). Theoretical calculations show that almost all brown dwarfs evolve from M to L to T spectral type as they age and cool (Burrows et al. 2001). M-dwarfs are characterized spectroscopically by line-absorption of TiO and VO in the optical, and H_2O and CO in the infrared. They have practically no continuum. This can be also seen in the UVES spectra of brown dwarfs in Cha I (Sect. 3). The detection of brown dwarfs cooler than M led to the introduction of two entirely new spectral types: L-dwarfs are objects with $T_{\rm eff}$ ranging from about 1000 K to 2000 K. Their spectra are characterized by

[4] It should be noted, that *atmosphere* is not a consistently used concept in astronomy/planetary science. Associated with evolutionary models, the term *atmosphere* is used in a more technical way and denotes the radiative outer layers, for which atmospheric calculations are performed. It includes at least the photosphere of an object but can sometimes also include deeper layers in order to increase the physical overlap between calculations for the interior and calculations for the radiative outer layers. The atmosphere of a terrestrial planet denotes the gaseous envelope, which surrounds the solid celestial body. Speaking of atmospheres of giant planets and brown dwarfs, one usually means all surface layers which display kinds of weather phenomena.

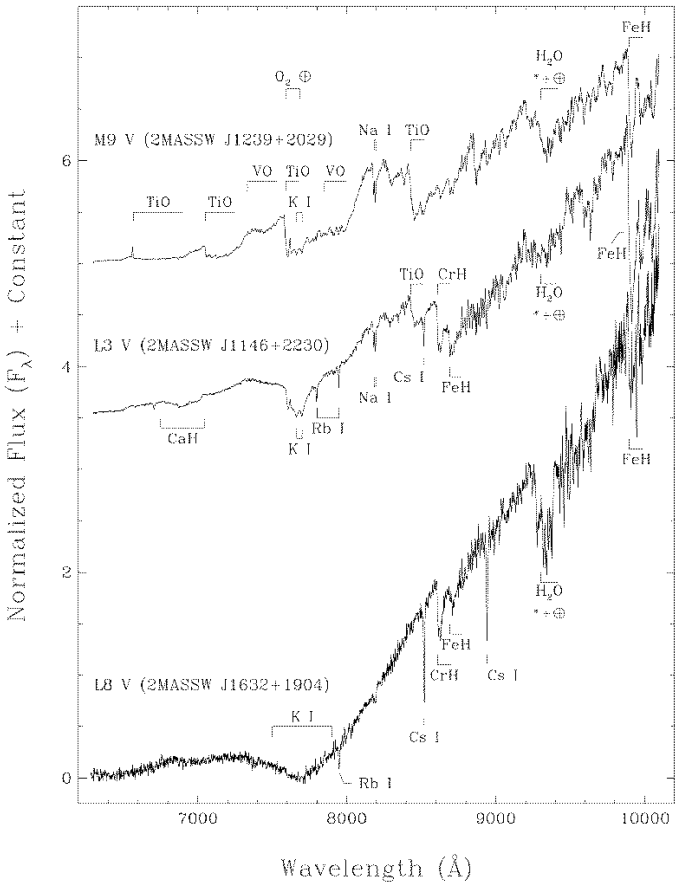

Figure 1.5: **Spectra of a late-M, early- to mid-L, and late-L-dwarfs.** From Kirkpatrick et al. (1999a). Prominent features are marked. Note the absence of oxide absorption in the L-dwarfs along with the dominance of alkali lines and hydride bands.

the weakening of TiO and VO features and the appearance of neutral alkali lines as well as strong metal-hydride bands (e.g. Kirkpatrick et al. 1999b). The even cooler T-dwarfs are characterized by the onset and growth of methane absorption in the H and K band and are therefore called *methane dwarfs* (Burgasser et al. 1999, 2002). Features of metal oxides are completely absent in the spectra of T-dwarfs.

1.4.2 Condensation, clouds and weather

Below a temperature of about 2800 K the condensation of dust sets in (e.g. Tsuji et al. 1996a,b, Fegley & Lodders 1996, Allard et al. 1997, Burrows & Sharp 1999). Different constituents of the atmosphere are condensing at certain atmospheric heights. The formation of condensates depletes the gas phase of a number of

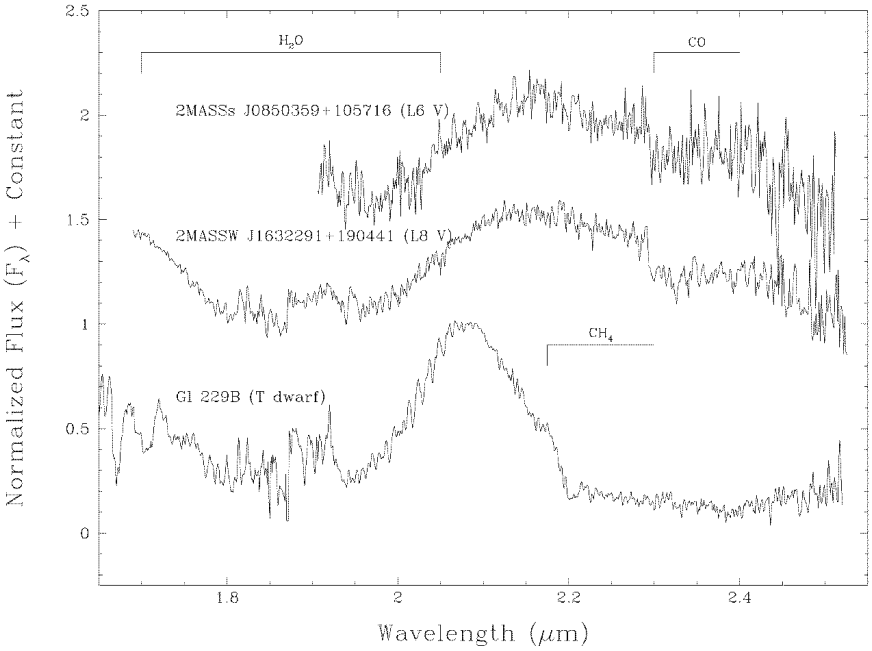

Figure 1.6: **Spectra of two mid- to late-L and a mid-T-dwarf.** From Kirkpatrick et al. (1999a). Gl 229 spectrum from Geballe et al. (1996). Note the absence of methane absorption and the continued presence of CO absorption in the late-L-dwarfs.

molecular species and therefore alters significantly the gas phase composition (*rain out*). For example, the vanishing of metal oxides, like TiO and VO with decreasing effective temperature, starting in L-dwarfs and progressing in T-dwarfs is due to the fact that these species are rained out in the atmosphere and are segregated in condensed form (e.g. $CaTiO_3$) below the photosphere. Furthermore, the formation of condensates may significantly alter the opacity of the photosphere and therefore the thermal structure (green house effect). The J-K colors of L-dwarfs become progressively redder with later spectral type (e.g. Kirkpatrick et al. 1999b), whereas the cool T-dwarfs (like Gl 229B) have blue J-K colors (e.g. Leggett et al. 1999). These spectroscopic observations are best fit by progressive appearance of more silicate dust in the atmosphere with later spectral type in the L-regime on one hand (e.g. Leggett et al. 1998, Chabrier et al. 2000) (*dusty L-dwarfs*) and with a settling of the silicate dust below the visible atmosphere in the T-dwarf regime on the other hand (e.g. Allard et al. 1996) (*relatively cloud-free T-dwarfs*). These examples demonstrate the crucial importance of accurate cloud models for the prediction of realistic colors and spectra of cool brown dwarfs. Also the establishment of an effective temperature scale for L-dwarfs needs a proper description of clouds.

Chemical equilibrium models (e.g. Fegley & Lodders 1994, Tsuji et al. 1996a, Burrows & Sharp 1999) predict, which species are expected to condensate in

an atmosphere. Below about 2800 K O-rich compounds start to condense in the atmosphere, first corundum Al_2O_3 and at lower temperatures ($T_{eff} \lesssim 1800$ K) perovskite $CaTiO_3$, iron Fe, forsterite Mg_2SiO_4 and enstatite $MgSiO_3$. These condensates rain out VO, TiO, Al, Ca, Ti, Fe, Mg, Si from the gas phase of the atmosphere. Below ∼500 K water clouds form and below ∼200 K clouds of ammonia NH_3 form.

Current cloud models (e.g. Tsuji et al. 1996a, Marley et al. 1999, Ackermann & Marley 2001) have to deal with several difficulties as unknown but important grain size, the mixture of various species in one cloud as well as the layered structure. The direct effect of clouds on the emergent fluxes of brown dwarfs/planets has yet to be clarified. However, it can be said, that for objects with temperatures between 1500 and 2400 K silicate and iron clouds play an important role, below ∼1000 K chloride and sulfide clouds, water clouds near 300 K and ammonia clouds below 200 K (Burrows et al. 2001).

Recent photometric observations (Tinney & Tolley 1999, Bailer-Jones & Mundt 2001, Martín et al. 2001) hint at significant variability in the light curves of brown dwarfs, which might be attributed to global scale weather patterns, as observed on Jupiter (Great Red Spot). Inhomogeneities in dust cloud coverages may cause observable photometric variations. If they are stable on orbital time scales, they cause a periodic variation at the rotational period. Most of the up to date observed variability for brown dwarfs show no or variable periods. Several authors suggest that we might see temporal variations of the cloud configuration, like the formation and dissipation of clouds on short time scales.

Photometric monitoring of young M-type brown dwarfs was carried out within the frame of the presented work. Significant variability was observed and is discussed in the context of clouds and magnetic activity (Sect. 6.)

1.5 Magnetic activity

For stars on the main-sequence, there is a well-known correlation between magnetic activity and rotation: the faster the rotation the more active the star is, measured in terms of chromospheric Hα, Ca II and Mg II emission, flare activity as well as coronal X-ray emission (Kraft 1967, Noyes et al. 1984, Marilli et al. 1986, Rutten 1986). Magnetic fields of stars with masses above ∼0.4 $M_\odot$, which have a radiative core in the interior and a convective envelope are thought to be generated by a so called $\alpha\Omega$ *dynamo* (or *solar dynamo*), which is driven by rotation. A poloidal magnetic field in the convective layer will be stretched and amplified into a strong large-scale toroidal field when it is dragged by convective overshooting into the radial shear in rotation that resides at the interface between convective and radiative zone (Spiegel & Weiss 1980, Spiegel & Zahn 1992). When

the star ages on the main-sequence, it looses angular momentum due to winds and its rotation is decelerated. As expected for a rotation-based dynamo, also the activity decreases with age (Wilson & Skumanich 1964) (rotation-activity-age correlation). Furthermore it has been observed that at a certain threshold rotation velocity the rotation-activity relation saturates (e.g. Stauffer et al. 1994b) and is even reversed for ultra-fast rotators (Randich et al. 1997). This behavior is not yet completely understood.

Stars of lower mass than $\sim 0.4\,M_\odot$, brown dwarfs as well as pre-main-sequence stars (T Tauri stars) have no radiative core but are fully convective according to the standard model. Hence, the solar dynamo operating at the interface between radiative and convective zone cannot work for them[5]. However, T Tauri stars are known to be extremely active stars and it is still unclear what kind of dynamo is generating the magnetic fields in them. Several extended studies of rotation and activity of T Tauri stars have been carried out but the rotation-activity relation in the pre-main sequence regime is still a matter of debate: a correlation between rotation and X-ray emission has been found for T Tauri stars in Taurus (Bouvier et al. 1990, Neuhäuser et al. 1995, Stelzer & Neuhäuser 2001), whereas a recent publication by Feigelson et al. (2002) reports the absence of a connection between X-ray emission and rotation for a large sample of T Tauri stars in Orion. Hα emission on the other hand is not a definite indicator for chromospheric activity at very young ages, since they often have circumstellar accretion disks, which are significant additional Hα emission sources. At these very young ages, however, magnetic activity might be also (partially) attributable to accretion phenomena.

Leaving the very young ages aside, in any case a change in the activity behavior was expected at the transition between solar-type stars to fully convective stars (at about spectral type M5.5). However, this has not been observed (e.g. Fleming et al. 1993, Giampapa et al. 1996) indicating that there is no abrupt change of the dynamo efficiency or the rotation-activity dependence at this spectral type. It has been suggested that a *turbulent dynamo* (Durney et al. 1993) or α^2 *dynamo* (Rädler et al. 1990), which is driven by a wide range of convective motion, works in fully convective stars/brown dwarfs. The magnetic field in solar-type stars might then be generated besides the solar dynamo also partially by the turbulent or α^2 dynamo operating throughout the convective zone and taking over completely when the star becomes fully convective (Giampapa et al. 1996). This would explain the absence of dramatic changes in activity at the boundary to fully convective objects.

Several observations in the last few years hint at decreasing activity and to a

[5] Recent calculations by Wuchterl & Klessen (2001) show that pre-main-sequence stars resulting from collapse are not fully convective. Even brown dwarfs can have a radiative core (Wuchterl 2002). In this case, the solar dynamo may operate also in pre-main-sequence stars, and low-mass objects.

break-up of the correlation between activity and rotation for very late M-dwarfs. In particular, near and below the substellar limit several rapid rotators are found with no or very little signs of chromospheric activity (e.g. Basri & Marcy 1995, Martín et al 1997, Delfosse et al. 1998a, Tinney & Reid 1998, Basri et al. 2000). Gizis et al. (2000) finds that the fraction of active (measured in terms of Hα emission) cool (late-M and L) dwarfs increases with later spectral type until reaching a maximum at around M7-M8 and decreases in turn for even later types. Furthermore, they find that younger brown dwarfs have less Hα emission hinting at a reversion of the conventional age-activity correlation for brown dwarfs. It should be noted, that this does not include very young brown dwarfs, which are indeed more active than older ones (X-ray emission, spots, see below). The indications that old brown dwarfs are relatively inactive is also supported by the finding that they have probably no or only very weak persistent X-ray emission (e.g. Rutledge et al. 2000).

Weakening of chromospheric and coronal activity in the substellar regime might be due to the poor electric conductivity of the cool and neutral atmospheres. At very cool temperatures magnetic Reynolds numbers are low, hence the magnetic field is decoupled from the gas and cannot be twisted. Such neutral atmospheres do not allow any near-surface dynamo action, whereas there might be subsurface dynamos operating. Hence, cool brown dwarfs might still have magnetic fields, but the atmosphere is nevertheless unable to transport magnetic energy through non-conductive surface layers and therefore no magnetic activity in the chromosphere and corona is expected (Meyer & Meyer-Hofmeister 1999, Gelino et al. 2001, Mohanty et al. 2002).

On the other hand, surprisingly several flares have been recorded for brown dwarfs in Hα (Reid et al. 1999a, Liebert et al. 1999), in X-rays (Rutledge et al. 2000) as well as in radio (Berger 2002). These detections show that flare events might be not uncommon for brown dwarfs and that the magnetic fields have not entirely disappeared. It is puzzling, how a neutral atmosphere unable to produce spots or to heat the chromosphere and corona can produce flares.

To summarize, the activity behavior of old brown dwarfs tends toward flaring activity and an absence of persistent chromospheric Hα or coronal X-ray emission. Counterexamples to this picture are: a methane dwarf with (non-flaring) Hα emission (Burgasser et al. 2000a) and a very rapid rotator (Kelu-1) with persistent Hα emission (Basri et al. 2000).

Very young brown dwarfs (a few Myrs) on the other hand seem to have more in common with T Tauri stars, as they (1) can be persistent X-ray sources (e.g. Neuhäuser & Comerón 1998, Neuhäuser et al. 1999, Garmire et al. 2000, Feigelson et al. 2002, Imanishi et al. 2001, Preibisch & Zinnecker 2001, 2002, Mokler et al. 2002), (2) have significant (often variable) Hα emission (e.g. Comerón et al. 2000, Zapatero Osorio et al. 2002a, 2002b) and (3) photometric monitoring give

evidence for surface spots (cf. Sect. 6). A study of the relation between rotation and activity in the substellar regime at this very young age is hampered, up to now, by the lack of observational constraints of rotation parameters: $v \sin i$ values are known for only two very young brown dwarfs and seven brown dwarf candidates (cf. Sect. 4) and rotational periods have been determined for three brown dwarf candidates so far (cf. Sect. 6).

Activity indicators are: cool spots, which are the foot-points of magnetic flux tubes. The magnetic fields suppress convective energy transport from the interior and cause therefore regions of locally cooler temperatures. They are visible with the naked eye (with a filter!) on our Sun in high activity seasons, they can be traced by photometric monitoring since the cool spots modulate the brightness of a star at the rotation rate and, last but not least, Doppler imaging allows the reconstruction of images of the stellar surface and therefore to make spot distributions visible on other stars than the Sun. Flares are explained by twisting of the fieldlines due to rotation and reconnection. Emission lines of Hα, CaII and MgII as well as X-ray emission of active stars are thought to be caused by heating of the chromosphere and corona (For an example, the temperature of the solar surface is about 6000 K, the temperature of the solar corona a few million degrees). It is not yet clear by what mechanism the energy is transported to the outermost layers of the solar atmosphere. It has been suggested that the release of magnetic stresses brought into the field by twisting and shearing subsurface motion or acoustic waves might be responsible for the heating.

1.6 Substellar tests

How to be sure that the target of your observations is a brown dwarf?

1.6.1 The lithium test

The fusion of lithium occurs at lower temperatures than the fusion of hydrogen. Stars burn their lithium in about the first 100 Myr, whereas brown dwarfs with masses below about 65 M_{Jup} never reach the temperatures required to burn lithium (D'Antona & Mazzitelli 1985). Brown dwarfs and very low-mass stars are fully convective, therefore the surface material is efficiently mixed to the core. This fact allows us to conclude from spectroscopic diagnostics of the atmospheric abundance to the core abundance. Rebolo et al. (1992) suggested to use the lithium resonance line at 6708 Å to discriminate between stars and brown dwarfs: The detection of lithium in an old ($>>$ 100 Myr), fully convective object indicates that its core never reached temperatures high enough to burn a substantial

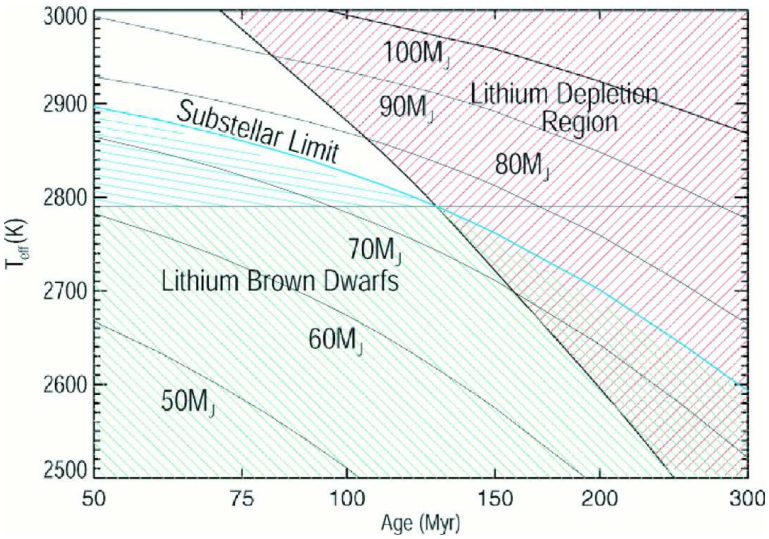

Figure 1.7: **Lithium depletion** during the evolution of very low-mass stars and brown dwarfs for different masses and temperatures. From Basri (2000) based on evolutionary models by Baraffe & Chabrier. Solid lines are cooling tracks for different masses. The substellar limit ($75\,M_{Jup}$, depending on metallicity) is noted in blue. In the Lithium depletion region (marked with red hatching) lithium is depleted to 99%. The horizontal line marks the temperature at which an object at the substellar boundary has just depleted its lithium. Below this line, the detection of lithium in an object guarantees its substellar nature. See the text for more details.

amount of its primordial lithium, hence it never burned hydrogen and is therefore a brown dwarf.

The limits to this test are: It does not apply to very young objects (younger than 100 Myr), because stars at this age have not yet depleted their lithium. Therefore young brown dwarfs, which will never burn lithium cannot be distinguished from young stars, which have *not yet* depleted all their lithium. Furthermore, the test does not apply for brown dwarfs with masses higher than the lithium burning minimum mass of $\sim 65\,M_{Jup}$ since the non-detection of lithium for brown dwarfs with masses above $\sim 65\,M_{Jup}$ does not rule out substellar nature.

Basri (2000) modified the criterion for the lithium test to the age-independent statement, that *any object with spectral type M7 or later that shows lithium must be substellar*. This can be seen by having a look at the lithium depletion region within an effective temperature vs. age diagram (Fig. 1.7). The non-detection of lithium for an object with known effective temperature gives a lower limit to its age and mass. Conversely, the detection of lithium for an object with known effective temperature gives an upper limit to its age and mass. According to models, for an object at a temperature of ~ 2700 K, 99% of the lithium is depleted exactly at the substellar limit. A temperature of ~ 2700 K transforms to about

spectral type M6. Therefore any object of later spectral type that shows lithium must be substellar.

1.6.2 Methane test

Methane absorption appears in the spectra of objects with a temperature below about 1300 K. The detection of methane in a spectrum clearly classifies the object as substellar because even the least massive and oldest stars have an effective temperature of 1500–1700 K. Methane absorption can be detected in the near infrared at $\sim$1.7 μm as well as at $\sim$2.3–2.4 μm.

1.6.3 Substellar test by mass determination

The substellar nature of very young objects, for which the lithium test is not applicable, can be performed by a direct or indirect determination of the mass and comparison with the theoretical hydrogen burning minimum mass (0.075-0.085 $M_\odot$, depending on metallicity). A dynamical mass determination is only possible for binaries, multiple systems or objects with an observable disk. An indirect mass estimation is possible by the determination of luminosity and effective temperature of the object and comparison of its position in the Hertzsprung-Russel diagram (HRD) with theoretical evolutionary tracks. (Some uncertainties may remain due to uncertainties in the temperature scale as well as uncertainties in the models themselves.

1.7 Multiplicity and circumstellar material

The study of brown dwarf multiple systems and their properties, like binary frequency, mass ratio and orbital separation, provide important clues to their formation history as described in Sect. 1.2. In addition, binaries are our only means to determine accurate masses and provide therefore an invaluable test of evolutionary models. In the last few years, several brown dwarfs in multiple systems have been discovered by high-resolution imaging applying speckle and adaptive optics (AO) techniques as well as coronographic methods, which are able to handle the large dynamical range of, for example, a brown dwarf orbiting a thousand times more luminous star. Furthermore, spectroscopy at high resolving power allowed to detect substellar companions to stars as low-mass as Jupiter. The combination of high-resolution spectroscopy and large aperture telescopes is capable of searching for companions to substellar objects themselves. The hitherto main observational results in the context of multiple systems involving brown dwarfs are summarized in this paragraph.

1.7.1 Brown dwarf companions to stars

One of the most striking findings in this context is maybe the almost complete absence of short-period, close (<3 AU) brown dwarf companions to sun-like stars. High-precision radial velocity surveys have brought up more than hundred planetary candidates in orbit around stars but only very few brown dwarf candidates despite the fact that these surveys are more sensitive to higher masses. This is referred to as the *brown dwarf desert* (Basri & Marcy 1997, Mayor et al. 1998a, 1998b, Marcy & Butler 1998, Halbwachs et al. 2000, Zucker & Mazeh 2001, Jorissen et al. 2001). Fig. 1.8 taken from Zucker & Mazeh (2001) displays the gap in the mass function of companions to stars (from planetary to stellar masses) at the masses of brown dwarfs.

On the other hand, several brown dwarfs have been detected in wide orbits around stars indicating that there is no brown dwarf desert at wide separations. The search for faint companions to stars by direct imaging yielded the discovery of at least nine brown dwarf companions to stars confirmed by both spectroscopy as well as proper motion, four more likely brown dwarfs in orbit around stars have been reported (see Table 1.1). The coolest companion among them is the T-dwarf

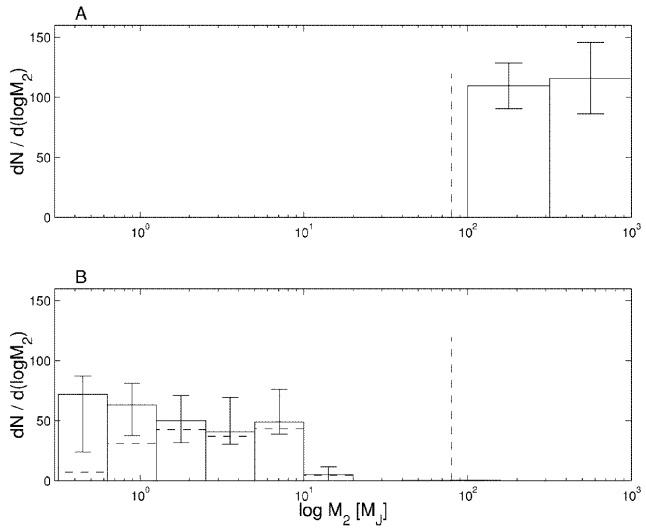

Figure 1.8: **Mass distribution of planetary and stellar companions to stars.** From Zucker & Mazeh (2001). Dashed lines represent the mass distribution without correction for selection effects. The vertical dashed lines mark the substellar boundary. Panel A (top) displays the mass distribution for stellar companions to stars, panel B (bottom) that one for substellar companions to stars. The gap between planetary companions to stars and stellar companions to stars, the *brown dwarf desert*, is a significant lack of close brown dwarf companions to stars. It suggests that planets and stars form two crucially different populations.

Table 1.1: **Compilation of known brown dwarf companions to stars.** For the last four objects, either the brown dwarf status of the companion (brown dwarf candidate: BDc) or the fact that the companion is really physically bound to the star (companion candidate: cc) has to be confirmed.

object	separation	note	reference
Gl 229 B	∼40 AU		Nakajima et al. 1995, Oppenheimer et al. 1995
G 196-3 B	∼340 AU		Rebolo et al. 1998
Gl 570 D	∼1500 AU		Burgasser et al. 2000b
TWA 5 B	∼110 AU		Lowrance et al. 1999, Neuhäuser et al. 2000
HR 7329	∼200 AU		Lowrance et al. 2000, Guenther et al. 2001
Gl 417B	∼2000 AU		Kirkpatrick et al. 2000, 2001
Gl 584C	∼3600 AU		Kirkpatrick et al. 2000, 2001
Gl 337C	∼900 AU		Wilson et al. 2001
Gl 618.1B	∼1100 AU	BDc	Wilson et al. 2001
HR 7672	∼14 AU	BDc	Liu et al. 2002
GG Tau Bb	∼207 AU	cc	White et al. 1999
Gl 86B	∼19 AU	cc	Els et al. 2001

Gl 570 D in a quadruple system (Burgasser et al. 2000b) and the youngest is the M8.5–M9 brown dwarf TWA 5B orbiting a pre-main-sequence star (Lowrance et al. 1999, Neuhäuser et al. 2000). Given the lack of brown dwarf companions at separations of 3 AU and smaller, a remarkable detection is also the L4.5 dwarf in a relatively close 14 AU orbit around the star HR 7672 (Liu et al. 2002). HR 7672 shows in addition a long-term radial velocity trend (Cumming et al. 1999), which is attributed to Doppler reflex motion caused by the companion. The separations range from 14 AU to 3600 AU. A study of frequency of brown dwarf companions to stars by Gizis et al. (2001) based on the three wide companions Gl 417B, Gl 584C and Gl 570D confirms that there is no brown dwarf desert at wide separations.

1.7.2 Brown dwarf binaries

One of the first discovered brown dwarfs, PPl 15, turned out to be a spectroscopic binary containing two gravitationally bound brown dwarfs (Basri & Martín 1999). Up to now, three more brown dwarf binaries, i.e. brown dwarf–brown dwarf pairs, have been detected by spectroscopy as well as proper motion (see Table 1.2). At least five more candidates for brown dwarf binaries are known, which await confirmation. Gl 569B is a confirmed brown dwarf binary in orbit around a M2.5 star and HD 130948B+C is an L-dwarf binary orbiting a star. Hints at the detection of a second brown dwarf spectroscopic binary come from UVES spectra of the

Table 1.2: **Compilation of known brown dwarf binaries (=brown dwarf-brown dwarf pairs).** SB: spectroscopic binary. For the last six objects, either the brown dwarf status of the binary components (brown dwarf candidates: BDc) or the fact that the components are really physically bound (binary candidate: bc) has to be confirmed.

object	separation	note	reference
PPl 15	0.03 AU	SB	Basri & Martín 1999
DENIS-P J1228.2-1547	∼5 AU		Martín et al. 1999, Koerner et al. 1999
2MASSW J1146	5–10 AU		Koerner et al. 1999, Reid et al. 2001
Gl 569B	1 AU		Martín et al. 2000, Lane et al. 2001, Kenworthy et al. 2001
HD 130948B+C	∼2 AU	BDc	Potter et al. 2002
2MsJ0850+1057	∼4 AU	bc	Reid et al. 2001
2MWJ2331–0406	∼14 AU	BDc	Close et al. 2002b
2MJ1426+1557	∼4 AU	BDc	Close et al. 2002a,b
2MWJ2140+1625	∼4 AU	BDc	Close et al. 2002b
2MWJ2113-1009	–	SB bc	Guenther et al. 2002

old brown dwarf candidate 2MWJ2113-1009 (Guenther & Wuchterl 2002).

The binary frequency for lower mass stars turned out to be significantly lower than for G dwarfs (∼ 57% Duquennoy & Mayor 1991). This was already noted by Fischer & Marcy (1992) and Reid & Gizis (1997a,b) and was very recently confirmed by Marchal (2002), who reports a multiplicity rate of 31±5% for (sub) stellar M-dwarfs in the solar vicinity based on a six year survey. In this sample, the binary frequency is monotonously decreasing with primary mass and the separation distribution for M-dwarfs is similar to that for G dwarfs. An even lower binary fraction was found by Close et al. (2002) (14%–24%) for 20 late M-dwarfs (M8–M9) as well as by Reid et al. (2001) (20%) for 20 L-dwarfs.

1.7.3 Planets around brown dwarfs

To date, there is no planet known orbiting a brown dwarf. The lowest mass star with a radial velocity planet candidate ($M \sin i$=0.2 M_{Jup}) is the M4-dwarf Gl 876, which has a mass of 0.3–0.4 $M_\odot$ (Delfosse et al. 1998b). We do not know, if the formation of planets around brown dwarfs is possible. One could argue that disk masses of brown dwarfs may be too small for the formation of planets. However, infrared excess emission has been observed for numerous brown dwarfs (see next section) hinting at significant circumstellar material even around substellar objects, out of which planets may form.

If brown dwarfs *have* planets, they are definitely easier to detect than planets around stars by both radial velocity as well as by direct imaging techniques. The radial velocity surveys trace the reflex motion of a host object due to an orbiting mass. A planet of a given mass causes a larger reflex motion and therefore larger radial velocity signal if its host object is less massive. In particular, a planet with a given mass is able to pull much more on a brown dwarf primary than on a stellar primary. A less massive (and therefore less luminous) parent object is also an advantage speaking of planet detections by direct imaging. Detecting a planet close to a thousand times brighter star is a matter of dynamical range, a problem which is less serious for a planet around a brown dwarf.

1.7.4 Circumstellar disks

Disks are a consequence of star formation by molecular cloud collapse. Thus, evidence for disks around brown dwarfs would shed light on their origin and furthermore hint to the possibility that brown dwarfs may also harbor planetary systems. Although circumstellar disks around mid- to late M-dwarfs and cooler objects might be expected to have insufficient mass to form companions around them, recent observational evidence hints at significant reservoirs of gas and dust even around these objects (e.g. Fernández & Comerón, 2001). In the last two years, indications for the presence of significant circumstellar material around numerous brown dwarfs have been found: one bona fide brown dwarf (Cha Hα 1) as well as three brown dwarf candidates (Cha Hα 2, 6 and 9) in Cha I display mid-infrared (6.7 μm) excess emission (Persi et al. 2000, Comerón et al. 2000); three brown dwarfs in ρ Oph show near-infrared excess (at 2.2 μm) (Wilking et al. 1999). A study of more than 100 brown dwarf candidates in Orion shows that a large fraction of them (>50%) display K-band excess (2.2 μm) and gives evidence that disks are common among very young brown dwarfs (Muench et al. 2001). These findings suggest that brown dwarfs

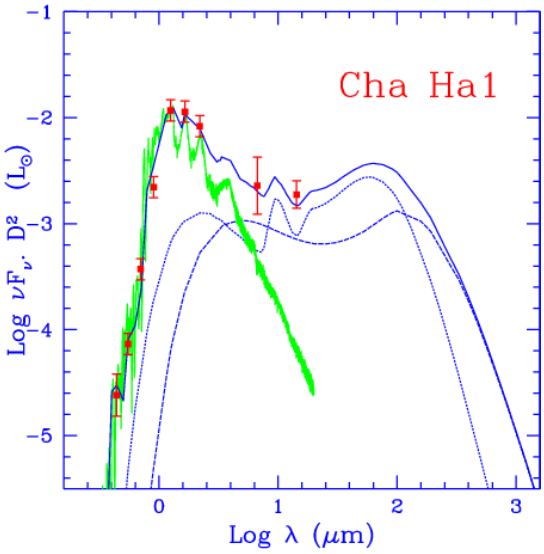

Figure 1.9: Observed and modeled spectral energy distribution of Cha Hα 1. From Natta & Testi (2001). Observed fluxes (red) from Comerón et al. (2000) and Persi et al. (2000), dashed lines: contribution from the disk, green: emission from Allard et al. (2001) model atmosphere, solid line: disk model predictions.

form rather like stars than planets. Infrared excess emission is emitted by the inner disk regions of brown dwarfs, therefore the sizes of the disks cannot be inferred from these observations. The presence of close-in circumstellar material around brown dwarfs may not exclude that the system has been ejected during its former live. It could be possible that such inner disks are not truncated by dynamical interactions. Millimeter observations are required to monitor the emission from the outer disk regions.

Natta & Testi (2001) demonstrate that the observed emission for Cha Hα 1, 2 and 9, for which excess emission was found in both mid-infrared bands (6.7 and 14.3 μm) but not in the near-infrared, can be described by models of a flared circumstellar disk identical to those of T Tauri stars but scaled down to brown dwarf disk masses (Fig. 1.9 displays the observed and modeled spectral energy distribution of Cha Hα 1). They show that the emission in the near-infrared is dominated by the stellar photosphere, whereas the main signature of the brown dwarf disks are to be found in mid-infrared excess emission. Natta & Testi further note that for Cha Hα 2 and Cha Hα 9 there is a tendency of the 14.3 μm data point to lie slightly (about 20%) below the model predictions. Apai et al. (2002) carried out additional mid-infrared observations at 9.8 and 11.9 μm of Cha Hα 2 filling the gap between the ISO measurements at 6.7 and 14.3 μm. These observations were aimed at the detection of the silicate emission at about 9.6 μm, which should be produced by a flared disk. A *flared disk* features a superheated surface layer, i.e. an optically thin 'disk atmosphere', which is expected to produce silicate emission, and an optically thick disk interior. A *flat disk* has no atmosphere but is completely optically thick. Apai et al. (2002) find no silicate feature and conclude that the disk of Cha Hα 2 is better described by an optically thick flat disk than by a T Tauri-like flared disk. This may not be the case for Cha Hα 1, since for this object, the flared disk model predicts the observed data points very well. Further mid-infrared observations also of Cha Hα 1 would be of interest.

Chapter 2

The brown dwarfs in Cha I

The Chamaeleon cloud complex is comprised of three main clouds. Cha I is the most active star forming cloud among them and one of the most promising grounds for observational projects on very low-mass objects since it is young, nearby (160 pc) and the extinction is low compared to other star forming regions. Recently twelve low-mass M6–M8–type objects, Cha Hα 1 to 12, have been detected in the center of Cha I with ages in the range of 1 to 5 Myrs (Comerón et al. 1999, 2000). Characteristic parameters of the objects are listed in Table 2.1. Fig. 2.1 displays the objects placed into the Hertzsprung-Russell diagram (HRD) and compared with current evolutionary tracks for brown dwarfs. The masses of all twelve objects lie below or near the border line separating brown dwarfs and very low-mass stars at about 0.08 $M_\odot$. Cha Hα 1, 7, 10 and 11 (M7.5–M8) are bona fide brown dwarfs with masses in the range of about 0.03 $M_\odot$ to 0.05 $M_\odot$ (Neuhäuser & Comerón 1998, 1999; Comerón et al. 2000). Cha Hα 2, 3, 6, 8, 9, 12 (M6.5–M7) are brown dwarf candidates, whereas Cha Hα 4 and 5 (M6) are also named brown dwarf candidates in this work but are more likely very low-mass stars. The tentativeness in the classification is mainly due to the relatively large errors in the derived temperatures (cf. error bar in Fig. 2.1, bottom panel) caused by an unsecure temperature scale for brown dwarfs.

Mid-IR ISO and ground based observations revealed that the brown dwarf Cha Hα 1 and the three brown dwarf candidates Cha Hα 2, 6 and 9 have optically thick circumstellar disks (Persi et al. 2000, Comerón et al. 2000, Apai et al. 2002). Natta & Testi (2001) demonstrate that the observed emission for these objects can be described by models of flared circumstellar disks identical to those of T Tauri stars. They show that the emission in the near-IR is dominated by the stellar photosphere, whereas the main signature of the brown dwarf disks are to be found in mid-IR excess emission. However, Apai et al. (2002) found that the mid-IR emission of Cha Hα 2 is better described by a model of a flat disk on the basis of the absence of silicate emission expected for a flared disk (cf. Sect. 1.7).

Table 2.1: **Parameters of brown dwarfs and very low-mass stars in Cha I.** Given are spectral types SpT, masses M_*, V and I band magnitudes, effective temperatures T_{eff} and luminosities L in units of the solar luminosity $L_\odot$ published by Comerón et al. (1999, 2000). The masses are estimates based on Baraffe et al. (1998) tracks and an intermediate temperature scale from Luhman (1999) for the Cha Hα objects and on Burrows et al. (1997) tracks and the dwarf temperature scale from Leggett et al. (1996) for the T Tauri stars, respectively. Sz 23 has a larger mass than provided by the model of Burrows et al. (1997), therefore, for this object the mass is derived from D'Antona & Mazzitelli (1997) tracks.

object	SpT	M_* [$M_\odot$]	V [mag]	I [mag]	T_{eff} [K]	log L [$L_\odot$]
Cha Hα 1	M7.5	0.04	21.0	16.2	2770	-1.96
Cha Hα 2	M6.5	0.07	19.8	15.1	2910	-1.47
Cha Hα 3	M7	0.06	19.5	14.9	2840	-1.46
Cha Hα 4	M6	0.1	18.5	14.3	2980	-1.25
Cha Hα 5	M6	0.1	19.2	14.7	2980	-1.31
Cha Hα 6	M7	0.05	19.8	15.1	2840	-1.57
Cha Hα 7	M8	0.03	22.2	16.9	2690	-2.19
Cha Hα 8	M6.5	0.07	20.1	15.5	2910	-1.65
Cha Hα 9	M6	0.07	23.1	17.3	2980	-2.26
Cha Hα 10	M7.5	0.04	21.6	16.9	2770	-2.28
Cha Hα 11	M8	0.03	21.9	17.4	2690	-2.44
Cha Hα 12	M7	0.05	20.6	15.6	2840	-1.60
B 34	M5	0.12	18.1	14.3	3031	-1.18
Sz 23	M2.5	0.3	18.0	14.4	3448	-1.18
CHXR 74	M4.5	0.17	17.3	13.6	3090	-0.82
CHXR 78C	M5.5	0.09	19.0	14.8	2940	-1.23
CHXR 73	M4.5	0.15	20.2	15.6	3035	-0.79

Mid-IR emission of the Cha Hα objects loosely correlates with Hα emission: objects without mid-IR excess emission always have small Hα emission equivalent width (< 5 Å), while objects with mid-IR excess emission can be found with any quantity of Hα emission (Comerón et al. 2000). Cha Hα 1 was the first brown dwarf detected in X-rays (Neuhäuser & Comerón 1998). Several of the brown dwarf candidates in Cha I, namely Cha Hα 3, 4, 5 and 6, are also detected as X-ray sources with L_x/L_{bol} values typical for young late-type stars (Neuhäuser et al. 1999, Comerón et al. 2000). Quiescent X-ray emission of brown dwarfs indicate that even substellar objects may drive coronal activity when they are young.

Furthermore, several very low-mass stars have been studied within the scope of the presented work. These are B 34, CHXR 74, Sz 23, CHXR73 and CHXR 78C. Their main properties are also given in Table 2.1.

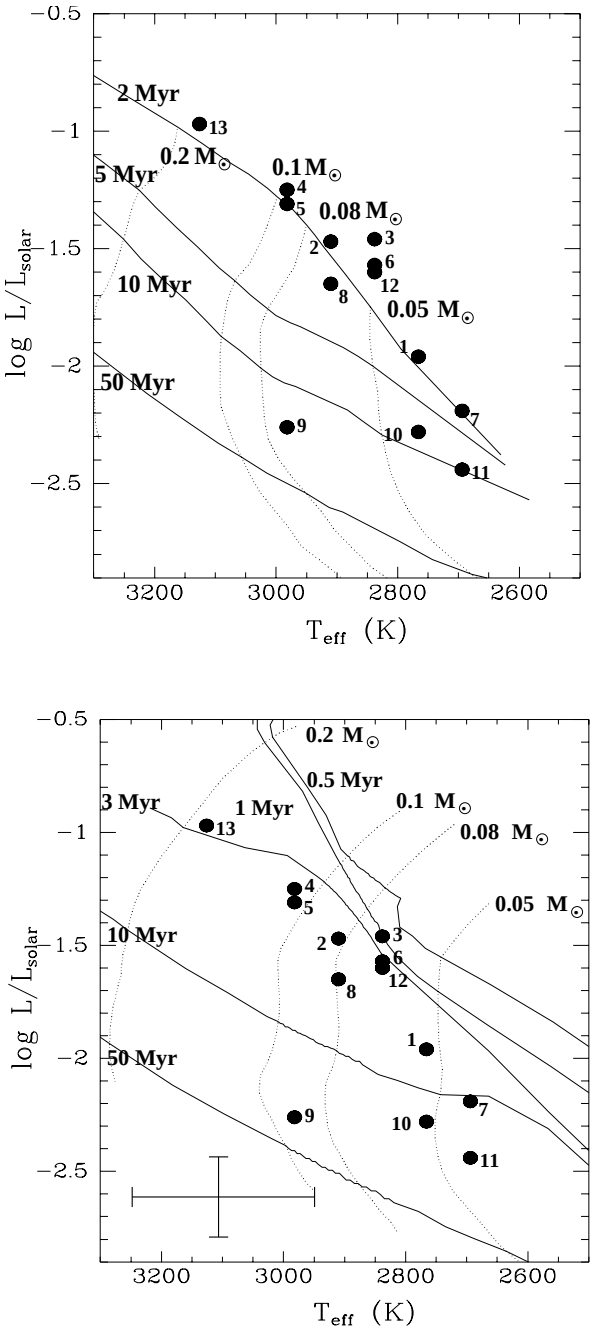

Figure 2.1: **HRD with bona fide and candidate brown dwarfs in Cha I.** From Comerón et al. (2000). Evolutionary tracks from Baraffe et al. (1998) (top) and Burrows et al. (1997) (bottom). All objects lie near or below the theoretical boundary between brown dwarfs and stars at $\sim$0.08 $M_\odot$. The additional object, Cha Hα 13, is an M5-type star found in the same survey.

Chapter 3

High-resolution spectroscopy (UVES/VLT)

Spectroscopy is one of the main observational tools for astronomers to gather detailed information about astronomical objects. Spectral features contain invaluable imprints from the regions where they emerge, such as element abundances, temperatures, gravities as well as radial and rotational velocities. Important progress was made in the last decade in stabilizing spectrographs and wavelength references allowing observers to achieve radial velocity precisions down to a few $\mathrm{m\,s^{-1}}$. This paved the way for the detection of the first extrasolar planets around stars in the last seven years by radial velocity surveys (cf. Sect. 1.1). With the combination of high-precision spectroscopy and large aperture telescopes of the 8 m to 10 m class, we are now capable of measuring radial and rotational velocities also for faint objects, like brown dwarfs. This is done within the framework of the presented thesis. First results have been published in Joergens & Guenther (2001).

Sect. 3.1 describes the acquisition and reduction of high-resolution UVES spectra for brown dwarfs and very low-mass stars in Cha I followed by a measurement of radial velocities in Sect. 3.2. Mean heliocentric radial velocities for individual objects are further exploited in Sect. 3.3 within the scope of a kinematic study of brown dwarfs and constraints for theories of the formation of brown dwarfs are derived. In Sect. 3.4 and 3.5 the measurements of projected rotational velocities $v \sin i$ based on line broadening and measurements of the equivalent width' of the lithium line are presented. An analysis of the time dependence of the radial velocities in the context of a search for substellar companions is presented in Sect. 3.6.

3.1 Data acquisition and analysis

Using the high-resolution UV-Visual Echelle Spectrograph (UVES) attached to the 8.2 m Kueyen telescope of the European Southern Observatory, high-resolution spectra of nine bona fide and candidate brown dwarfs (Cha Hα 1 to 8 and 12) as well as of three very low-mass mid-M-type T Tauri stars (B 34, CHXR 74 and Sz 23) in Cha I have been taken. UVES is a cross-dispersed echelle spectrograph (Dekker et al. 2000) operated at the Unit Telescope 2 of the Very Large Telescope (VLT) in Paranal, Chile, and is ideally suited for high precision spectroscopy of faint objects. The spectroscopic observations have been carried out in March, April and May 2000 as well as in January and February 2002. For each object at least two spectra separated by a few weeks have been obtained in order to monitor time dependence of the radial velocities. An observing log is given in the appendix in Table 6.1 and 6.2.

The observations have been performed with the red arm of the two-armed UVES spectrograph equipped with a mosaic of two CCDs. The mosaic is made of a $2\mathrm{K} \times 4\mathrm{K}$ EEV chip (pixel size $15\,\mu$m) for the blue part of the red arm and a MIT-LL CCD with a higher near-infrared quantum efficiency for the red part of the red arm. The wavelength regime from 6600 Å to 10400 Å was covered with a spectral resolution of $\lambda/\Delta\lambda = 40\,000$. A slit of $1''$ to $1.2''$ was used.

An echelle spectrograph contains two light dispersive elements, in the case of UVES this being two gratings: a high dispersion echelle grating cross-dispersed by a low dispersion grating. The cross-disperser grating determines the distance between the echelle orders. The result is a high-resolution, closely spaced array of side-by-side orders of large spectral coverage.

A standard CCD reduction of the two-dimensional UVES echelle frames, including bias correction, flat fielding and cosmic ray elimination, has been performed. Subsequently, one-dimensional spectra have been extracted, including subtraction of sky background light and finally the spectra have been wavelength calibrated using the echelle package of IRAF[1]. Details about individual reduction steps are given in the following.

1. **Cutting the mosaic frames**
   In a first step the two-dimensional frames containing the spectra obtained with the mosaic of the two CCDs have been cut into two pieces and handled separately in the following data reduction.

[1] IRAF is distributed by the National Optical Astronomy Observatories, which is operated by the Association of Universities for Research in Astronomy, Inc. (AURA) under cooperative agreement with the National Science Foundation.

2. **Bias correction**
   The *bias* is an offset voltage applied to the CCD, which has to be subtracted from all science and flat field frames. A master bias frame has been created by taking the median of several individual exposures with zero integration time and smoothing the result. The master bias has been subtracted from all science and flat field exposures in order to remove the electronic pedestal level of the CCD as well as any underlying bias structures.

3. **Flat field correction**
   Flat fielding is done by dividing the science spectra by a *flat field* in order to correct for small scale pixel-to-pixel variations caused by microscopic inhomogeneities of the CCD or dust particles. Flat fields are the response of the entire instrumentation (telescope, spectrograph, CCD detector) to the illumination with a light source with a flat (i.e. without spectral features) energy distribution. In addition to the pixel-to-pixel variations, they contain large scale intensity variations due to the blaze function of the echelle grating as well as the wavelength dependent sensitivity of the CCD. A master flat field frame has been created by taking the median of several spectra obtained by illumination with a flat field lamp. The master flat is normalized by fitting its intensity along the dispersion by a third order fit, while setting all points outside the order aperture to 1 and dividing the master flat by this fit. This procedure ensures that all large-scale structures are eliminated from the master flat. The flat field is, in addition to the correction of pixel-to-pixel variations of the science spectra, also used for the determination of the echelle order shape and the presence of bad columns on the detector.

4. **Cosmic ray elimination**
   A correction of *hot pixels* caused by high-energetic particles has been performed. Pixels deviating by more than a certain threshold, which depends on the noise of the image, are replaced by the mean of a given number of neighbouring pixels.

5. **One-dimensional extraction**
   The location of the echelle orders on the two-dimensional frames are determined by means of a flat field. The pixels containing the science spectra are traced and one-dimensional sums along the orders are extracted. Furthermore, in the procedure of one-dimensional extraction, the sky background is determined from specified lines below and above the spectrum and subtracted from it.

6. **Wavelength calibration**
   The wavelength calibration is done in a first step by the use of calibration spectra obtained with a Thorium-Argon lamp along with a Thorium-Argon

line list. General limits to this calibration are set by the non-simultaneous observation of science and calibration spectra, which results in slightly different illuminations of the spectrograph slit. In order to achieve a relatively high wavelength and therefore radial velocity precision, an additional correction by means of telluric lines has been applied (see Sect. 3.2).

3.2 Radial velocities

The determination of precise radial velocities requires the superposition of a wavelength reference on the stellar spectrum to ensure that the light beams of the source and the reference follow exactly the same path in the spectrograph. For high-precision radial velocity surveys for extrasolar planets often an Iodine gas absorption cell is used, which is put in front of the spectrograph and superimposes Iodine lines on the stellar spectrum in the blue part of the optical wavelength region. However, the Iodine cell cannot be used for spectroscopy of brown dwarfs since they are extremely red objects. A gas absorption cell for the red part of the optical regime or the infrared is not (yet) available. For the analysis of the UVES spectra, therefore telluric O_2 lines (B-band centered at 6880 Å) have been used as **wavelength reference**. They are produced in the Earth's atmosphere and are 'automatically' imposed on the stellar spectrum in the red regime. It has been shown that they are stable up to $\sim 20\,\mathrm{m\,s^{-1}}$ (Balthasar et al. 1982, Caccin et al. 1985). Fig. 3.1 displays a part of a spectrum of Cha Hα 4 featuring stellar TiO absorption bands, the lithium line as well as plenty of telluric lines.

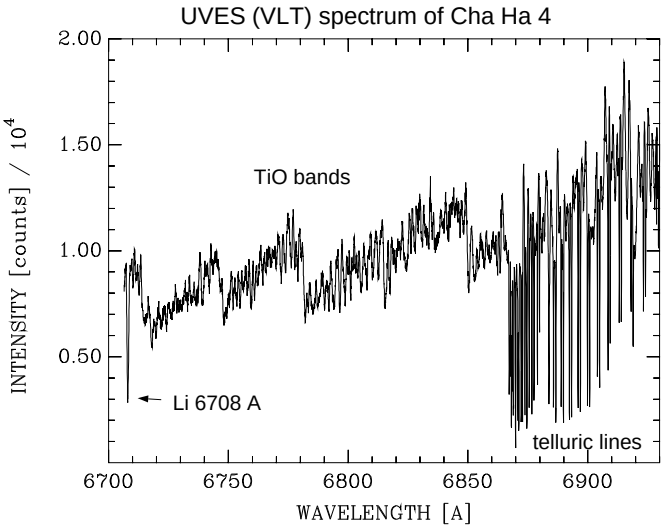

Figure 3.1: Small part of an UVES echelle spectrum of Cha Hα 4.

Radial velocities have been determined by a **cross-correlation** of plenty of stellar lines of the object spectra against a template spectrum and locating the correlation maximum. A mean UVES spectrum of the very low-mass M4.5-type star CHXR 74 served as template. The zero point of its velocity has been determined

Table 3.1: **Radial velocities for bona fide and candidate brown dwarfs in Cha I.** Given are the date of the observation, heliocentric Julian day (HJD) at the middle of the exposure, the measured radial velocity as well as the estimated error. The asterisk in the last column marks radial velocities based on the average of two single measurements (see Table 6.1 and 6.2 for the individual radial velocities). The errors for these are standard deviations.

Object	Date	HJD	RV $[\mathrm{km\,s^{-1}}]$	ΔRV $[\mathrm{km\,s^{-1}}]$
Cha Hα 1	2000 Apr 04	2451638.56395	16.167	0.53
	2000 Apr 24	2451658.57346	16.648	0.67
Cha Hα 2	2000 Apr 04	2451638.59431	16.015	0.50
	2000 Apr 24	2451658.60407	16.282	0.56
Cha Hα 3	2000 Apr 04	2451639.49340	14.357	0.45
	2000 Apr 24	2451658.61991	14.758	0.45
Cha Hα 4	2000 Mar 14	2451617.73646	14.909	0.38 *
	2000 Mar 24	2451627.80388	14.866	0.19 *
	2000 Mar 31	2451635.51085	14.773	0.14
	2000 Apr 23	2451658.52150	14.908	0.05 *
	2000 May 22	2451687.50595	14.830	0.08 *
	2002 Jan 17	2452291.78912	14.949	0.48 *
	2002 Jan 18	2452292.82508	14.754	0.12 *
	2002 Jan 24	2452298.70540	14.635	0.08 *
	2002 Feb 02	2452307.71979	15.064	0.39 *
	2002 Feb 04	2452309.74222	14.821	0.001 *
	2002 Feb 13	2452318.71915	14.985	0.07 *
Cha Hα 5	2000 Apr 05	2451639.51485	15.499	0.45
	2000 Apr 24	2451658.63522	15.446	0.42
Cha Hα 6	2000 Apr 05	2451639.58967	16.093	0.50
	2000 Apr 24	2451658.65099	16.652	0.50
Cha Hα 7	2000 Apr 05	2451639.55225	16.513	0.56
	2000 Apr 24	2451658.68756	17.664	0.56
Cha Hα 8	2000 Apr 05	2451639.61095	14.787	0.50
	2000 Apr 24	2451658.72597	14.935	0.50
Cha Hα 12	2000 Apr 05	2451639.63487	15.021	0.50
	2000 Apr 25	2451659.59469	13.905	0.53

by means of a fit to the prominent lithium line at 6708 Å. For the measurements of Doppler shifts of stellar features, appropriate wavelength regions have been selected, which are not affected by telluric lines, cosmetic defects of the CCD or fringes of the CCD in the near infrared.

Table 3.2: **Radial velocities for very low-mass T Tauri stars in Cha I.** Given are the date of the observation, heliocentric Julian day (HJD) at the middle of the exposure, the measured radial velocity RV as well as the estimated error. The asterisk in the last column marks radial velocities based on the average of two single measurements (see Table 6.1 and 6.2 for the individual radial velocities). The errors for these are standard deviations.

Object	Date	HJD	RV [km s^{-1}]	ΔRV [km s^{-1}]
B 34	2000 Mar 13	2451616.83205	15.795	0.09 *
	2000 Mar 25	2451628.61377	15.746	0.04
	2000 Mar 31	2451634.55482	15.749	0.09 *
	2000 Apr 23	2451657.53470	15.667	0.11 *
	2000 May 22	2451686.51384	15.814	0.13 *
CHXR 74	2000 Mar 13	2451616.78715	15.376	0.09 *
	2000 Mar 31	2451634.52092	14.499	0.05 *
	2000 Apr 22	2451656.51247	14.854	0.27 *
	2000 May 21	2451686.48261	14.276	0.06 *
Sz 23	2000 Mar 14	2451617.68093	14.652	0.04
	2000 Mar 25	2451628.66914	15.926	0.07
	2000 Mar 31	2451634.59142	15.564	0.13 *
	2000 Apr 22	2451657.49636	14.740	0.23 *
	2000 May 20	2451685.48812	15.233	0.08 *

A **heliocentric correction** has been applied to the observed radial velocities taking into account the diurnal, monthly and annual motion of the Earth due to the Earth's rotation, the motion of the Earth's center about the Earth-Moon barycenter as well as the motion of the Earth-Moon barycenter about the center of the Sun, respectively. Heliocentric radial velocities for individual spectra along with error estimates are given in Table 3.1 and 3.2.

A radial velocity **precision** between 80 m s^{-1} and 600 m s^{-1}, depending on the S/N of the individual spectra, was achieved (last column of Table 3.1 and 3.2). For several objects the radial velocity derived for one night is based on two consecutive single spectra providing two independent measurements (see Table 6.1 and 6.2 in the appendix for a detailed listing of radial velocities of individual spectra). This allows a solid estimation of the error based on the standard deviation for two such data points. Errors derived in that way are marked in Table 3.1 and 3.2 with an asterisk. These error measurements depend, as expected, linearly on the S/N of the spectra. This linear relationship is used in turn to estimate errors for radial velocities which are based on only one measurement per night. It should be noted, that the precision of the radial velocities is limited by the S/N of the spectra and

not by systematic effects. The relatively high precision that was achieved for the *relative* velocities does not apply to the **absolute velocities** due to additional uncertainties in the zero point of the template. An additional error of about $300\,\mathrm{m\,s^{-1}}$ is assumed for the absolute velocities.

Mean heliocentric radial velocities (Table 3.3) for each studied object are further exploited in Sect. 3.3 within the scope of a kinematic study of brown dwarfs. An analysis of the time dependence of the radial velocities in the context of a search for substellar companions is presented in Sect. 3.6.

3.3 Kinematics of brown dwarfs in Cha I

In this section, a kinematic study of the young bona fide and candidate brown dwarfs in Cha I is presented based on mean radial velocities measured from UVES spectra. The kinematics of this small homogenous group of brown dwarfs is compared to the kinematics of young very low-mas stars in the same region as well as to that of the surrounding molecular gas of the star forming cloud in which they are embedded. Based on this precise kinematic study of very young brown dwarfs constraints for theories of the formation of brown dwarfs are derived.

The mean radial velocities based on UVES spectra (Table 3.3) are consistent with radial velocities measured by Neuhäuser & Comerón (1999) within the given errors for Cha Hα 1, 3, 4, 5 and B 34. However, the values for Cha Hα 2, 7, 8, CHXR 74 and Sz 23 are discrepant by $1\,\sigma$ and the radial velocity for Cha Hα 6 by $2\,\sigma$. This may be a hint at long-term single-lined spectroscopic binaries. Cha Hα 12 was not observed by the other group.

3.3.1 Velocity dispersion of brown dwarfs

Neuhäuser & Comerón (1999) determined a mean radial velocity of $\sim$14.6 $\mathrm{km\,s^{-1}}$ and a total range of 11 $\mathrm{km\,s^{-1}}$ for Cha Hα 1 to 8 from medium resolution spectra. The measurements of precise radial velocities for Cha Hα 1 to 8 and Cha Hα 12 with UVES allow the study of the kinematics of these bona fide and candidate brown dwarfs with high accuracy. It was found that their radial velocities lie close together, only spanning a range of 2.6 $\mathrm{km\,s^{-1}}$. The mean radial velocity is 15.6 $\mathrm{km\,s^{-1}}$ and the radial velocity dispersion is 2.2 $\mathrm{km\,s^{-1}}$ (cf. Table 3.3 and Fig. 3.2).

3.3.2 Velocity dispersion of the molecular gas

The Cha Hα objects are located at the periphery of one of the six cloud cores (No. 5) in Cha I in a region with a relatively high density of young stellar objects. The mean radial velocity of the molecular gas of the Cha I cloud and also of the cloud core No. 5 is 15.3 km s^{-1} (Mizuno et al. 1999). The mean radial velocity of the studied brown dwarfs is consistent with this velocity of the gas and therefore with the objects being kinematic members of Cha I. Mizuno et al. (1999) determined the radial velocity dispersion of the gas of core No. 5 to 1.2 km s^{-1}. The brown dwarfs show a slightly larger radial velocity dispersion (2.2 km s^{-1}) than the surrounding molecular gas.

3.3.3 Velocity dispersion of T Tauri stars in Cha I

In the following, the radial velocity distribution of the bona fide and candidate brown dwarfs is compared with those of T Tauri stars. Radio observations by Mizuno et al. (1999) revealed that the three main clouds in the Chamaeleon star forming region differ to a large extent in their star formation properties and also the radial velocities of the molecular gas vary between the clouds (differences up to 3.6 km^{-1}), whereas they are relatively constant ($\sim$1 km s^{-1}) within each single cloud. Therefore it is reasonable to compare the kinematics of the brown dwarfs

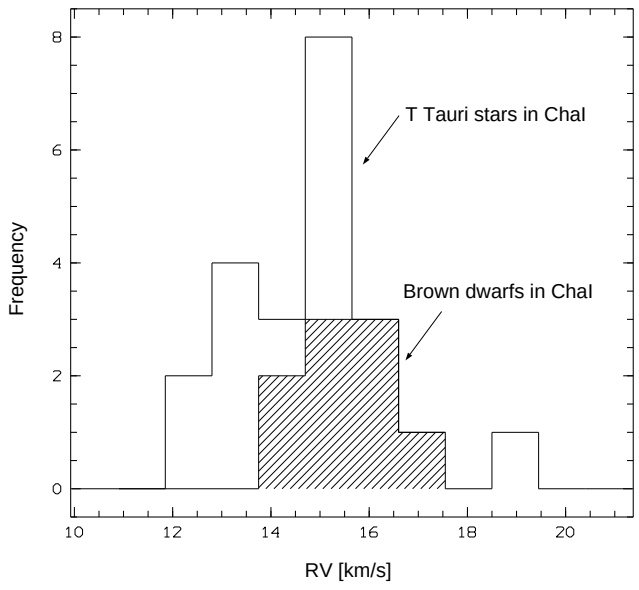

Figure 3.2: **Distribution of mean radial velocities** for nine bona fide and candidate brown dwarfs (hashed) and for 22 T Tauri stars in Cha I.

Table 3.3: **Mean radial and rotational velocities for brown dwarfs and very low-mass stars in Cha I.** Parameters derived from UVES spectra: mean heliocentric radial velocity <RV>, projected rotational velocity $v \sin i$ and equivalent width EW of lithium (6708 Å). <RV> is the weighted mean of the individual values (Table 3.1, 3.2), the given error is the standard deviation of the individual values plus 300 m s^{-1} for the error in the zero offset. Last columns: (sub)stellar radii and upper limits for rotational periods.

object	<RV> [km s^{-1}]	$v \sin i$ [km s^{-1}]	EW(Li) [Å]	$R_\star$ [$R_\odot$]	P_{max} [d]
Cha Hα 1	16.35± 0.65	7.6±2.2	0.14 ±0.10	0.46	3.1
Cha Hα 2	16.13± 0.49	12.8±1.2	0.30 ±0.08	0.73	2.9
Cha Hα 3	14.56± 0.58	21.0±1.6	0.26 ±0.08	0.77	1.9
Cha Hα 4	14.85± 0.42	18.0±2.3	0.46 ±0.11	0.89	2.5
Cha Hα 5	15.47± 0.34	15.4±1.8	0.44 ±0.10	0.83	2.7
Cha Hα 6	16.37± 0.70	13.0±2.8	0.32 ±0.08	0.68	2.6
Cha Hα 7	17.09± 1.11	≤ 10	≤ 0.09	0.37	–
Cha Hα 8	14.86± 0.40	15.5±2.6	0.33 ±0.15	0.59	1.9
Cha Hα 12	14.50± 1.09	25.7±2.6	0.37 ±0.10	0.66	1.3
B 34 (CHXR 76)	15.75± 0.36	15.2±1.9	0.60 ±0.13	0.93	3.1
CHXR 74 (B 27)	14.56± 0.83	14.1±1.6	0.63 ±0.04	1.36	4.9
Sz 23	15.03± 0.88	17.3±3.4	0.31 ±0.08	0.72	2.1

in Cha I with those of T Tauri stars also confined to the Cha I star forming cloud.

Radial velocities of T Tauri stars in Cha I have been measured by Dubath et al. (1996), Covino et al. (1997), Neuhäuser & Comerón (1999) and in the scope of the presented work and are listed in Table 3.4. Furthermore, unpublished radial velocities of T Tauri stars based on FEROS spectra have been included (Guenther et al., in prep.). The T Tauri stars have radial velocities in the range of [12.5...19.0 km s^{-1}] with a mean radial velocity of 14.8 km s^{-1} and a dispersion of 3.6 km s^{-1} (cf. Fig. 3.2).

The mean radial velocity of the T Tauri stars matches very well the ones of the bona fide and candidate brown dwarfs in Cha I, whereas the dispersion as well as the total range of radial velocities of the T Tauri stars is significantly larger than the ones of the brown dwarfs. Stellar activity of T Tauri stars probably account for this discrepancy. It has been shown that T Tauri stars exhibit a *radial velocity noise* of the order of $\sim$2 km s^{-1} (Guenther et al. 2000) due to magnetically induced surface features, which cause a shifting of the photocenter of the visible stellar

Table 3.4: **List of T Tauri stars in Cha I with known radial velocities** with a precision of 2 km s^{-1} or better from: [1] Dubath et al. (1996), [2] Covino et al. (1997), [3] Guenther et al.,in prep. and from UVES observations (B 34, CHXR 74, Sz 23: see Table 3.3). For objects with two references for the radial velocity, the weighted average as well as the standard deviation of the two values are given. For Sz 41 also $v \sin i$ is the weighted average of two different measurements.

object	other names	RV [km s^{-1}]	$v \sin i$ [km s^{-1}]
Sz 4[1]		16.5±1.3	16.6±3.3
Sz 6[1]	CR Cha, CHXR 6, RXJ1059.1-7701	14.9±0.8	38.0±1.5
Sz 15[1]	GSC09414-00267	17.2±0.6	4.9±7.9
Sz 19[1]	DI Cha, CHXR 23, Hen3-593, HIP54365	13.5±0.6	35.7±1.1
Sz 20[1]	VV Cha, CHXR 24	15.4±1.3	23.9±2.7
Sz 41[1,2]	CHXR 50, RXJ1112.7-7637	14.0±2.0	30.5±1.9
RXJ1109.4-7627[2]	CHXR 37	13.1±2.0	14.5±3
B 33[2]	CHXR 25	13.0±2.0	–
F 34[2]		14.0±2.0	55±3
RXJ1111.7-7620[2]	CHX18N	19.0±2.0	23±3
CS Cha[1,3]	Sz 9, CHXR 10, B 10, RXJ1102.5-7733	14.8±0.1	15.2±1.5
CT Cha[1,3]	Sz 11, CHXR 13	15.1±0.4	16.2±2.3
CV Cha[1,3]	Sz 42, CHXR 51, RXJ1112.5-7644	15.1±0.5	27.2±17.7
SX Cha[3]	Sz 2	13.4±0.9	–
SY Cha[3]	Sz 3, CHXR 1	12.7±0.1	–
TW Cha[3]	Sz 5, CHXR 5, B 5, Hen3-546	15.7±1.2	–
VW Cha[3]	Sz 24, CHXR 31, B 40, RXJ1108.1-7742 Hen3-598	15.1±0.1	–
VZ Cha[3]	Sz 31, CHXR 39, Hen3-605	14.7	–
WY Cha[1,3]	Sz 36, CHXR 46, RXJ1109.9-7629b	12.5±0.6	$7.5\ ^{+2.7}_{-4.8}$

disk and therefore mimic a radial velocity variation. Moreover it may also play a role that the brown dwarfs and brown dwarf candidates are all situated in a small area at the periphery of one cloud core whereas the T Tauri stars are distributed over the whole Cha I region. The radial velocities of the six cloud cores within Cha I differ by ±0.25 km s^{-1} (Mizuno et al. 1999).

3.3.4 Constraints for formation theories

It is still unknown how brown dwarfs form (Sect. 1.2). Recently, it has been proposed that brown dwarfs are formed due to the ejection of protostars in the early accretion phase, which are thenceforward cut off from the gas reservoir and cannot accrete to stellar masses (Reipurth & Clarke 2001).

The presented kinematic study indicates that the radial velocity dispersion of the very young bona fide and candidate brown dwarfs in Cha I is relatively small. This gives suggestive evidence that there is no run-away brown dwarf among them. It cannot be ruled out that some of them have a larger three-dimensional velocity dispersion since radial velocities are tracing only space motions in one dimension, namely in the line-of-sight. However, the studied brown dwarfs in Cha I (age: 1–5 Myr) occupy a field of less than $12' \times 12'$ at a distance of 160 pc. Brown dwarfs born within this field and ejected during the early accretion phase in directions with a significant fraction perpendicular to the line-of-sight, would have flown out of the field a long time ago. This is the case even for the smallest ejection velocities of $2\,\mathrm{km\,s^{-1}}$ calculated by theorists (Bate et al. 2002, Sterzik & Durisen 2002). Therefore, the measurement of radial velocities is the very method to test if objects born in the field have significantly high velocities due to dynamical interactions during their formation process.

Very recent dynamical calculations (Bate et al. 2002, Sterzik & Durisen 2002) hint at rather small ejection velocities, suggesting the possibility that the imprint of the ejection in the kinematics might not be an observable effect. Calculations of Bate et al. (2002) yield to a velocity dispersion of ejected brown dwarfs of $2\,\mathrm{km\,s^{-1}}$ in three-dimensions and $1.2\,\mathrm{km\,s^{-1}}$ in one-dimension. Sterzik & Durisen (2002) find about the same dispersion. On the other hand, they predict that 10% of the brown dwarfs have a larger velocity than $5\,\mathrm{km\,s^{-1}}$ due to dynamical interactions. The velocities of the bona fide and candidate brown dwarfs in Cha I cover a total range of only $2.6\,\mathrm{km\,s^{-1}}$. Therefore, it is concluded that the ejection-model for the formation of brown dwarfs is not a likely formation mechanism for the brown dwarfs in Cha I.

Some or all of the brown dwarfs may still have been 'ejected' with less than escape velocity into an extended orbit around another component of a multiple system. None of the studied brown dwarfs is closer to a known T Tauri star than 4600 AU, i.e. it is unlikely that one of them is still bound to a star. There is still the possibility that the parent star itself was later ejected with escape velocity and left an unbound brown dwarf.

3.4 Projected rotational velocities $v \sin i$

Projected rotational velocities have been measured based on the line broadening of spectral features. The telluric lines have been used for the determination of the instrumental profile of the spectrograph and a solar-like center-to-limb variation has been assumed. The results are given in Table 3.3. The measured $v \sin i$ values for the bona fide and candidate brown dwarfs in Cha I range from $8\,\mathrm{km\,s^{-1}}$ to $26\,\mathrm{km\,s^{-1}}$. For Cha Hα 7 only an upper limit of $v \sin i$ was determined due to a low S/N of its spectra. These very young bona fide and candidate brown dwarfs are therefore moderately fast rotators in contrast to the very fast rotating old brown dwarfs, which have rotational velocities up to $60\,\mathrm{km\,s^{-1}}$ (e.g. Basri & Marcy 1995, Martín et al 1997, Tinney & Reid 1998, Basri et al. 2000).

Projected rotational velocities $v \sin i$ are lower limits of the rotational velocity v since the inclination i of the rotation axis remains unknown. Based on $v \sin i$ and the radius of the object a spectroscopic period $P_{v \sin i}$, which is an upper limit of the rotational period, can be derived:

$$P_{v \sin i}[\mathrm{d}] = 50.6145 \frac{R[\mathrm{R}_\odot]}{(v \sin i)[\mathrm{km\,s^{-1}}]} \quad .$$

In order to derive $P_{v \sin i}$ for the brown dwarfs and very low-mass stars in Cha I, their radii have been estimated by means of the Stefan-Boltzmann law from bolometric luminosities and effective temperatures given by Comerón et al. (1999) and Comerón et al. (2000) for the T Tauri stars and the bona fide and candidate brown

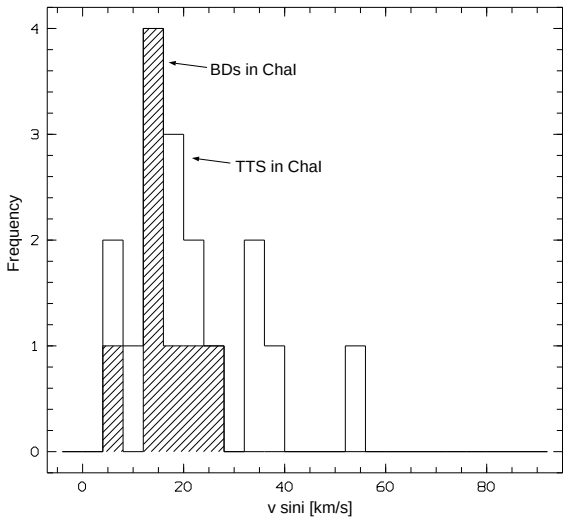

Figure 3.3: **Distribution of $v \sin i$** for brown dwarfs (hashed) and T Tauri stars in Cha I.

dwarfs, respectively. The approximate upper limits for the rotational periods of the bona fide and candidate brown dwarfs range between one and three days (Table 3.3). A further exploration of the rotational properties of the target brown dwarfs was done by a photometric monitoring campaign (Sect. 5), which yielded the determination of rotational periods for three brown dwarf candidates.

Fig. 3.3 shows the $v\,sini$ distribution of brown dwarfs in comparison with that of T Tauri stars in Cha I (see Table 3.4 and 3.3 for $v \sin i$ values of T Tauri stars). Both distributions peak at a $v \sin i$ of 17 to 21 $\mathrm{km\,s^{-1}}$, indicating that there is no crucial difference between the rotational velocities of the studied very young brown dwarfs and that of T Tauri stars.

3.5 Lithium equivalent width

All brown dwarfs and low-mass stars observed with UVES show lithium absorption at 6708 Å. The measured equivalent width is given in Table 3.3 for all objects. For Cha Hα 7 only an upper limit of the lithium equivalent width was determined due to a low S/N. For eight of the twelve bona fide and candidate brown dwarfs in Cha I, lithium detection and equivalent width measurements (with moderate S/N) have been reported by Neuhäuser & Comerón (1999). The UVES observations allow the addition of the lithium detection of Cha Hα 12.

The lithium detection of objects in the star forming region Cha I does not automatically imply their substellar nature since stars at this age (a few million years) have not yet depleted their primordial lithium and can therefore not be distinguished from brown dwarfs, which will never deplete their lithium, as described in Sect. 1.6.1. However, for objects with spectral type M7 and later, the lithium detection *is* a solid indication for their substellar nature: Either the object is young (≤ 100 Myr), then a spectral type of M7 or later implies substellar nature or the object is old (> 100 Myr), then the lithium detection guaranties substellarity. On the basis of these arguments, Cha Hα 1, 7, 10 and 11 (spectral type M7.5–M8) are bona fide brown dwarfs and Cha Hα 3, 6 and 12 (M7) are brown dwarf candidates, taking an error of 0.5 sub-types in the spectral types into account.

3.6 Radial velocity survey for substellar companions

Up to now, only two spectroscopic brown dwarf binaries are known and no planet orbiting a brown dwarf (cf. Sect. 1.7). Binaries and higher order multiple systems are of great interest since they provide important clues to their formation history on one hand, and since they allow constraints of their masses on the other hand.

The orbital motion of close binaries can be monitored by means of spectroscopic observations of their radial velocities. Fig 3.4 illustrates the orbital motion of a high-mass primary due to an unseen low-mass companion. In the case of the sketch, the orbiting object is a planet and causes a periodic wobble of the host star. As the star is moving towards the observer, spectral lines are shifted to shorter wavelength (blue-shift) and as the star is moving away from the observer the spectral lines are shifted to longer wavelength (red-shift). The variation of the radial velocity $v_{\rm rad}$ due to this *Doppler effect* causes a shifting of the wavelength of spectral lines of:

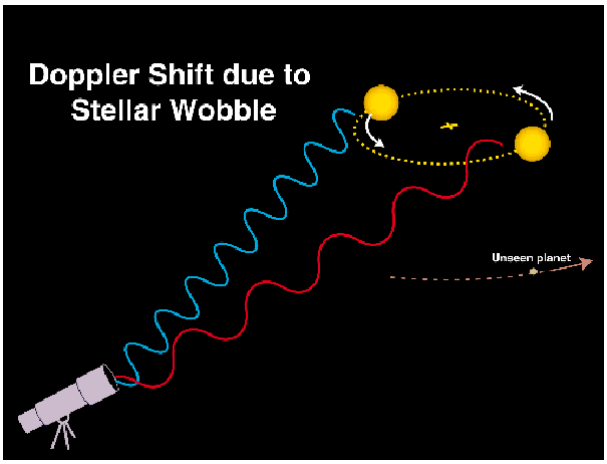

Figure 3.4: **Illustration of the Dopplershift caused by an unseen planet.** See text for details.

$$\frac{\Delta\lambda}{\lambda} = \frac{v_{\rm rad}}{c} \tag{3.1}$$

where c is the speed of light.

The observed radial velocity due to orbital motion in a binary system is given by the following equation

$$V_{\rm rad} = \frac{2\pi a \sin i}{P(1-e^2)^{1/2}}[cos(\theta+\omega) + e\cos\omega] \tag{3.2}$$

(a semimajor axis, i inclination, P orbital period, e eccentricity), where $K = (2\pi a \sin i)/[P(1-e^2)^{1/2}]$ is the *semiamplitude* of the velocity curve. For a *double-lined* spectroscopic binary, where the velocity curves of both components can be determined from observations, i.e. K_1 and K_2, the minimum masses for

Table 3.5: **Upper mass limits for companions around brown dwarfs and very low-mass stars in Cha I.** Based on the scatter of the radial velocity an upper limit for the semiamplitude K_1 and for the minimum mass $M_2 \sin i$ have been derived. A semimajor axis of 0.1 AU was assumed for all objects but Sz 23, for which 0.3 AU were applied. The primary masses for the objects are from Comerón et al. (1999, 2000).

object	max. K_1 [km s^{-1}]	max. $M_2 \sin i$ [M_{Jup}]
Cha Hα 1	0.24	0.6
Cha Hα 2	0.13	0.4
Cha Hα 3	0.20	0.6
Cha Hα 4	0.22	0.8
Cha Hα 5	0.03	0.1
Cha Hα 6	0.28	0.6
Cha Hα 7	0.58	1.1
Cha Hα 8	0.07	0.3
Cha Hα 12	0.56	1.5
B 34	0.07	0.3
CHXR 74	0.55	2.6
Sz 23	0.64	7

both components, $M_1 \sin i$ and $M_2 \sin i$ can be derived. For *single-lined binaries*, only the velocity curve of the primary, and hence only K_1 can be determined. This allows the determination of the quantity known as the *mass function*:

$$f(M) = \frac{M_2^3 \sin^3 i}{(M_1 + M_2)^2} = 1.04 \times 10^{-7} (1 - e^2)^{3/2} K_1^3 P \quad M_\odot \tag{3.3}$$

In order to search for spectroscopic (brown dwarf or planetary) companions to the bona fide and candidate brown dwarfs in Cha I as well as to the three very low-mass T Tauri stars, time sequences of radial velocity measurements based on UVES observations were performed. For each of the objects Cha Hα 1, 2, 3, 5, 6, 7, 8 and 12 spectra have been taken in two nights separated by a few weeks. For Cha Hα 4, B 34, CHXR 74 and Sz 23 between four and eleven spectra have been taken, separated by weeks to years. The measured radial velocities along with the heliocentric Julian date can be found in Table 3.1 and 3.2. No clear indications for companions have been found.

An upper limit for the semiamplitude K_1 of a variation caused by a hypothetical companion was determined for each object by assuming that the total variability amplitude was recorded. Subsequently, upper mass limits for the hypothetical companions have been estimated based on K_1 by applying Eq. 3.3 and Kepler's

third law. For this calculation an orbital separation of 0.1 AU was assumed for all but Sz 23, for which 0.3 AU were applied taking into account its higher mass. Primary masses M_1 from Comerón et al. (1999, 2000) have been used. Furthermore, circular orbits and an inclination of 90° were assumed. The assumption of $i = 90°$ means that the derived mass limits are upper limits for the minimum masses $M_2 \sin i$. The results are listed in Table 3.5.

The radial velocities for Cha Hα 1, 2, 3, 5, 6, 7, 8 and 12 are constant within the measurements uncertainties. Fig. 3.5 displays radial velocity vs. time for these objects. The upper limits for the semiamplitude range between 30 m s^{-1} for Cha Hα 5 and 600 m s^{-1} for Cha Hα 7 and 12. The deduced upper limits for the lower mass limits $M_2 \sin i$ range between a tenth of a Jupiter mass (Cha Hα 5) and 1–2 Jupiter masses (Cha Hα 7 and 12).

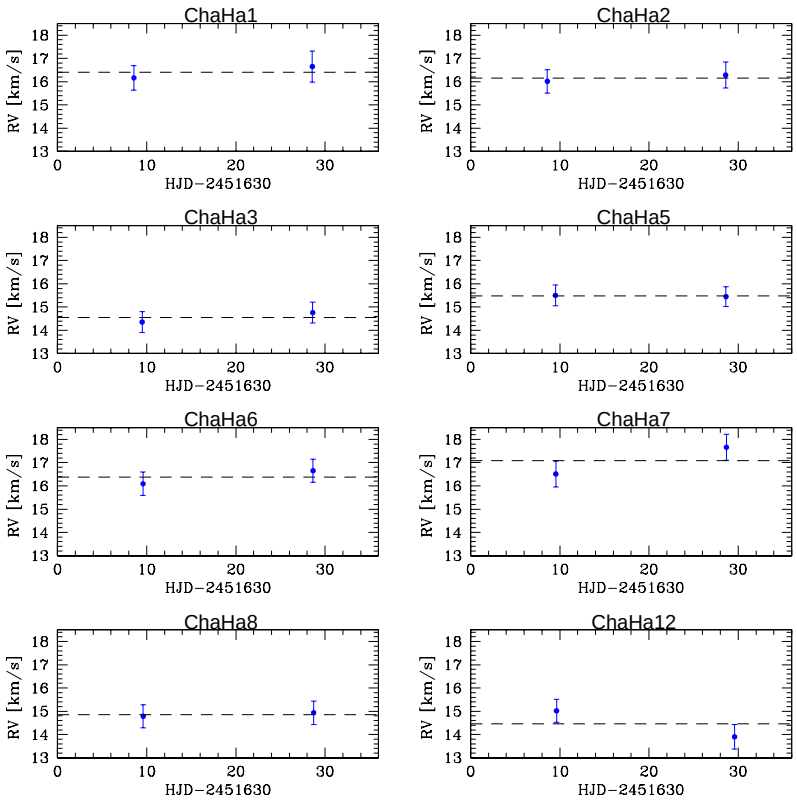

Figure 3.5: **Radial velocity vs. time for Cha Hα 1, 2, 3, 5, 6, 7, 8 and 12.** radial velocity measurements based on high-resolution spectra obtained with UVES at the VLT. Error bars indicate 1 σ errors. The mean radial velocity is marked with a dashed line.

Radial velocity time series for Cha Hα 4, B 34, CHXR 74 and Sz 23 are displayed in Fig. 3.6 and 3.7. B 34 shows a very constant radial velocity with a scatter of smaller than 150 m s^{-1} over a total time basis of 70 days. This puts the upper limit for the semiamplitude for a companion to 74 m s^{-1} and the upper limit for the mass $M_2 \sin i$ to 0.3 M_{Jup}. Cha Hα 4, CHXR 74 and Sz 23 show small but significant variations of their radial velocity, which correspond to companion masses $M_2 \sin i$ of 0.8 M_{Jup}, 2.6 M_{Jup} and 7 M_{Jup}, respectively.

In summary, no evidence for brown dwarf companions or giant planets ($\gtrsim 1\,M_{Jup}$) to the studied sample of bona fide and candidate brown dwarfs has been found. These results suggest that binaries among brown dwarfs in Cha I are rather rare. On the other hand, there are hints of significant radial velocity variations of Cha Hα 4, CHXR 74 and Sz 23. Assuming that they are caused by orbiting companions, they correspond to minimum masses $M_2 \sin i$ of 0.8 M_{Jup}, 2.6 M_{Jup} and 7 M_{Jup}, respectively.

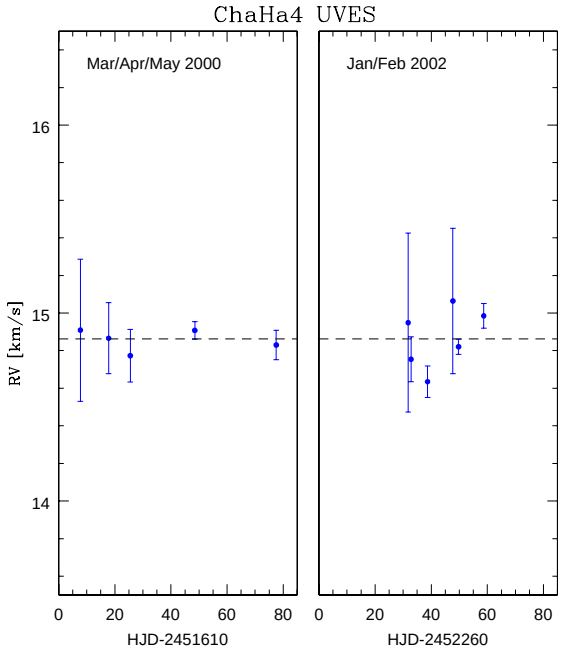

Figure 3.6: **Radial velocity vs. time for Cha Hα 4.** Radial velocity measurements are based on high-resolution spectra obtained with UVES at the VLT. Error bars indicate 1 σ errors.

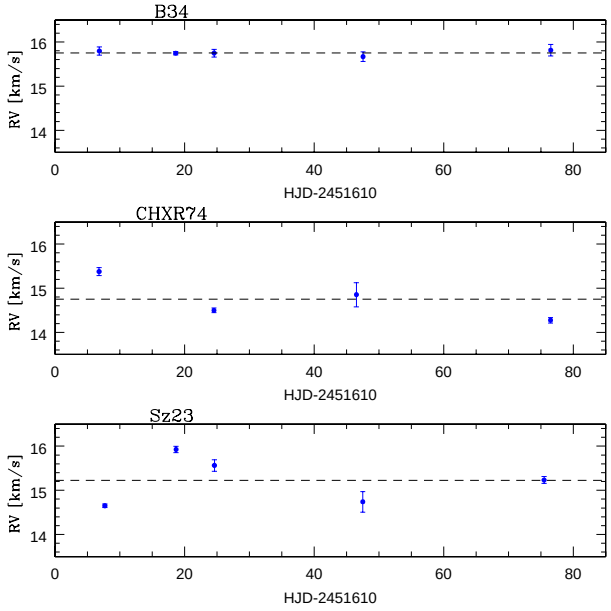

Figure 3.7: **Radial velocity vs. time for B 34, CHXR 74 and Sz 23.** Radial velocity measurements are based on high-resolution spectra obtained with UVES at the VLT. Error bars indicate 1 σ errors.

Chapter 4

High-resolution imaging (HST/VLT/NTT)

The radial velocity survey presented in the last chapter of the bona fide and candidate brown dwarfs Cha Hα 1–12, is sensitive to close companions at separations of 2–3 AU at maximum. A complementary search for wide visual companions was performed by means of space- and ground-based high-resolution images. A direct imaging campaign was carried out with the Wide Field Planetary Camera (WFPC2) on board the Hubble Space Telescope (HST) as well as with the ground-based instrument Son of Isaac (SofI) at the New Technology Telescope (NTT) at ESO. Furthermore, images obtained by Comerón et al. (2000) with the FOcal Reducer/low dispersion Spectrograph (FORS1) at the Very Large Telescope (VLT) were retrieved from the public VLT data archive and reanalysed. Some of the data presented in this chapter have been published in Neuhäuser, Brandner, Alves, Joergens et al. (2002a) and Joergens et al. (2001).

4.1 HST observations and data reduction

Deep images in the R and I band as well as in the Hα filter have been obtained with the HST Wide Field Planetary Camera No. 2 (WFPC2) in eight HST orbits in 2000 and 2001. Images have been taken of Cha Hα 1–5 and Cha Hα 7–12. Observations of Cha Hα 6 were not possible due to missing guide stars. The observing log of the HST observations is given in Table 4.1.

The HST observations were performed in the optical wavelength range instead of the infrared because the Near-Infrared Camera NICMOS on board HST was not available in 2000 and 2001. Observations in the Hα filter were carried out in order to detect faint Hα emission sources not detected in previous Hα surveys (Comerón

Table 4.1: **Observing log of HST observations.** Remarks: There are no other (archived or scheduled) HST observations with any of the targets in the field-of-view (as of Sept. 2001). (**) The observations in the I filter failed due to technical problems, hence no data in I. (***) Cha Hα 8 and a few of its companion candidates were also in the field-of-view of these observations, namely at the edge of chip WF2.

Object in Cha I	filter	exposure [seconds]	JD date
Cha Hα 1 & 7	F656N (Hα)	2 × 500	2451952
	F675W (R)	2 × 100	12 Feb 2001
	F814W (I)	2 × 100	
Cha Hα 2 & 9	F656N (Hα)	2 × 500	2451842
	F675W (R)	2 × 100	25 Oct 2000
	F814W (I)	2 × 100 (**)	
Cha Hα 3	F656N (Hα)	2 × 700	2451733
	F675W (R)	300 + 80	8 Jul 2000
	F814W (I)	160 + 40	
Cha Hα 4,10,11 & 8 (***)	F656N (Hα)	4 × 500	2451783
	F675W (R)	2×(300+100)	27 Aug 2000
	F814W (I)	2×(300+100)	
Cha Hα 5	F656N (Hα)	2 × 700	2451778
	F675W (R)	300 + 80	22 Aug 2000
	F814W (I)	160 + 40	
Cha Hα 8	F656N (Hα)	2 × 700	2451752
	F675W (R)	300 + 80	27 Jul 2000
	F814W (I)	160 + 40	
Cha Hα 12	F656N (Hα)	2×(260+70)	2451914
	F675W (R)	2×(10+40)	05 Jan 2001
	F814W (I)	2×(10+40)	

et al. 1999, 2000), which would be good candidates for hitherto unknown brown dwarfs.

The WFPC2 contains four cameras, each containing a 800×800 pixel Loral CCD. Three cameras (WF2, WF3, WF4) operate at an **image scale** of 0.1″ per pixel and comprise the Wide Field Camera (WF) with an L-shaped field-of-view. The fourth camera operates at 0.046″ per pixel and is referred to as the Planetary Camera (PC). Whenever possible, several objects have been placed in one field-of-view and observed with the WF chips in order to maximize the observing efficiency. Isolated objects have been observed with the PC chip, which has a smaller field-of-view but a better angular resolution.

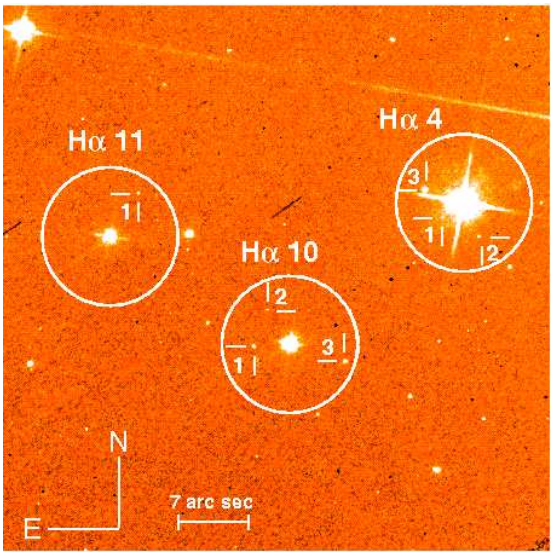

Figure 4.1: **HST I band image of Cha Hα 4, 10, and 11** obtained with the WF4 chip on 27 Aug 2000. The exposure time is 800 sec. The circles around the three main targets each have radii of 7″.

Data reduction was performed with the IRAF package *stsdas* written for the analysis of HST data. All exposures were split into two to four to facilitate cosmic ray rejection. After corrections for cosmic rays with *crrej*, the split exposures were added up. The contribution from the sky background was very small ($\sim$ 1 count) in most images because the targets are located in the dark cloud Cha I, which shields most background objects. Near the bright (V=8.5 mag) A0e star HD 97048 it was slightly enhanced.

Source detection was done by visual inspection of the images. Any faint, non-extended object within a few arc sec to one of the targets, can be either a real companion or an unrelated fore- or background object. However, an unambiguous confirmation of the companionship can be done only by means of additional observations:

1. With spectroscopy of a companion candidate, it can be checked if it is as cool as expected from the magnitude difference to the primary.
2. With follow-up deep imaging at different epochs, it can be tested if the primary and the companion candidate are a common proper motion pair and therefore most certainly physically bound.

Without these follow-up observations, a first check of the companionship was done by examination of the colors of the candidates (Sect. 4.3). Somewhat arbitrarily, a maximum separation between a primary and a potential companion of

about 1000 AU was assumed, which corresponds to about 7″ at the distance of Cha I. All non-extended, faint objects found within a radius of 7″ to one of the Cha Hα targets are regarded henceforth as *companion candidates*. They are listed in Table 4.2 labeled with the name of their primary and a cc number. For example, Cha Hα 4/cc 1 refers to the companion candidate No. 1 around Cha Hα 4. Faint objects outside 7″ are considered as unrelated objects located most likely in the background of Cha I.

For Cha Hα 4, 8, 10 and 11, several **companion candidates** were detected within a radius of 7″. Fig. 4.1 shows the HST I band image of Cha Hα 4, 10, 11 as an example. HST images of Cha Hα 5 (Fig. 4.2) display one companion candidate at a separation of 1.5″ (cf. also Sect. 4.4). Furthermore, HST images of Cha Hα 2 (Fig. 4.8) reveal an elongation of the primary hinting at a binary system as discussed in Sect. 4.5.

Aperture photometry was performed for all companion candidates (detected by visual inspection) with a 0.5″ radius and a source-free background field annulus located around the measured object. The counts were transformed to magnitudes m according to the HST data reduction manual[1] by:

$$m[mag] = -2.5 \cdot \log(DN/exp) + ZP - 0.1 \tag{4.1}$$

with DN the number of counts, exp the exposure time in seconds, and ZP the zero point of the magnitude scale. 0.1 mag is subtracted in order to transform from the 0.5″ radius to the infinite aperture. In addition, a correction for the charge-transfer-efficiency (CTE) loss was done according to Whitmore et al. (1999). The CTE correction is especially important for weak sources such as the brown dwarf companion candidates.

The **magnitudes** determined in this way are given in Table 4.4. The R and I magnitudes (Vega system) of Cha Hα 1 to 12 agree well ($\pm$0.1 mag) with previously determined ground-based R and I magnitudes (Cousins bands) of the objects (Comerón et al. 2000).

The HST Hα magnitudes correlate with previous ground-based measurements of the Hα equivalent width (Comerón et al. 2000) within a certain error range. This indicates that they are basically consistent with them and that the **Hα emission** of the objects are variable, which is not unexpected for such young objects. In the last column of Table 4.4, equivalent width measurements of Hα from Comerón et al. (1999, 2000) and Neuhäuser & Comerón (1999) are listed, which also show that the Hα emission of the objects is rather variable.

The achieved **dynamic range** of the observations, i.e. the observable magnitude difference between a primary and its companion candidate, was determined for

[1] http://www.stsci.edu/documents/dhb/web

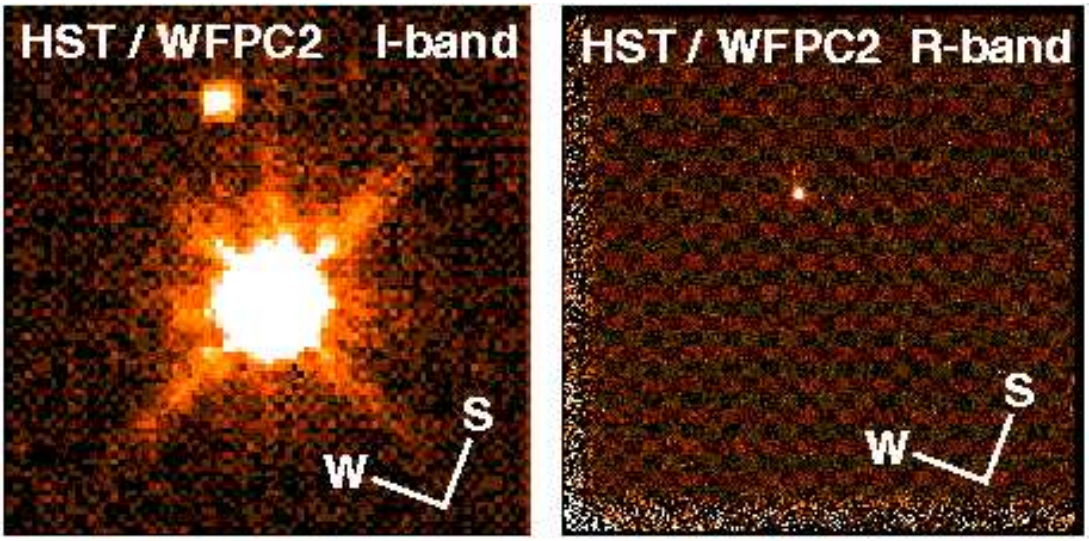

Figure 4.2: **HST R and I band images of Cha Hα 5.** Left panel: I band image ($4'' \times 4''$ field). A companion candidate $1.5''$ southwest of Cha Hα 5 is detected. Right panel: R band image with the whole PC field ($\sim 15'' \times 15''$), where no objects other than the primary and one companion candidate are detected. Also in the I and Hα images taken with the HST, no other objects are detected.

the deepest images obtained with each chip. For the PC chip it was determined based on I band images of Cha Hα 5 and 8. The dynamic range achieved with the WF chips was determined based on the longest exposures of Cha Hα 4, 10 and 11 (WF4) and Cha Hα 8 (WF2). The dynamic range for each companion separation is given by the flux ratio between a primary and the flux being 3σ above the background level at this separation. For example, the presented PC observations are able to detect an object which is 10 mag fainter than its primary (i.e. log flux ratio is -4) and located at a distant of at least $2''$ from the primary.

The mean brightness of the primaries Cha Hα1–12 is 16.0 mag in the I band. Thus, with the presented PC observations, one is capable of detecting a companion as faint as 26 mag (in I band) at $2''$ separation. In order to translate these magnitude limits into lower limits of detectable companion masses, a comparison with theoretical models has to be done. Assuming a color index ($I-K_s$) of ~ 4.5 mag for an L- or T-dwarf, a magnitude limit of 26 mag in the I band corresponds to a limit of 21.5 mag in the K_s band. This K_s magnitude along with a bolometric correction of $B.C._K$=2 mag (as for Gl 229 B, Leggett et al. 1999) corresponds to a companion mass of 1 M_{Jup} according to models by Burrows et al. (1997) for the distance and age of the targets. Therefore, the presented PC observations allow the detection of a 1 M_{Jup} companion at $2''$ around a primary with an I band magnitude of 16 mag.

Table 4.2: **List of wide companion candidates found in HST images** sorted by increasing separations up to 7″. Object designations are the positions for the epoch J2000.0. *cc* denotes *c*ompanion *c*andidate. The offsets (typically better than ±0.1″) of the companion candidates are given with respect to the primary. Spectral types for the primaries are from Comerón et al. (2000).

Object designation	other name	HST chip	separation [″] $\Delta\alpha$	$\Delta\delta$
110717.0-773454	Cha Hα 1	WF4	primary	M7.5
110743.0-773359	Cha Hα 2	WF4	primary	M6.5
110752.9-773656	Cha Hα 3	PC	primary	M7
110819.6-773917	Cha Hα 4	WF4	primary	M6
110819.7-773918	Hα 4/cc 1	WF4	2.0 E	1.3 S
110819.5-773920	Hα 4/cc 2	WF4	1.4 W	3.3 S
110819.8-773918	Hα 4/cc 3	WF4	3.5 E	1.3 N
110825.6-774146	Cha Hα 5	PC	primary	M6
110825.5-774147	Hα 5/cc 1	PC	1.0 W	1.1 S
110840.2-773417	Cha Hα 6	not observed		M7
110738.4-773530	Cha Hα 7	WF2	primary	M8
110747.8-774008	Cha Hα 8	PC	primary	M6.5
110747.9-774007	Hα 8/cc 1	WF2	1.4 E	1.3 N
110747.8-774010	Hα 8/cc 2	WF2	0.4 W	2.3 S
110747.7-774012	Hα 8/cc 3	PC	1.3 W	4.0 S
110748.0-774004	Hα 8/cc 4	PC	2.9 E	3.5 N
110747.7-774014	Hα 8/cc 5	PC	0.8 W	5.8 S
110747.6-774003	Hα 8/cc 6	PC	3.0 W	5.3 N
110747.9-774015	Hα 8/cc 7	PC	1.7 E	6.7 S
110747.4-774006	Hα 8/cc 8	PC	6.6 W	2.4 N
110719.2-773252	Cha Hα 9	WF2	primary	M6
110825.6-773930	Cha Hα 10	WF4	primary	M7.5
110825.8-773930	Hα 10/cc 1	WF4	3.4 E	0.3 S
110825.7-773927	Hα 10/cc 2	WF4	2.2 E	3.2 N
110825.3-773932	Hα 10/cc 3	WF4	5.2 W	1.7 S
110830.8-773919	Cha Hα 11	WF4	primary	M8
110830.6-773915	Hα 11/cc 1	WF4	2.7 W	4.0 N
110637.4-774307	Cha Hα 12	WF4	primary	M7

To summarize, all companions with a mass above about $1M_{Jup}$ outside of $2''$ ($\sim$300 AU) and all companions down to a few M_{Jup} at $\sim$100 AU should have been detected with the presented observations. Outside of $0.35''$ ($\sim$50 AU), all companions with masses above $\sim 5M_{Jup}$ ($K_s \simeq 18$ mag) should have been detected.

4.2 Ground-based imaging with VLT and NTT

Images of the targets in the V, R and I band have been previously obtained by Comerón et al. (2000) with the FOcal Reducer/low dispersion Spectrograph No. 1 (FORS1) at the ESO 8.2 m Antu telescope, Unit Telescope 1 (UT1) of the **VLT**. These data have been retrieved from the public VLT data archive and reanalysed for the purpose of a search for companions. The FORS1 observations have been carried out during sub-arc sec seeing conditions with a pixel scale of $0.2''$/pixel. Some of the companion candidates found in HST images were also detected in the FORS1 V, R and I band images. Their magnitudes are given in Table 4.4.

Furthermore, infrared images in the J, H and K_s filter were obtained with the infrared camera Son of Isaac (SofI) at the ESO 3.6 m New Technology Telescope (**NTT**) at La Silla during a seeing of about 0.6 to $0.7''$. These observations were mainly carried out in March 2001 with the small SofI field in order to achieve the highest possible angular resolution ($0.147''$/pixel). Two more images (H & K_s) were already taken in March 2000 with the large SofI field ($0.29''$/pixel) containing

Table 4.3: **Observing log of ground-based VLT and NTT images.**

Instr.	Cha Hα	filter	exp.	date	FWHM
FORS1	4,5,8,10,11	V	60s	26 Jan 1999	0.78"
FORS1	4,5,8,10,11	R	60s	26 Jan 1999	0.87"
FORS1	4,5,8,10,11	I	60s	26 Jan 1999	0.80"
SofI	4,5,8,10,11	H	200s	14 Mar 2000	0.68"
SofI	4,5,8,10,11	K_s	200s	14 Mar 2000	0.58"
SofI	4,10,11	J	600s	3 Mar 2001	0.60"
SofI	4,10,11	H	1200s	3 Mar 2001	0.58"
SofI	4,10,11	K_s	5400s	3 Mar 2001	0.73"
SofI	5	J	600s	7 Mar 2001	0.74"
SofI	5	K_s	5400s	4 Mar 2001	0.58"
SofI	8	J	600s	3 Mar 2001	0.64"
SofI	8	H	1200s	3 Mar 2001	0.72"

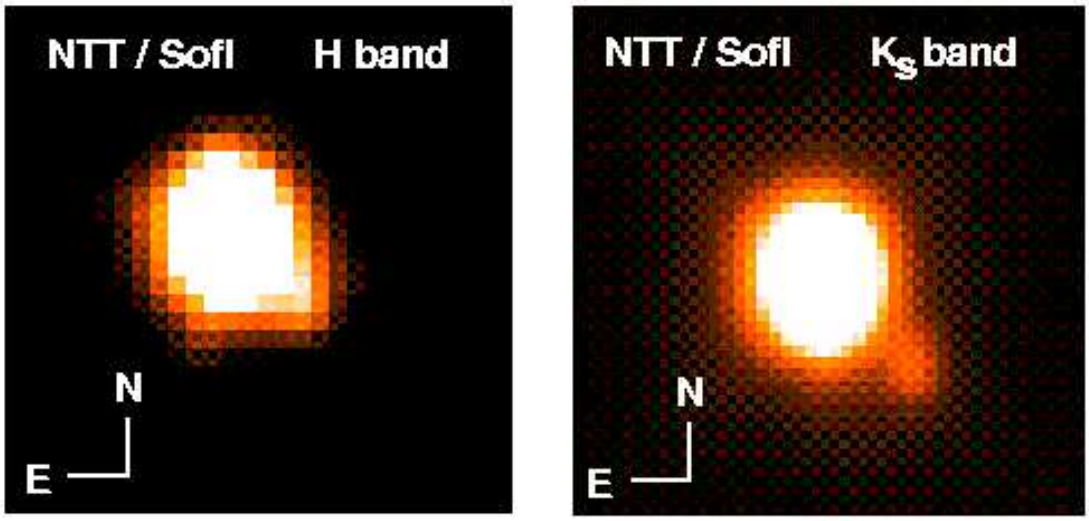

Figure 4.3: **NTT H and K_s band images of Cha Hα 5.**

several Cha Hα primaries in the field-of-view. Darks, flat fields and standards were taken in the same nights and a standard data reduction was performed with the *eclipse* tool[2] provided by ESO. The observing log of all ground-based observations is given in Table 4.3.

Standard **aperture photometry** was performed with MIDAS[3] for most of the ground-based images from the VLT as well as from the NTT observations. However, for the very close companion candidate near Cha Hα 5 a more sophisticated approach was needed to measure the VRIJ magnitudes. This is described in Sect. 4.4.

All determined **magnitudes** are given in Table 4.4. The magnitudes for the primaries Cha Hα 1–12 derived from VLT images are from Comerón et al. (2000), whereas the magnitudes for companion candidates in the very same images are determined within the scope of the presented search for companions. The JHK_s magnitudes derived for the primaries from SofI images agree well with those given in Comerón et al. (2000), who had obtained their data with IRAC2 at the ESO/MPG 2.2m. The IJK_s magnitudes for the primaries listed in Table 4.4 also agree well with DENIS magnitudes given by Neuhäuser & Comerón (1999) for Cha Hα 1–8.

Several objects which have been detected in the HST I band images are undetected in other filters. Lower limits for the magnitudes in filters where an object is not detected, are derived from the mean background intensity (and its variation) from ± 4 pixels (for HST images) and ± 3 pixels (for ground-based images) around

[2] www.eso.org/projects/aot/eclipse
[3] www.eso.org/projects/esomidas

Table 4.4: **Space- and ground-based VRI and JHK magnitudes for all companion candidates.** V,R_C,I_C from VLT/FORS1, R_V,I_V,m(Hα) from HST/WFPC2, and J,H,K_s from NTT/SofI. VLT/FORS1 observations as well as JHK_s magnitudes for Cha Hα 1, 2, 3, 7, and 9 are from Comerón et al. (2000). VLT/FORS1 VRI magnitudes for companion candidates were determined from the Comerón et al. (2000) VLT/FORS1 images. Typical precision: 0.05 mag for bright primary objects and 0.1 mag for companion candidates, but $\geq$ 0.2 mag for objects fainter than 23 mag as well as for Cha Hα 5/cc 1 (see Sect. 4.4). n/o: not observed. W_λ from Comerón et al. (1999, 2000) and Neuhäuser & Comerón (1999). Hα always in emission.

Object	V (VLT)	R_C (VLT)	R_V (HST) m_{F675W}	I_C (VLT)	I_V (HST) m_{F814W}	J	H	K_s	Hα (HST) m_{F656N}	$W_{\lambda(H\alpha)}$ [Å]
Cha Hα 1	21.0	18.7	18.96	16.17	16.16	13.55	12.78	12.28	17.72	35-99
Cha Hα 2	19.8	17.60	17.42	15.08	n/o	12.59	11.43	11.15	16.76	32-71
Cha Hα 3	19.51	17.38	17.27	14.89	14.97	12.46	11.64	11.11	16.81	5-14
Cha Hα 4	18.52	16.70	16.68	14.34	sat.	12.19	11.38	11.09	16.69	5-11
Hα 4/cc 1	$\geq$ 22.5	$\geq$ 22.2	$\geq$ 23.6	$\geq$ 19.0	23.0	$\geq$ 18.4	$\geq$ 18.1	$\geq$ 17.3		
Hα 4/cc 2	$\geq$ 22.8	$\geq$ 22.3	24.1	$\geq$ 20.7	22.2	18.5	17.4	17.3		
Hα 4/cc 3	23.0	21.6	21.7	20.4	20.2	17.7	16.7	16.2		
Cha Hα 5	19.18	17.14	17.03	14.68	14.67	12.14	11.21	10.56	16.62	8-11
Hα 5/cc 1	23.1:	21.1:	21.22	19.0:	19.20	16.8:	15.0:	14.4:		
Cha Hα 6	19.75	17.60	n/o	15.13	n/o	12.43	11.61	11.09	n/o	59-76
Cha Hα 7	22.2	19.5	19.69	16.86	16.78	13.89	13.00	12.51	19.02	35-45
Cha Hα 8	20.1	17.96	17.84	15.47	15.50	12.9	12.0	11.4	17.46	8-9
Hα 8/cc 1	$\geq$ 23.2	$\geq$ 21.5	$\geq$ 23.5	$\geq$ 19.3	23.4	$\geq$ 17.5	$\geq$ 16.6	$\geq$ 14.7		
Hα 8/cc 2	$\geq$ 23.6	$\geq$ 22.5	$\geq$ 23.5	$\geq$ 20.4	23.6	$\geq$ 17.0	$\geq$ 18.1	$\geq$ 16.6		
Hα 8/cc 3	$\geq$ 23.3	23.2	22.7	21.3	21.3	18.8	16.7	15.8		
Hα 8/cc 4	$\geq$ 23.3	22.9	22.9	21.5	21.7	19.9	17.8	17.0		
Hα 8/cc 5	$\geq$ 23.5	$\geq$ 23.2	$\geq$ 24.8	$\geq$ 22.0	21.7	$\geq$ 20.3	$\geq$ 20.1	$\geq$ 18.3		
Hα 8/cc 6	$\geq$ 23.4	$\geq$ 23.1	23.1	$\geq$ 21.9	22.6	$\geq$ 20.6	$\geq$ 20.0	$\geq$ 19.3		
Hα 8/cc 7	$\geq$ 23.5	22.9	22.5	21.0	21.0	18.4	16.8	15.4		
Hα 8/cc 8	$\geq$ 23.4	$\geq$ 23.1	$\geq$ 24.9	$\geq$ 21.6	22.6	$\geq$ 20.6	$\geq$ 19.9	$\geq$ 18.9		
Cha Hα 9	23.1	20.1	20.05	17.34	n/o	13.92	12.59	11.82	20.02	16
Cha Hα 10	21.6	19.4	19.35	16.90	16.79	14.41	13.68	13.30	19.21	9
Hα 10/cc 1	$\geq$ 23.1	$\geq$ 23.1	23.3	21.7	21.8	19.0	17.6	17.1		
Hα 10/cc 2	$\geq$ 23.5	$\geq$ 23.0	24.9	$\geq$ 21.2	22.9	$\geq$ 18.5	$\geq$ 20.3	$\geq$ 19.9		
Hα 10/cc 3	$\geq$ 23.3	23.0	23.0	21.4	21.5	19.6	18.5	17.9		
Cha Hα 11	21.9	19.9	19.69	17.35	17.41	14.72	14.03	13.60	18.95	23
Hα 11/cc 1	$\geq$ 22.9	$\geq$ 22.9	23.4	22.2	22.2	21.1	19.3	18.7		
Cha Hα 12	20.6	18.3	18.34	15.58	15.72	n/o	n/o	n/o	18.03	20

the pixel, where the peak of the companion candidate should be located according to its position in the HST I band images. The given limits correspond to an intensity of 3σ above the mean background. No additional companion candidates (within $7''$) were detected in the ground-based images.

4.3 Colors of companion candidates

A first check as to whether or not a companion candidate is truly bound was done by testing if the companion candidate is as cool as can be expected from the magnitude difference by means of optical and infrared colors.

Figs. 4.4 and 4.5 display a color-magnitude diagram R_V vs. (R_V-I_V) and a color-color diagram (J−H) vs. $(H-K_s)$, respectively. Given the faint magnitudes of the companion candidates, all of them would have masses around or below the deuterium burning limit, assuming that they are at the distance of the primaries and suffer the same extinction. For such low masses, they should be very faint and red in the optical. However, with the possible exception of Cha Hα 5/cc 1 and Cha Hα 4/cc 2, the companion candidates are all too bright in R and I given their JHK_s magnitudes. Thus, they are probably reddened background giants

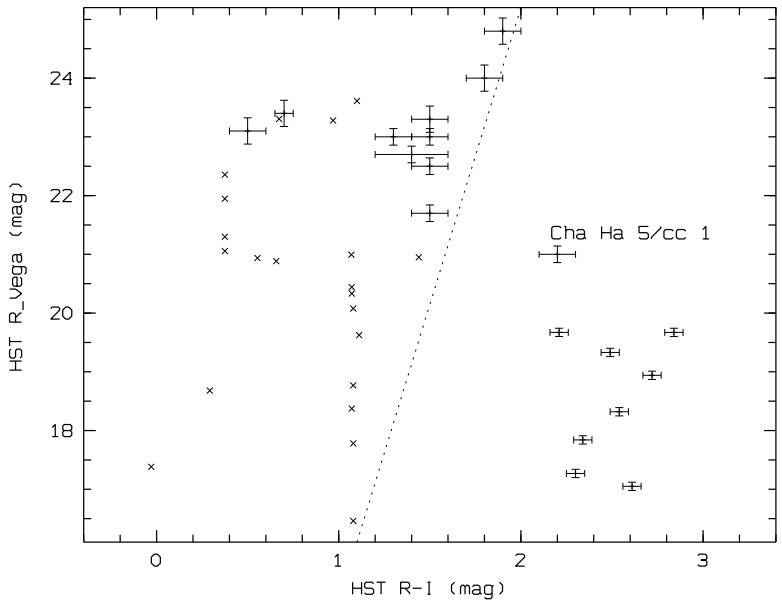

Figure 4.4: **Color-magnitude diagram: R_V vs. (R_V-I_V).** All primary objects Cha Hα 1–12 (with small error bars), all companion candidates within 7″ (with larger error bars), and all other objects (without error bars) detected in HST images are plotted. Data from Table 4.4. Note the bimodal distribution: All primaries and one companion candidate (Cha Hα 5/cc 1) are located in the lower right part of the diagram, whereas all other objects are located to the left of the inserted dotted line. This suggests that all objects on the left side of the dotted line are located in the background, while those in the lower right are members of Cha I.

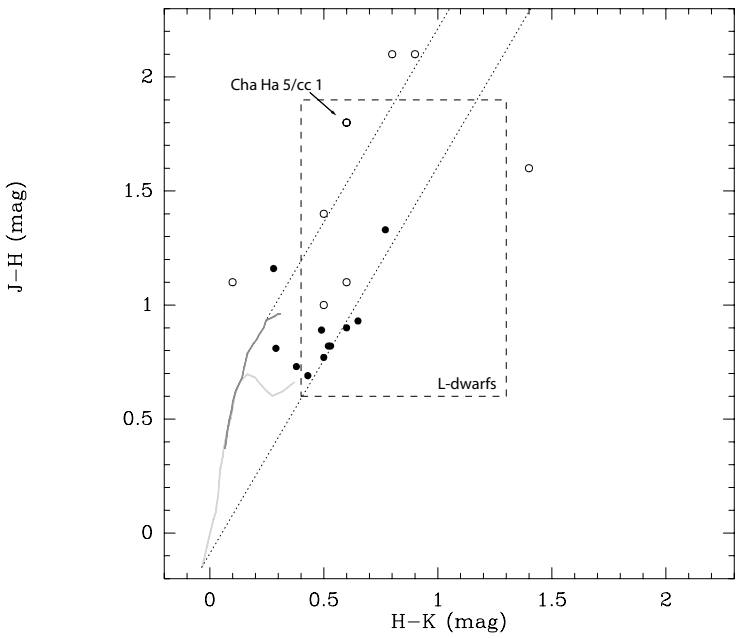

Figure 4.5: **Color-color diagram: (J−H) vs. (H−K_s).** Filled circles mark primaries Cha Hα 1–12 and open circles companion candidates. Error bars are omitted for clarity, errors range between ~ 0.07 mag for the brightest primaries and ~ 0.15 mag for the faintest companion candidates. Solid lines indicate the locations of points corresponding to un-reddened main-sequence and giant stars (Bessel & Brett 1988). The two parallel dotted lines define the reddening band for both main-sequence and giant stars taken from Rieke & Lebofsky (1985). The dashed box indicates the locations of L-dwarfs according to Burgasser et al. (2002) and Leggett et al. (2002). The companion candidate located to the right of both dotted lines is Cha Hα 8/cc 7. The leftmost companion candidate (bluest in H−K_s) is Cha Hα 4/cc 2, located near the early T-dwarf area. Cha Hα 5/cc 1 is marked by an arrow.

or extragalactic objects. It is noted that Cha Hα 8/cc 7 is located in the area of infrared excess hinting at circumstellar material.

For Cha Hα 5/cc 1 and Cha Hα 4/cc 2, the observed magnitudes and colors are consistent with either a moderately reddened L- or T-type companion or, alternatively, with a highly reddened background star. The companion candidate near Cha Hα 5 is discussed separately in the next section (Sect. 4.4). The other possibly interesting object, Cha Hα 4/cc 2, has colors of (J−H) = 1.10 ± 0.14 and (H−K_s) = 0.10 ± 0.14 mag and is the bluest in (H−K_s) (Fig. 4.5). The T3-dwarf SDSSpJ102109.69-030420.1 has similar (2MASS) colors according to Burgasser et al. (2002), namely (J−H) = 0.93 ± 0.15 and (H−K_s) = 0.23 ± 0.20 mag[4]. If

[4] but somewhat different colors according to Leggett et al. (2002), namely (J−H) $\simeq 0.47$ and (H−K) $\simeq 0.15$ mag

Cha Hα 4/cc 2 is really an early T-dwarf companion, it will definitely be a planetary mass-object. However, its angular separation is 3.6″, i.e. ∼570 AU at 160 pc, and therefore much larger than expected for planets.

As mentioned above, one possibility to confirm a companion candidate is to measure proper motions and verify that primary and companion are co-moving. For HST companion candidates, which are also detected in ground-based images, observations at several epochs are already available. However, the resolution of the ground-based images is too low to measure their proper motions with the required precision. It can only be said that the ground-based separations are not inconsistent with those measured in the HST images. A check for common proper motion is possible in a few years with the HST PC pixel scale (45.5 mas).

4.4 The companion candidate near Cha Hα 5

HST R and I band images of Cha Hα 5 are shown in Fig. 4.2. A faint object is visible at a separation of 1.5″ to the southwest of Cha Hα 5 referred to as Cha Hα 5/cc 1. This companion candidate is also marginally resolved in ground-based VRIJHK$_s$ images (Figs. 4.3 and 4.6) at best in the K$_s$ band image taken with SofI in March 2001. The companion candidate is not detected in Hα, while all primary objects including Cha Hα 5 are detected.

Aperture photometry was performed for the HST images as well as for the ground-based H and K$_s$ band images (Fig. 4.3) of this object. However, due to the small separation between the primary and the companion candidate, this was not possible for the VRIJ images since the magnitude differences in these filters are even higher. The point-spread-functions (PSFs) of the primary and the companion candidate are significantly superposed in these images. This can be clearly seen in the right panels of Fig. 4.6, where the combined flux is plotted as a function of the separation to the primary. The faint companion candidate shows up as a bump in the wing of the PSF of the primary.

Therefore, for the V, R, I and J band images, firstly the flux was determined for each pixel within a radius of 4″ around the center of Cha Hα 5 and plotted as a function of the separation to the primary (Fig. 4.6, right panels). Those functions are a superposition of two Moffat functions (Moffat 1969). Thereafter, the peak flux of the companion candidate was derived by subtracting the flux value of the upper envelope at 1.5″ separation from the flux value of the lower envelope at the same separation. Based on this peak flux of the companion candidate and the peak flux of the primary, the magnitude difference between the primary and the companion candidate has been determined and hence, the magnitude of the companion candidate. The magnitudes derived in that way from the R and I band images are consistent with the R and I magnitudes determined from HST images,

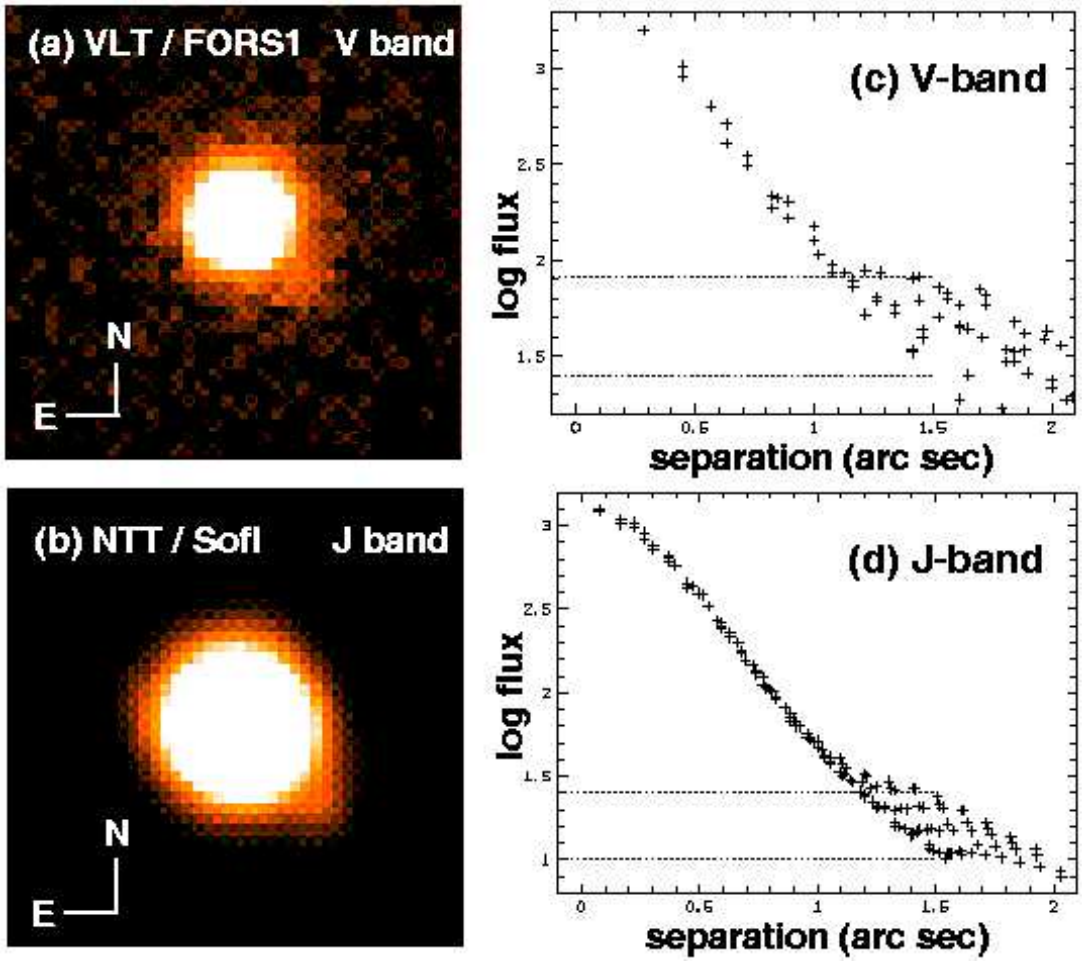

Figure 4.6: **V and J band images of Cha Hα 5 and its companion candidate.** **a)** VLT V band image. **b)** NTT J band image. **c)** and **d)** PSF of Cha Hα 5 with the faint companion candidate as the bump in its wing, plotted as log of flux (in V and J, respectively) vs. separation in arc sec from the primary. The magnitude of the companion was computed by subtracting the contribution of the primary at 1.5″ separation (lower envelope of the data points) from the peak of the bump (upper envelope) and comparing it to the observed flux and known magnitude of the primary. The dotted lines mark the maximum flux of the companion and the flux contribution of the primary at 1.5″ separation, respectively.

where the companion candidate is well resolved from the primary (±0.10 mag in R and ±0.19 mag in I) demonstrating that it is a reliable procedure.

A first check of the companionship of Cha Hα 5/cc 1 was done by means of optical and infrared colors as for the other companion candidates. Its colors are marginally consistent with a highly-reddened K giant in the background of Cha I or with an early- to mid-L type object at the distance of the primary. However,

very recent follow-up spectroscopy of this companion candidate (Neuhäuser et al. 2002b) showed that it is a K-type background star.

4.5 Hints of binarity of Cha Hα 2

In the previous sections, an investigation for clearly resolved companions, at least in HST images, has been carried out. In order to search for closer companions, an analysis of the PSF in HST images of Cha Hα 1–12 has been performed checking for significant elongations due to unresolved companions. For this purpose, the ratio between the Full Width at Half-Maximum (FWHM) in the direction of the strongest elongation and the FWHM perpendicular to it has been determined for every primary and every band observed with the HST (R, I, and Hα). These measurements of the observed PSF elongations have been plotted vs. the magnitudes for each object and band (Fig. 4.7).

While most PSFs are consistent with a single point source (elongation ~ 1), there is one notable outlyer, namely Cha Hα 2, for which the PSF for both the R and Hα observation is elongated by a factor of ~ 1.5 towards the NE-SW direction (the object was not observed in the I filter due to technical problems with WFPC2 shutter). All three other sources of the same observation are consistent with point sources. The Cha Hα 2 PSFs are $\sim 5.5\sigma$ deviant from the other Cha Hα primaries and Cha Hα 2 may therefore be a binary.

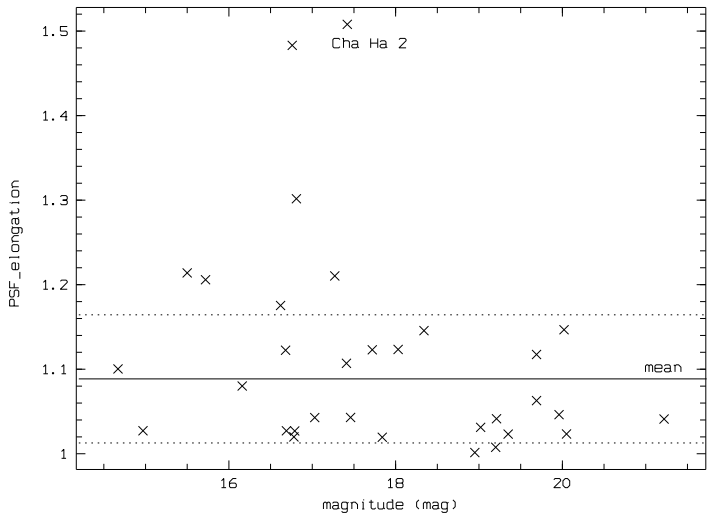

Figure 4.7: **Apparent elongation of the point-spread-functions (PSF) vs. magnitude of Cha Hα 1–12** (and Cha Hα 5/cc 1). Only Cha Hα 2 (observed in R and Hα, not in I) appears to be elongated. The mean elongation of all other PSFs are 1.089 ± 0.076 (horizontal line).

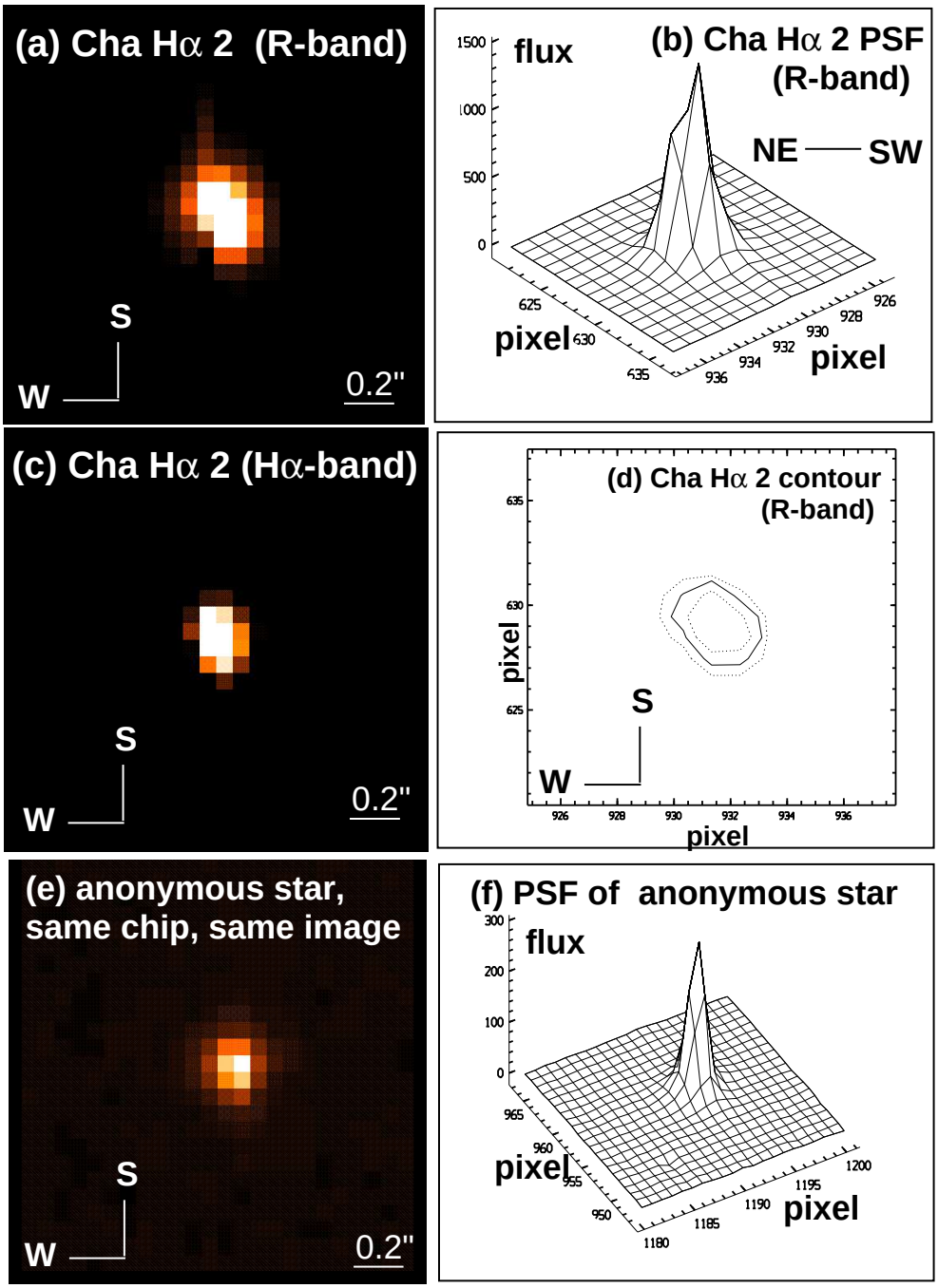

Figure 4.8: **HST R and Hα images of Cha Hα 2** (WF4 chip) show a $\sim 0.2''$ elongation of its PSF. b) three-dim. display of the PSF of Cha Hα 2 showing a faint secondary bump to the NE. d) Contour plot of the PSF of Cha Hα 2. e) HST R band image of another star (same chip and observation). f) PSF of that comparison star. While the PSF of Cha Hα 2 is always slightly elongated, the PSF of the (anonymous) comparison star is consistent with a point source.

The HST images of Cha Hα 2 are displayed in the left panels of Fig. 4.8. Further investigation of the HST R band image of Cha Hα 2 shows that without corrections for the superposition, the SW component is a factor of ~ 1.56 brighter than the NE component. After subtracting the PSF of the brighter (SW) component from the fainter one, the NE component is fainter by ~ 0.2 mag. The position angle of the NE companion candidate relative to the SW primary is $\sim 40°$ (measured as usually from N to E), and the separation between the close pair is almost $0.2''$, i.e. slightly less than two pixels. This angular separation corresponds to about 30 AU at the distance of Cha I. The R_V band magnitude of the unresolved object was determined to $R_V = 17.42$ mag (Table 4.4), therefore the two components would have R_V magnitudes of ~ 17.45 mag and ~ 17.65 mag.

The resolution of the ground-based FORS1 and SofI images is too low to resolve this elongation.

It cannot be excluded completely that the apparent elongation is caused by, e.g., bad pixels. Furthermore, there is also the possibility that the apparent companion is an unrelated background object. Therefore, follow-up observations are necessary in order to confirm the binary hypothesis.

Cha Hα 2 (M6.5) is located close to the sub-stellar limit (cf. HRD in Fig. 2.1) and can therefore either be a very low-mass star or a relatively massive brown dwarf (Comerón et al. 2000). The HST imgages hint at an approximately equal-brightness and hence, equal-mass binary. Thus, both of its components would still be very close to the sub-stellar limit, i.e. either low-mass stars or brown dwarfs. More precise imaging photometry (e.g. with the PC or NICMOS on board the HST) and resolved spectroscopy is necessary to further investigate if Cha Hα 2 is a binary. If it is a binary, the orbital motion should be detectable in a few decades yielding orbital parameters and masses of the components.

Chapter 5

Photometric monitoring

A photometric monitoring campaign of bona fide and candidate brown dwarfs in the Cha I star forming cloud has been carried out in two filters in order to study the time dependence of their brightness and color. It is known that magnetically driven surface features (spots) of stars modulate the brightness of the star as it rotates (cf. Sect. 1.5). Fig. 5.1 illustrates the light curve of a star due to the periodic appearing and disappearing of a cool spot. The presented photometric observations of brown dwarfs are aimed at the study of such spot-driven variabilities in the substellar regime in order to test if brown dwarfs have magnetic spots. Furthermore, since surface features modulate the emitted flux *at the rotational period*, the photometric study is aimed at the determination of rotation rates for brown dwarfs. Rotational periods are fundamental (sub)stellar properties. The knowledge of rotational periods for objects covering a wide range of ages is important for the understanding of the evolution of angular momentum. Scanning the period–age–diagram observationally for brown dwarfs with ages of less than 100 Myr provides in addition, a significant test of substellar evolutionary theories since the onset of deuterium burning is expected to have an observable effect on the angular

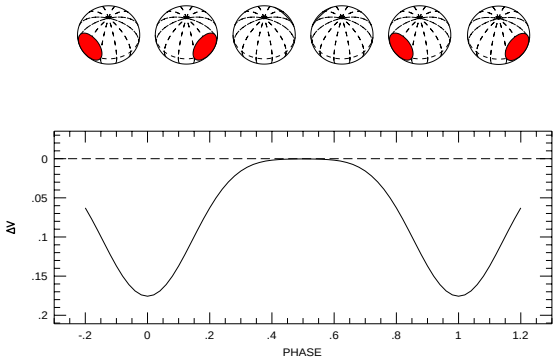

Figure 5.1: **Modulation of the brightness due to a spot.** Kindly provided by G. Torres. A cool spot on the surface of a (sub)stellar object causes a periodic dimming of the total brightness at the rotation period. Plotted are the relative V magnitudes ΔV over the orbital phase.

momentum evolution. The contraction of brown dwarfs is expected to be temporarily decelerated or even stopped in the first several million years of their lifetime due to the ignition of deuterium (e.g. Burrows et al. 2001). Furthermore, rotation rates are critical parameters for rotationally induced phenomena, like dynamo activity (supposed to cause surface spots) and meteorological processes. However, the number of brown dwarfs with known rotational periods is rather small (see Sect. 5.1) and in particular at very young ages almost no rotation rates have been measured so far. First results of the here presented photometric data have been published in Joergens et al. (2002).

5.1 Hitherto known periods for brown dwarfs

A few studies of the photometric behavior of brown dwarfs have been carried out so far. In Table 5.1 all brown dwarfs for which photometric periods have been published in the literature, are compiled and ordered by increasing age. Given that S Ori 31 and CFHT-PL 8 are probably not brown dwarfs and that for LP 944-20 no definite period was found, the number of known periods for brown dwarfs add up to only five, all for old field brown dwarfs.

Table 5.1: **Compilation of brown dwarfs with known photometric periods.** Note that S Ori 31 and CFHT-PL 8 are probably stars but have been included because of their closeness to the hydrogen burning mass limit. Masses are estimates. Ages of the field brown dwarfs BRI 0021-0214 to SDSS 0539 are generally unknown but supposed to be of the order of 1 Gyr. The spectral type of S Ori 31 is an estimate. Amplitudes are measured in broad band I filters, except for the ones marked with an asterisk, these refer to narrow band observations. See references for details: [1] Bailer-Jones & Mundt (2001), [2] Terndrup et al. (1999), [3] Tinney & Tolley (1999), [4] Martín et al. (2001), [5] Clarke et al. (2002).

object	age [Gyr]	mass [$M_\odot$]	SpT	period	amplitude [mag]
S Ori 31[1]	1-5 Myr		(M6.5)	7.5 h	0.012
CFHT-PL 8[2]	0.1-0.12	0.08	–	0.4 d	0.028
LP 944-20[3]	0.5-0.65	0.06	M9	–	0.04*
BRI 0021-0214[4]	∼1		M9.5	0.8 d, 0.2 d	0.018, 0.007
2M1334[1]	∼1		L1.5	2.7 h, 6.3 h, 1.0 h	0.020
Kelu-1[5]	∼1	<0.07	L2	1.8 h	0.012*
2M1146[1]	∼1		L3	5.1 h	0.015
SDSS 0539[1]	∼1		L5	13.3 h	0.011

The nature of the detected variations are not finally clarified. For very cool objects (spectral type late M, L) surface spots might not play a significant role but another important process may affect the time dependence of the observed flux of the objects: Below a temperature of about 2800 K the condensation of dust sets in (e.g. Tsuji et al. 1996a,b, Allard et al. 1997, Burrows & Sharp 1999) as described in Sect. 1.4.2. Inhomogeneities in dust cloud coverages may cause observable photometric variations. Tinney & Tolley (1999) report variations of an M9 dwarf in narrow band filters, which are sensitive to changes in TiO absorption features and therefore to clouds. Bailer-Jones & Mundt (2001) detected significant periods for four M and L dwarfs, two of them are consistent with rotational velocities. Furthermore, they find that for one variable object there is no common period in data taken with a separation of one year and suggest that one sees the formation and dissipation of clouds rather than rotationally driven features. Martín et al. (2001) report also a varying periodicity found in I band photometry of the M9.5 dwarf BRI 0021-0214. The authors suggest that the variations are caused by inhomogeneous clouds rather than spots because the object is very inactive in terms of Hα and X-ray emission despite a very fast rotation. Clarke et al. (2002) found periodic variations of the brightness of Kelu-1. The detected period of 1.8 h is consistent with the rotational velocity. In recent observations (Clarke & Tinney 2002), no evidence for variability in dust sensitive molecular lines was found and the nature of the variations remains still unclear. Eislöffel & Scholz (2001) studied the photometric behavior of very low mass stars and brown dwarfs in the young (∼36 Myr) cluster IC4665 and report the finding of rotational periods below one day for five candidate brown dwarfs. These measurements probe the age range < 100 Myr in terms of rotational properties and details on periods and amplitudes will be given in a forthcoming publication (pers. comm.).

5.2 Data acquisition

A field of $13' \times 13'$ in the Cha I cloud was monitored photometrically in six consecutive half nights with the imaging camera DFOSC at the Danish 1.5 m telescope at ESO, La Silla, Chile. Images have been obtained in the Bessel R and the Gunn i filter between May 31 and June 5 in 2000. The first two nights have been partly cloudy and therefore fewer images (with lower S/N) have been taken in these two nights.

The exposure times have been chosen to detect periods on time scales of expected rotational periods of the objects. Projected rotational velocities $v \sin i$ of these moderately fast rotators (cf. Sect. 3.4) indicate that their rotational periods are within the range of a few days. The objects span a large dynamical range (I=13.6 to 17.4 mag) therefore i band images with two different exposure times of about

400 s and about 900 s have been obtained. R band images have been taken with only one exposure time of about 1000 s.

Aperture photometry was performed for the twelve bona fide and candidate brown dwarfs Cha Hα 1 to 12, the very low-mass T Tauri stars CHXR 73, CHXR 78C, B 34 as well as for several reference stars in the field with IRAF. All counts within an aperture of given radius centered on the object are integrated. The sky background was determined from a source-free annulus outside this aperture and subtracted from the object counts. The T Tauri stars CHXR 74 and Sz 23 are also in the field of view but have been saturated. The calculation of differential magnitudes allowed the compensation for variable atmospheric conditions at least to a certain degree. The i band images are affected by fringes. A correction of fringes is possible if the flat fielding is done by using a so called superflat, which is created by a series of science images with offsets greater than the largest structure in the field. However, the observed field of view contains large reflecting clouds of the star forming region, thus the science frames themselves cannot be used. The fringe correction would have been possible only with the observation of an additional field but was spared for time efficiency at the expense of some photometric accuracy. From the analysis of carefully chosen reference stars the photometric error was estimated to be about 0.015 mag or less for objects as bright as the reference stars or brighter: The standard deviation of the reference stars is 0.009 to 0.014 mag in the i band and 0.005 to 0.006 mag in the R band (cf. Fig. 5.3 to 5.5 for the dispersion of the reference stars).

5.3 Time series analysis

In order to search for periodicity in the obtained light curves of the targets the string-length method (Dworetsky 1983) was applied. This method is ideally suited for unevenly spaced data as in the case of the presented light curves. The algorithm phase folds the data with a trial period and calculates the string length between successive data points. This is done for all periods within a given period range. The period which generates the minimum string length is the most likely period.

The significance of the detected periods was estimated by cross checking a randomized data set sampled with the same time steps as the real data but with arbitrary magnitudes within the limits of the real magnitudes. For each suspected period, 10000 randomized data sets were checked. The percentage of samples that have a longer (i.e. less significant) string length for any period than that of the suspected period yields the confidence level (a 99.9% confidence level corresponds to the case that all randomized samples have a longer string length than the string length for the suspected period). Besides this significance test, a major emphasis

was put on a direct check by eye of the original as well as the phase folded light curves.

It is well known that in addition to intrinsic periodicities of the monitored objects the light curves may show alias periods due to the sampling rate of the data. The most common alias periods $P_{\rm false}$ are

$$P_{\rm false}^{-1} = 1.0027\,{\rm d} \pm P_{\rm true}^{-1} \tag{5.1}$$

(Dworetsky 1983). This equation relates the true period with possible alias periods, which are inherent to the data due to an observing frequency of one sidereal day.

In general, more images have been obtained in the i band than in the R band and in addition the i band data have a higher S/N. Therefore for each object, firstly the i band data were studied and it was given them a higher weight. The search for periodicity has been carried out for periods in the range of 1.5 hours to 5 days. The minimum period is set by twice the average sampling rate of about 45 min. The maximum is chosen to be slightly smaller than the total time coverage of about 5.5 d.

5.4 Rotational periods

Significant periods have been measured for three brown dwarf candidates (Cha Hα 2, 3, 6) as well as for two very low-mass T Tauri stars (B 34, CHXR 78C) within the range of 2.2 d to 4.5 d and with i band amplitudes between 0.06 mag and 0.14 mag (Joergens et al. 2002). The results are presented in Table 5.2 and Fig. 5.3, 5.4 and 5.5.

For Cha Hα 4, 5, 8, 12 and CHXR 73 no clear variations are detected and limits for variability amplitudes for these objects are derived (Table 5.2). The S/N of Cha Hα 1, 7, 9, 10 and 11 in the obtained images is too low for a further exploration. These objects should be re-observed with a larger telescope.

Details of the results of the period analysis on individual objects as well as original and phase folded light curves are presented in the following subsections. Objects are ordered by decreasing mass: from about 0.12 $M_\odot$ for B 34 to about 0.05 $M_\odot$ for Cha Hα 6. These masses are rough estimates based on luminosities and effective temperatures and a comparison with theoretical evolutionary tracks by Baraffe et al. (1998) for the Cha Hα objects (Comerón et al. 2000) and by Burrows et al. (1997) for the T Tauri star B 34 (Comerón et al. 1999), respectively. The x and y axes of all light curves span the same range in magnitudes (0.2 mag) as well as in time (6.5 d) for convenient comparison.

5.4.1 B 34 ($\sim 0.12\,M_\odot$)

The brightness of the T Tauri star B 34 varies with a peak-to-peak amplitude of 0.14 mag in the i band and 0.18 mag in the R band during the six nights of the observations (Fig. 5.3). The light curves show a smooth variability apart from one runaway data point in the 3rd night, which is present in both filters and may therefore be an intrinsic increase of the brightness due to a flare-like event.

The period search analysis of the i band light curve of B 34 yields a clear period of 4.5 d with a confidence level above 99.9%. Searching for periods in the R band data yields rather a plateau with a range of 4.2 d to 4.9 d for the string length than a clear minimum, i.e. the period search algorithm is unable to distinguish between the significance of periods within this range. This can be understood if one takes into account that these periods are very close to the total time basis of the data set (5.5 days) and that the R band brightness of the first two nights is only constrained by one data point each. Therefore, any errors of these points greatly affect the period search. The R band data folded with the i band period of 4.5 d looks very smooth (Fig. 5.3). It is concluded that the common period is 4.5 d. The phase folded (R-i) color curve (Fig. 5.2) shows that B 34 is redder during minimum light as expected for brightness variations caused by starspots.

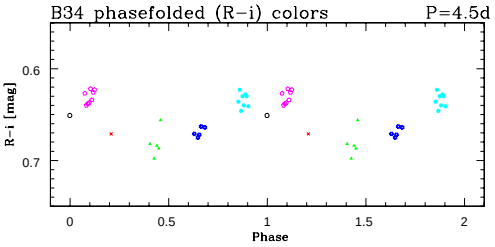

Figure 5.2: **Phase folded (R-i) colors of B 34.** Different symbols denote data points obtained in different nights.

5.4.2 CHXR 78C ($\sim 0.09\,M_\odot$)

The T Tauri star CHXR 78C changes its brightness with an amplitude of 0.07 mag in i and 0.10 mag in R (Fig. 5.4). The period search algorithm returns a period of 4.0 d for the i band light curve and a period of 3.9 d for the R band light curve, both with a confidence level above 99.9% . The phase folded light curves look convincingly smooth for both periods. Therefore, somewhat arbitrarily 3.9 d have been taken based on an eye check of the phase folded light curves with the awareness that the analysis is not sensitive to period differences of 0.1 d.

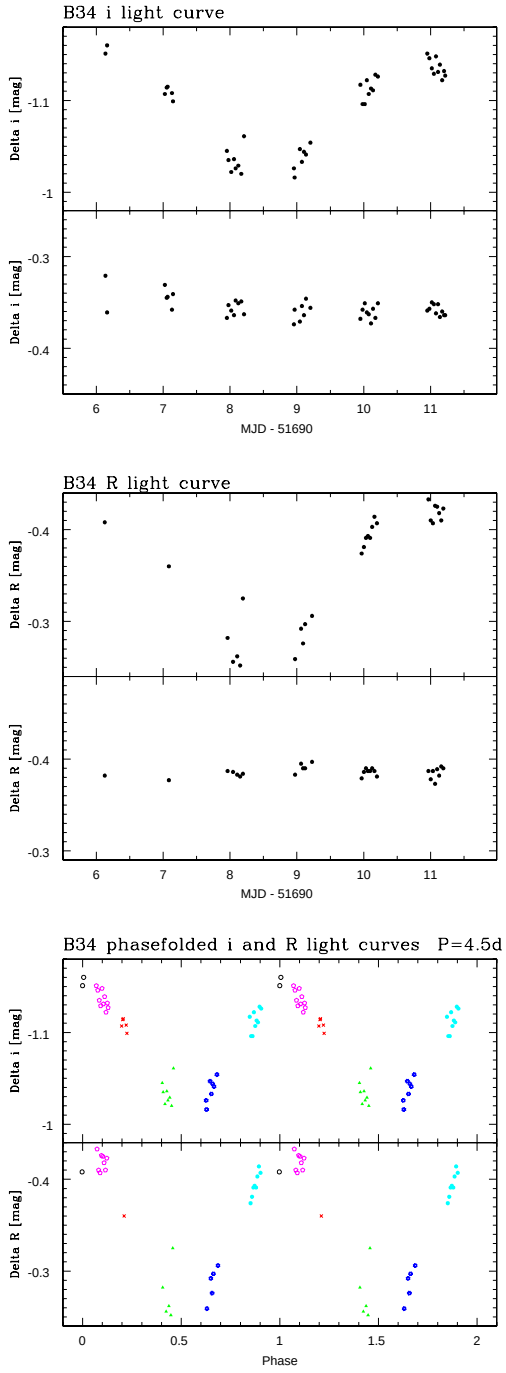

Figure 5.3: **Light curves of the very low-mass T Tauri star B 34.** Top and middle panel: i and R band original light curves (relative magnitudes), each with reference star magnitudes plotted below for comparison. Bottom panel: i and R light curves phase folded with the determined period. Different symbols in the phase folded light curves denote data points obtained in different nights.

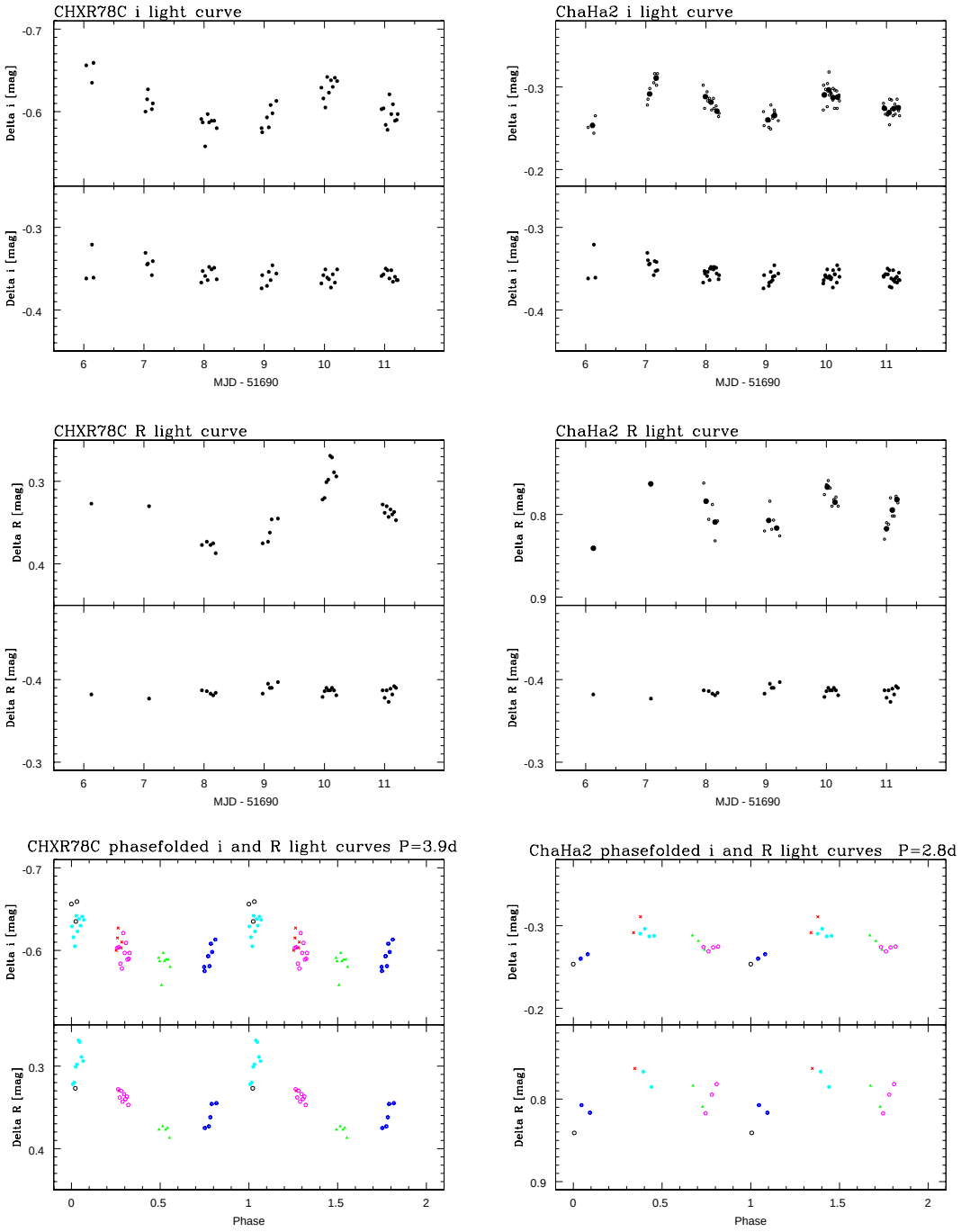

Figure 5.4: Light curves of the very low-mass T Tauri star CHXR 78C and the brown dwarf candidate Cha Hα 2. Panels are as in Fig. 5.3.

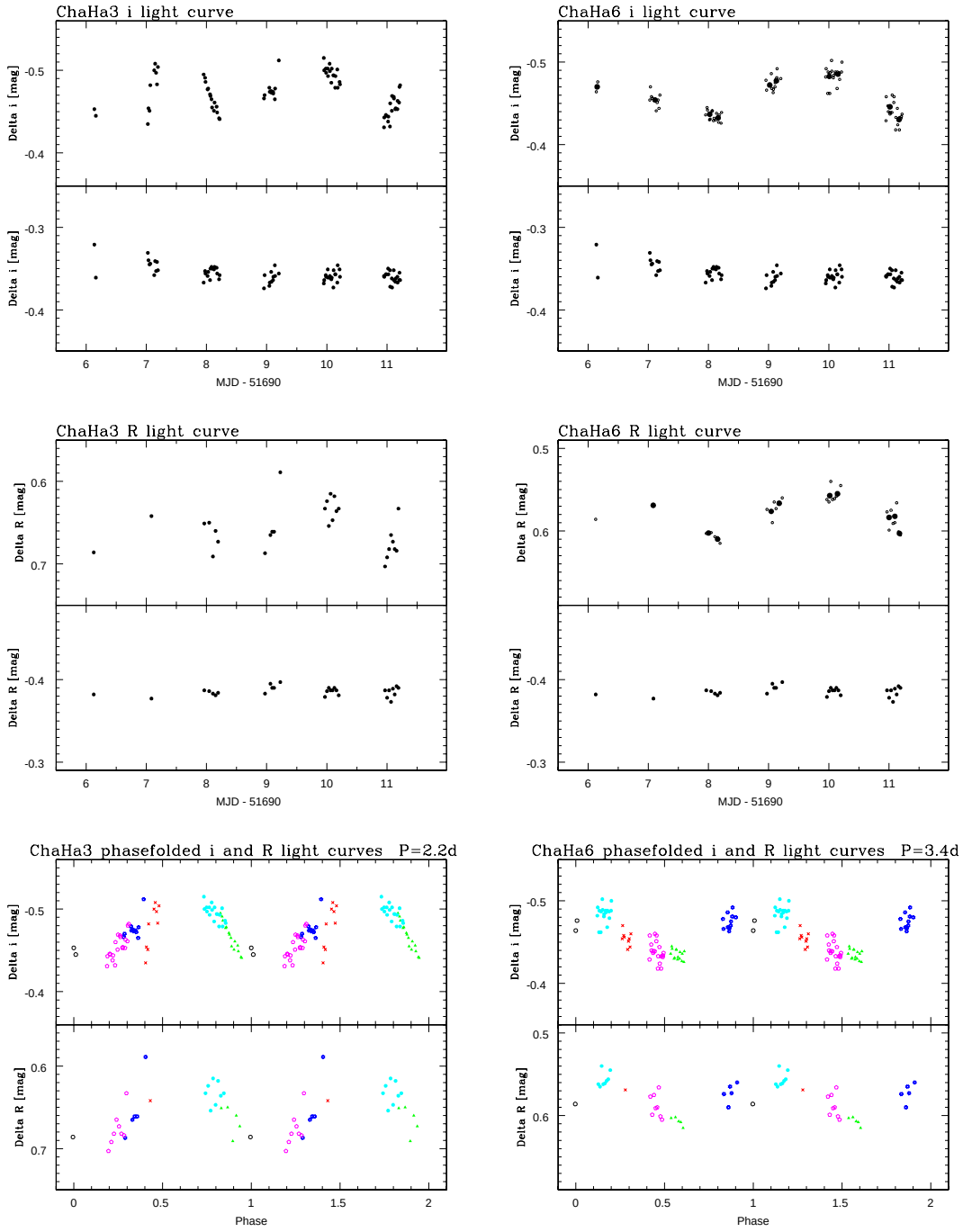

Figure 5.5: **Light curves of the brown dwarf candidates Cha Hα 3 and Cha Hα 6.** Panels are as in Fig. 5.3.

Table 5.2: **Rotational periods and photometric amplitudes** for brown dwarfs and very low-mass stars in Cha I. Rotational periods $P_{\rm phot}$ and photometric amplitudes Δ i and Δ R derived from i and R band light curves. Radii R_* are based on luminosities and effective temperatures (Comerón et al. 2000). $P_{v \sin i}$ denotes rotational periods derived from radii and $v \sin i$ measurements (see Sect. 3.4). $\Delta P_{v \sin i}$ is a $1\,\sigma$ error. For CHXR 78C no $v \sin i$ measurements are available.

object		periods			phot. amplitude	
	R_* [$R_\odot$]	$P_{\rm phot}$ [d]	$P_{v \sin i}$[d]	$\Delta P_{v \sin i}$[d]	Δ i [mag]	Δ R [mag]
B 34	0.93	4.5	3.1	$^{+1.7}_{-1.0}$	0.14	0.18
CHXR 78C	0.94	3.9	–	–	0.07	0.10
Cha Hα 2	0.73	2.8	2.9	$^{+1.4}_{-1.0}$	0.05	0.06
Cha Hα 3	0.77	2.2	1.9	$^{+0.8}_{-0.6}$	0.08	0.09
Cha Hα 6	0.68	3.4	2.6	$^{+2.0}_{-1.0}$	0.06	0.06
CHXR 73	1.46	–	–	–	0.05	0.03
Cha Hα 4	0.89	–	–	–	0.03	0.03
Cha Hα 5	0.83	–	–	–	0.02	0.04
Cha Hα 8	0.59	–	–	–	0.04	0.02
Cha Hα 12	0.66	–	–	–	0.03	0.04

5.4.3 Cha Hα 2 ($\sim 0.07\,M_\odot$)

In order to increase the S/N for the faint brown dwarf candidate Cha Hα 2 adjacent data points have been binned in groups of about five. Fig. 5.4 displays the original data as well as the overplotted binned data. The binned light curves have variability amplitudes of 0.05 mag in i and 0.06 mag in R. A minimum string length was found for a period of 2.8 d for the i band data with a confidence level larger than 99%. The light curves folded with this period (Fig. 5.4) support this result. The data analysis yields also the two less significant periods 0.73 d and 1.56 d, which cannot be rejected at once by a look at the phased light curves. However, they are related with the more significant 2.8 d period by Eq. 5.1 with $P_{\rm true}$=2.8 d and are therefore revealed as alias periods inherent to the data due to the sampling frequency of one day. It was therefore concluded that 2.8 d is the intrinsic period of the object. The R band light curve of Cha Hα 2 shows similar variations and trends as the i band light curve (Fig. 5.4, middle). However, the period analysis of the R band data does not confirm the 2.8 d period on a high

confidence level. It gives a minimum string length for 1.6 d (the alias in the i band) and only a second minimum for 2.8 d. The enhancement of the alias compared to the true period can be attributed to the smaller number of R band images as well as their lower S/N. The R band data folded with a period of 2.8 d show a smooth curve similar to the one of the i band and it was confidently concluded that 2.8 d is an intrinsic period of this object.

It should be noted that HST images of Cha Hα 2 hint at a companion at about 30 AU around Cha Hα 2 (see Sect. 4) unresolved in the DFOSC aperture photometry. If Cha Hα 2 is really a binary, the period found for Cha Hα 2 is presumably the period of one of the two components.

5.4.4 Cha Hα 3 ($\sim$ 0.06 M$_\odot$)

The brown dwarf candidate Cha Hα 3 exhibits variations with an i amplitude of about 0.08 mag and an R amplitude of about 0.09 mag (Fig. 5.5). The i band flux of this object seems to be modulated with a clear sine wave. However, the first three data points in the second night deviate from this behavior. The period analysis without these three points yields a highly significant period of 2.2 d with a confidence level above 99.9%. This suggests that 2.2 d is an intrinsic period of this object, although strong reasons have not been found to reject these three data points. The light curve phase folded with this period is displayed in Fig. 5.5. The R band data reflect the general trends also seen in the i band but are more noisy. They support a period of 2.2 d but do not confirm it with high significance. The R band data of nights 3 to 6 show a minimum string length for a period of 0.06 d but this can be rejected on the basis of a check of the data folded with this period. There is a second minimum at 2.2 d. The R band data folded with 2.2 d look quite smooth hinting at 2.2 days as being an intrinsic period of this object.

5.4.5 Cha Hα 6 ($\sim$ 0.05 M$_\odot$)

In order to increase the S/N of the brown dwarf candidate Cha Hα 6, adjacent data points have been binned in groups of two or three. See Fig. 5.5 for the original data and the overplotted binned data. The binned data of the object shows variabilities with an amplitude of 0.06 mag in both bands. The study of periodicities for the i band data results in a minimum string length for a period of 3.49 d with a confidence level of 96%. There are two less significant minima at 0.77 d and 1.43 d, which are related to the 3.49 d period by Eq. 5.1 indicating that these are aliases. The analysis of the R band data is hampered by the small number of data points. Particularly in the first night there is only a single data point which has a large uncertainty due to the poor weather conditions. It was

therefore ignored for the further analysis of the R band data and the search for periods. A minimum string length was found for a period of 3.34 d and two less significant minima for 0.78 d and 1.58 d. The alias periods for 3.34 d are 0.77 d and 1.42 d, therefore 0.78 and 1.58 are likely to be aliases. Fig. 5.5 (bottom) displays the light curves of Cha Hα 6 folded with 3.4 d, the average of the periods found for the i and R bands. Conclusively, this brown dwarf candidate has an intrinsic photometric period of 3.4 d$\pm$0.1 d.

5.5 Discussion

The periods determined for Cha Hα 2, Cha Hα 3 and Cha Hα 6 are among the first photometric periods determined for very young substellar objects and the longest found for any brown dwarf so far. Furthermore, the objects have relatively large variability amplitudes compared to hitherto monitored brown dwarfs. Causes of these variations as well as constraints for the evolution of angular momentum in the substellar regime are discussed in the following sections.

5.5.1 Rotational modulation due to spots

The detected periodic photometric variations of the brown dwarf candidates as well as of the T Tauri stars are interpreted as modulation of the emitted flux by rotation due to spots based on the following arguments:

1. The detected periods are consistent with rotational velocities $v \sin i$ and are therefore likely rotational periods. See Sect. 5.5.2 for more details.

2. The monitored (R-i) colors of these objects show larger amplitudes for shorter wavelength in agreement with the expectations for spots. This is true for all but Cha Hα 6, which shows the same amplitude in both the i and R band. Nevertheless, there may be slight differences between the amplitudes in the two bands, which are swallowed by the measurements uncertainties.

3. Young stars are known to have dominant surface features (e.g. Bouvier et al. 1993 and references therein), which are attributed to magnetic dynamo action. Though the studied brown dwarfs as well as the T Tauri stars have very low masses, they are relatively hot due to their young age. Thus, the atmospheric temperatures may be hot enough for a sufficient ionization fraction of the plasma in the atmospheres providing enough free charge carriers to allow for magnetically induced surface features.

4. The temperatures of these young objects are too hot (between 3030 K for B 34 and 2840 K for Cha Hα 3 and 6) for significant dust condensation according to model atmosphere calculations (e.g. Tsuji et al. 1996a,b, Allard et al. 1997, Burrows & Sharp 1999). Therefore, non-uniform condensate-coverage that has been suggested to explain the photometric variability detected for some L and M type old and hence cool (brown) dwarfs (Tinney & Tolley 1999, Bailer-Jones & Mundt 2001, Martín et al. 2001, Clarke et al. 2002) is an unlikely cause for the variabilities detected for the studied Cha I objects.

5.5.2 Comparison with spectroscopic velocities $v \sin i$

Measurements of the rotational broadening of spectral features in high-resolution UVES spectra yielded projected rotational velocities $v \sin i$ ranging from 8 to 26 km s^{-1} for nine out of twelve bona fide and candidate brown dwarfs in Cha I, as described in Sect. 3.4. These very young bona fide and candidate brown dwarfs are therefore moderately fast rotators in contrast to the very fast rotating old brown dwarfs, which have rotational velocities up to 60 km s^{-1} (Basri & Marcy 1995, Martín et al 1997, Tinney & Reid 1998, Basri et al. 2000). For the T Tauri star B 34 a $v \sin i$ of 15 km s^{-1} was determined.

The detected periods for Cha Hα 2, 3, 6 and B 34 are consistent within the measurement uncertainties with their spectroscopic velocities $v \sin i$ indicating that they are likely rotational periods of the objects (for CHXR 78C no $v \sin i$ measurement is available). Rotational periods $P_{v \sin i}$, which are upper limits of the true rotational periods, have been derived from radii and $v \sin i$ values and are given in Table 5.2. The radii have been determined based on luminosities and effective temperatures from Comerón et al. (1999, 2000) applying the Stefan-Boltzmann law.

It is noteworthy, that the observed periods P_{phot} are always – with the exception of Cha Hα 2 - larger than the calculated periods $P_{v \sin i}$ but do still agree with them when the errors are taken into account, hinting at a systematic effect. A $1\,\sigma$ error of $P_{v \sin i}$ with propagated errors of the luminosity $L_{\rm bol}$, the effective temperature $T_{\rm eff}$ and $v \sin i$ is given in Table 5.2. $P_{v \sin i}$ scales with $\sqrt{L_{\rm bol}}$, $T_{\rm eff}^{-2}$ and $v \sin i^{-1}$. Reasons for systematic deviations of the estimated $P_{v \sin i}$ from the observed $P_{\rm phot}$ may be either that the luminosities (bolometric correction, distance) have been systematically underestimated; the rotational velocities $v \sin i$ have been systematically overestimated; the effective temperatures have been systematically overestimated and/or the radii are systematically too small.

5.5.3 Radii of brown dwarfs

The radii of the very young brown dwarfs and brown dwarf candidates Cha Hα 1 to 12 estimated from luminosities and effective temperatures are ranging from 0.3 $R_\odot$ for Cha Hα 11 ($\sim$0.03 $M_\odot$) to 0.9 $R_\odot$ for Cha Hα 4 ($\sim$0.1 $M_\odot$). These radii are strikingly large for brown dwarfs but they are fully consistent with the extremely young age of the objects and the fact that they are still in a contracting stage. Models of Chabrier & Baraffe (1997) show that a brown dwarf with a mass of 0.06 $M_\odot$ has a radius of $\sim$0.55 $R_\odot$ at 3 Myr and a radius of $\sim$0.45 $R_\odot$ at 5 Myr in their calculations. Only after $\sim$500Myr, brown dwarfs have more or less shrunken to their final size of about 0.1 $R_\odot$ independent of their mass (Chabrier et al. 2000). After that age only a marginal further reduction of the size of a brown dwarf within the next 10 Gyr to 0.08–0.09 $R_\odot$ is expected. Compare also Fig. 1.4 taken from Burrows et al. (2001).

It is supposed that the young very low-mass objects in σ Orionis studied by Bailer-Jones & Mundt (2001) have similar radii as the Cha Hα objects because of the similar age of this cluster. Bailer-Jones & Mundt (2001) give an upper limit of 0.2 $R_\odot$ for all of their targets. This does not seem to apply for the objects in the σ Orionis cluster, which have ages within the range of 1 to 5 Myr and masses between 0.02 and 0.12 $M_\odot$. As an example, for the L1.5 dwarf S Ori 47 estimations of the effective temperature and the luminosity are available (Zapatero Osorio et al. 1999) indicating that the radius of this low-mass brown dwarf ($\sim$0.015 $M_\odot$) is as large as 0.35 $R_\odot$. The S Ori objects studied by Bailer-Jones & Mundt are of significantly higher mass and their rotational periods are therefore not necessarily below one day but they have rather values in the range of a few days. If the period of 7.5 h reported by Bailer-Jones & Mundt (2001) for S Ori 31 is the rotational period of this object, the rotational velocity would be about 100 km s^{-1} assuming a radius of 0.6 $R_\odot$. This would be surprisingly fast for such a young object. A measurement of the spectroscopic velocity $v \sin i$ of S Ori 31 would help to clear the cause of the 7.5 h periodicity. However, high-resolution spectroscopy for this faint object is challenging even with large telescopes.

5.5.4 Evolution of angular momentum

In the current picture of angular momentum evolution, young solar-mass stars as well as brown dwarfs are supposed to undergo a spin up due to contraction on the Hayashi track. Interaction with an accretion disk can hold up the acceleration of the rotation by magnetic braking until the inner disk is dissipated. As the star ages on the main sequence, angular momentum loss through stellar winds spins down the star again. In contrast, at the very low masses of brown dwarfs, there is supposed to be no braking due to winds, which would explain the observed (very)

fast rotation of old brown dwarfs, which have $v \sin i$ values ranging from 5 km s^{-1} up to 60 km s^{-1} (e.g. Basri & Marcy 1995, Martín et al 1997, Tinney & Reid 1998, Basri et al. 2000). Furthermore, brown dwarfs with ages between about 36 Myr and 1 Gyr seem to have rotational periods shorter than one day (see Sect. 5.1 for references). The lower age limit at about 36 Myr is set by rotational periods determined for brown dwarf candidates in the young cluster IC 4665 (Eislöffel & Scholz 2001), which has an age of ∼36 Myr (Mermilliod 1981).

However, the periods that have been measured for the three brown dwarf candidates Cha Hα 2, 3 and 6 range between about 2 and 3 days and are therefore larger than any period reported up to now for such low-mass objects. The relatively long rotational periods and moderately fast rotational velocities of the brown dwarf candidates in Cha I are explained naturally within the current picture of angular momentum evolution by the fact that they are still in an early contracting stage and/or they have suffered until very recently a braking due to their interaction with an accretion disk. The very young brown dwarfs in Cha I will most certainly spin up further during their continuous contraction and may very well reach the very high rotational velocities found for old field brown dwarfs.

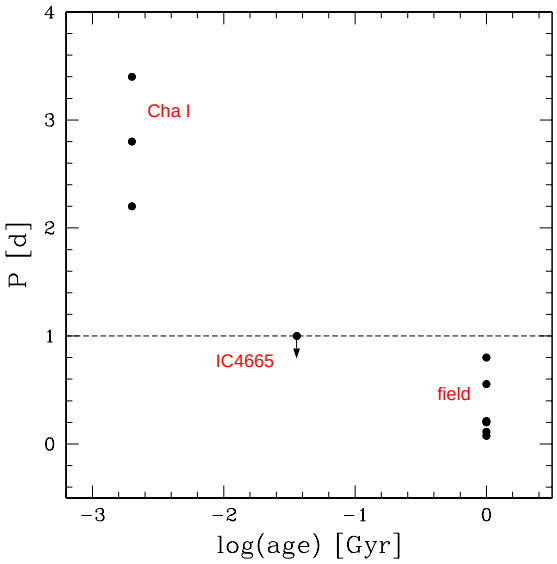

Figure 5.6: **Evolution of angular momentum from 1 Myr to 1 Gyr.** Rotational period P vs. age for Cha Hα 2, 3 and 6, brown dwarfs in the cluster IC4665 (Eislöffel & Scholz 2001) and brown dwarfs in the field (see Table 5.1 for references).

In Fig. 5.6 the available periods for brown dwarfs are plotted versus a logarithmic age scale. The derived rotation periods for brown dwarfs in Cha I at 1–5 Myr and those in the literature at >36 Myr give first indications that most of the acceleration of brown dwarfs takes place in the first 30 Myr or less of their lifetime. It is known that Cha Hα 2 and 6 have optically thick disks (Comerón et al. 2000), therefore magnetic braking due to interactions with the disk may play a role for them. This is suggested by the fact, that among the three brown dwarf candidates with determined periods, the one without a detected disk, Cha Hα 3, has the shortest period. If the interaction with the disk is responsible for the braking, the results from Eislöffel & Scholz (2001) indicate that brown dwarf inner disks

have been dissipated at an age of 36 Myr. These limits for the time scale of disk dissipation for brown dwarfs are in agreement with that for T Tauri stars, which are known to dissolve their inner disks within about the first 10 Myr (e.g. Calvet et al. 2000).

5.6 Summary

Based on the presented photometric i and R band observations, photometric periods have been determined for the three M6.5–M7 type brown dwarf candidates Cha Hα 2, Cha Hα 3 and Cha Hα 6 of 2.2 to 3.4 days. These are the longest photometric periods found for any brown dwarf so far. If interpreted as rotationally induced they correspond to moderately fast rotational velocities, which is fully consistent with their $v \sin i$ values (cf. Sect. 3.4) and their relatively large radii. Furthermore, periods have been also detected for the two M5–M5.5 type very low-mass stars B 34 and CHXR 78C.

The observed periodic variations of the brown dwarf candidates as well as of the T Tauri stars are interpreted as modulation of the flux at the rotation period due to magnetically driven surface features on the basis of a consistency with $v \sin i$ values as well as (R-i) color variations typical for spots. Furthermore, the temperatures even for the brown dwarfs in the sample are relatively high (> 2800 K) because the objects are very young. Therefore, the atmospheric gas should be sufficiently ionized for the formation of spots on one hand and the temperatures are too high for significant dust condensation and hence variabilities due to clouds on the other hand. These first indications for surface spots on very young brown dwarfs support the overall picture of magnetic activity of brown dwarfs, which is emerging in the last years: old (cool) brown dwarfs tend towards an absence of persistent activity, whereas very young brown dwarfs seem to have more in common with T Tauri stars as they are relatively active in terms of X-ray emission (e.g. Neuhäuser et al. 1999) and Hα emission.

The periods measured for the three brown dwarf candidates provide valuable data points in an as yet almost unexplored region of the substellar period-age diagram. A comparison of the determined rotational periods at the age of a few million years with rotational properties of older brown dwarfs (>36 Myr, Eislöffel & Scholz 2001) shows that most of the acceleration of brown dwarfs during the contraction phase takes place within the first 30 Myr or less and suggests that the disk dissipation for brown dwarfs occurs between 1–5 Myr and 36 Myr in agreement with disk dissipation time scales for T Tauri stars.

Last but not least, the measured periods for brown dwarfs at 1–5 Myr take us one step further towards scanning the evolution of periods for ages below 100 Myr and therefore to hopefully detect the expected plateau due to the onset of deuterium

burning predicted by theoretical calculations (e.g. Burrows et al. 2001, cf. also Fig. 1.4). This would provide a significant test of theoretical evolutionary models. A larger sample of brown dwarfs at various ages and in particular in the Megayear regime with known rotation rates is much needed not only to further constrain the substellar angular momentum evolution but also to allow a statistical treatment of rotation rates and activity indicators.

Chapter 6

Summary and outlook

Since the first brown dwarfs were detected in 1995, more than 300 of such objects intermediate between stars and planets have been found. However, the mechanism that leads to the formation of brown dwarfs is still poorly constrained. Its exploration is expected to provide valuable informations also for the formation processes of giant planets and (low-mass) stars. In the presented work a population of twelve very young bona fide and candidate brown dwarfs in the Cha I star forming region, Cha Hα 1 to 12 was studied in terms of their kinematic properties, the occurrence of multiple systems among them as well as their rotational characteristics. These brown dwarfs are only a few million years old and their observation allows insights into the formation and early evolution of brown dwarfs.

A variety of data obtained at numerous telescopes was presented, ranging from high-resolution spectra, over deep high-resolution space- and ground-based images to photometric time series:

High-resolution spectroscopic observations were conducted with the echelle spectrograph UVES attached to the 8.2 m Unit Telescope 2 of the Very Large Telescope at ESO. These observations allowed the measurement of radial and rotational velocities for such faint objects as the brown dwarfs in Cha I. A kinematic study of the sample showed that their radial velocity dispersion is relatively small and provided constraints for their formation. In addition, for nine bona fide and candidate brown dwarfs as well as for three very low-mass T Tauri stars in the field, spectra have been taken separated by a few weeks in order to search for radial velocity variations due to orbiting substellar (brown dwarf or planetary) companions.

Complementary to the radial velocity survey, a search for wide companions was performed by means of optical **high-resolution images** obtained with the Wide Field Planetary Camera on board the Hubble Space Telescope. Additional

ground-based images were taken in the near-infrared with SofI at the NTT and in the optical with FORS1 at the VLT. With the combination of the radial velocity and the direct imaging survey, a wide range of possible companion separations was covered with a sensitivity to detect companions as low mass as Jupiter. However, somewhat surprisingly no companions (neither spectroscopic nor visual) have been found hinting at a rather low multiplicity fraction of the studied brown dwarfs.

Finally, a **photometric monitoring campaign** at the Danish 1.5 m telescope at ESO has been carried out in order to study the time dependence of the brightness of the objects. Rotational periods have been measured for three brown dwarf candidates by tracing modulations of the light curves due to magnetically induced surface spots. The determined rotational periods along with rotational velocities derived from UVES spectra shed light on the rotational characteristics of very young substellar objects.

The UVES observations as well as the photometric monitoring campaign included also observations of very low-mass T Tauri stars in the field, which have masses near the substellar limit.

6.1 Kinematics of brown dwarfs in Cha I – constraints for their formation

It is still unknown, how brown dwarfs form. The mass distribution of companions (from planetary to stellar masses) to stars indicate that planets and stars form two entirely different populations. This suggests that brown dwarfs either are the high-mass extension of planets or the low-mass extension of stars. In this picture, brown dwarfs may either form like planets in a disk around a star or like stars by direct collapse of Jeans-unstable cloud cores. However, the finding of an almost complete absence of brown dwarfs as close companions to stars (brown dwarf desert) render a planet-like formation unlikely. On the other hand, a star-like formation scenario for brown dwarfs may be the formation of brown dwarfs out of relatively small, dense cloud cores. However, it is not clear if cloud cores exist which are cold and dense enough to become gravitationally unstable for brown dwarf masses. Recently, it has been proposed alternatively, that brown dwarfs are ejected protostars which have been cut off from the gas reservoir in the early accretion phase of the star formation process and could have therefore not accreted to stellar masses (Reipurth & Clarke 2001).

A kinematic study of very young brown dwarfs in the Cha I star forming cloud based on the measurement of precise radial velocities from high-resolution UVES spectra of nine of the twelve Cha Hα objects was performed. It indicates that the

radial velocity dispersion of the very young bona fide and candidate brown dwarfs in Cha I is relatively small. The radial velocity dispersion of the brown dwarfs was determined to $2.2\,\mathrm{km\,s^{-1}}$ in comparison with that one of the surrounding molecular gas of $1.2\,\mathrm{km\,s^{-1}}$ and that one of T Tauri stars in the field of $3.6\,\mathrm{km\,s^{-1}}$. This gives suggestive evidence that there is no run-away brown dwarf among the studied sample. It cannot be ruled out that some of them have a larger three-dimensional velocity dispersion. However, brown dwarfs born within the observed field and ejected during the early accretion phase in directions with a significant fraction perpendicular to the line-of-sight, would have flown out of the field a long time ago. This is true even for the smallest ejection velocities calculated by theorists. Therefore, the measurement of radial velocities is the very method to test if objects born in the field have significantly high velocities due to dynamical interactions during their formation process.

Very recent dynamical calculations (Bate et al. 2002, Sterzik & Durisen 2002) hint at rather small ejection velocities suggesting the possibility that the imprint of the ejection in the kinematics might not be an observable effect. They predict a velocity dispersion of ejected brown dwarfs of $2\,\mathrm{km\,s^{-1}}$ in three-dimensions and $1.2\,\mathrm{km\,s^{-1}}$ in one-dimension. On the other hand, they predict that 10% of the brown dwarfs have a larger velocity than $5\,\mathrm{km\,s^{-1}}$ due to dynamical interactions. The velocities of the bona fide and candidate brown dwarfs in Cha I cover a total range of only 2.6 km/s. Therefore, it is concluded that the ejection-model for the formation of brown dwarfs is not a likely formation mechanism for the brown dwarfs in Cha I.

6.2 Multiplicity of brown dwarfs and very low-mass stars in Cha I

The study of brown dwarf multiple systems and their properties, like binary frequency, mass ratio and orbital separation, provide important clues to their formation history. In addition, binaries are our only means to determine accurate masses and therefore provide a valuable test of evolutionary models. About four confirmed brown dwarf binaries (brown dwarf–brown dwarf pairs) are known to date, one of them, PPl 15 is a spectroscopic binary (Basri & Martín 1999), the others are wide binaries with separations in the range of 1 to 10 AU. About the same number of candidates for brown dwarf binaries are awaiting confirmation. There is no planet known orbiting a brown dwarf. The lowest mass star with a radial velocity planet candidate is the M4-dwarf Gl 876, which has a mass of 0.3–0.4 $\mathrm{M_\odot}$ (Delfosse et al. 1998b).

In order to study the multiplicity of the brown dwarf population in Cha I, a radial velocity survey for close spectroscopic companions as well as a deep direct

imaging survey for wide visual companions have been carried out. With these two complementary search methods, a wide range of possible companion separations has been covered. The exact separations depend on the companion masses. For example, for brown dwarf companions ($>13\,M_{Jup}$) to the targets, separations <3 AU and between 50 and 1000 AU were covered. With more restricted separations (<0.1 AU and 300–1000 AU) the surveys were sensitive also to companion masses down to $1\,M_{Jup}$.

The radial velocity survey was carried out with the high-resolution echelle spectrograph UVES at the VLT. Time-resolved spectra have been taken of nine bona fide and candidate brown dwarfs, Cha Hα 1–8 and 12, as well as of three very low-mass T Tauri stars, B 34, CHXR 74 and Sz 23. The radial velocities for eight out of nine observed bona fide and candidate brown dwarfs were found to be constant within the measurements uncertainties. Upper limits for the companion mass $M_2 \sin i$ have been derived and range for them between a tenth of a Jupiter mass and 1–2 Jupiter masses. The very low-mass T Tauri star B 34 displays also a constant radial velocity ($\leq 70\,m\,s^{-1}$) setting the upper limit for a companion mass $M_2 \sin i$ to $0.3\,M_{Jup}$. The radial velocities for Cha Hα 4 and the very low-mas T Tauri stars CHXR 74 and Sz 23 show small ($\leq 600\,m\,s^{-1}$) but significant variations of their radial velocity, which correspond to companion masses $M_2 \sin i$ of $0.8\,M_{Jup}$, $2.6\,M_{Jup}$ and $7\,M_{Jup}$, respectively. The nature of these variations has still to be clarified. Such small amplitude variations can also be mimicked by surface spots as has been shown for T Tauri stars (Guenther et al. 2000). From the results of the radial velocity survey, it is concluded that spectroscopic binaries among the studied brown dwarfs in Cha I as well as close-in giant planets around them are rather rare.

The direct imaging survey for wide visual companions around Cha Hα 1–12 was carried out with deep HST as well as NTT and VLT images. A companion candidate has been found around Cha Hα 5 at a separation of $1.5''$ (~ 240 AU). Its color is consistent with an early- to mid-L type object at the distance of the primary. However, recent follow-up spectroscopy of this companion candidate (Neuhäuser et al. 2002b) showed that it is a highly reddened K-type background star. There are hints of binarity of Cha Hα 2 from an elongated PSF in HST images. Follow-up images are planned in order to confirm or reject the binary hypothesis for Cha Hα 2.

To summarize, despite the hints at Cha Hα 2 being a wide binary from HST images no indications for brown dwarf binaries among the twelve bona fide and candidate brown dwarfs in Cha I have been found. Furthermore, despite the variations of the radial velocity of Cha Hα 4, which could be due to a companion of less than $1\,M_{Jup}$, no evidence for low-mass companions around the twelve targets has been found. There is the possibility that there are planetary mass companions with masses below one Jupiter mass since the presented observations were

not sensitive enough to detect those. Furthermore, spectroscopic binaries in the sample might not have been detected due to the non-observation at the critical orbital phases. However, the overall picture that arises is that the multiplicity fraction of the studied brown dwarfs is rather low ($\leq 10\%$).

This seems to be in contrast with the high multiplicity fraction observed for very young stars and may suggest that brown dwarfs form not by direct collapse of unstable cloud cores as stars. However, a significant comparison of the multiplicity fraction of stars and brown dwarfs at very young ages is still hampered by small-number statistics in the substellar regime. Such a study has to compare multiplicity fractions in a certain separation range, which has to agree for both samples. Furthermore, it is possible that the gravitational collapse of cloud cores of brown dwarf masses does not yield as much multiple systems as the collapse of clouds of solar masses. In addition, stars can have companions, which have only a tenth of the mass of the primary, whereas a companion of a brown dwarf with such a low mass ratio would be already a planet. However, there is still a lot to do for observers as well as for theorists in order to understand in which way objects of brown dwarf masses are formed.

6.3 Rotation rates, surface spots and substellar angular momentum evolution

Rotation rates are fundamental (sub)stellar properties. Their knowledge for objects covering a wide range of ages and masses is important for the understanding of the evolution of angular momentum. Scanning the period–age diagram for ages below 100 Myr observationally for brown dwarfs provides in addition, a test of substellar evolutionary theories since the onset of deuterium burning is expected to have an observable effect on the angular momentum evolution. The contraction of brown dwarfs is temporarily decelerated or even stopped in the first several million years of their lifetime due to the ignition of deuterium (e.g. Burrows et al. 2001). However, since age estimates are also often model dependent, the significance of such a test might be somewhat limited. Furthermore, rotation rates are critical parameters for rotationally induced phenomena, like dynamo activity (supposed to cause surface spots) and meteorological processes.

Based on photometric i and R band observations, rotational periods have been determined for the three M6.5–M7 type brown dwarf candidates Cha Hα 2, Cha Hα 3 and Cha Hα 6 of 2.2 to 3.4 days. In addition, projected rotational velocities $v \sin i$ have been measured from line broadening of spectral features in UVES spectra for the nine bona fide and candidate brown dwarfs Cha Hα 1–8 and Cha Hα 12 in the range of 8 km s^{-1} to 26 km s^{-1}.

The photometric periods for the three brown dwarf candidates are the longest periods found for any brown dwarf so far. If interpreted as rotationally induced they correspond to moderately fast rotational velocities, which is fully consistent with their $v \sin i$ values and their relatively large radii.

Furthermore, photometric periods have been also determined for the two M5–M5.5 type very low-mass stars B 34 and CHXR 78C as well as $v \sin i$ values for the three M2.5–M5 type very low-mass stars B 34, CHXR 74 and Sz 23.

The observed periodic variations of the brown dwarf candidates as well as of the T Tauri stars are interpreted as modulation of the flux at the rotation period due to magnetically driven surface features on the basis of a consistency check with $v \sin i$ values as well as (R-i) color variations typical for spots. Furthermore, the temperatures even for the brown dwarfs in the sample are relatively high (> 2800 K) because the objects are very young. Therefore, the atmospheric gas should be sufficiently ionized for the formation of spots on one hand and the temperatures are too high for significant dust condensation and hence variabilities due to clouds on the other hand. These first indications for surface spots on very young brown dwarfs support the picture of magnetic activity on brown dwarfs which is emerging in the last years: old (cool) brown dwarfs tend toward an absence of persistent activity, whereas very young brown dwarfs seem to have more in common with T Tauri stars as they are relatively active in terms of X-ray emission (e.g. Neuhäuser et al. 1999), Hα emission and spot activity (this work). This is not surprising since young very low-mass T Tauri stars (mid-M type) and young relatively high-mass brown dwarfs (late-M) are located next to each other in the HRD, while old brown dwarfs (L- and T-type) are somewhat separated from them.

The periods measured for the three brown dwarf candidates at 1–5 Myr provide valuable data points in an as yet almost unexplored region of the substellar period-age diagram. They take us one step further towards constraining the substellar evolution of angular momentum for ages below 100 Myr. A comparison of the determined rotational periods at the age of a few million years with rotational properties of older brown dwarfs (>36 Myr, Eislöffel & Scholz 2001) shows that most of the acceleration of brown dwarfs during the contraction phase takes place within the first 30 Myr or less. It is known that Cha Hα 2 and 6 have optically thick disks (Comerón et al. 2000), therefore magnetic braking due to interactions with the disk may play a role for them. This is suggested by the fact, that among the three brown dwarf candidates with determined periods, the one without a detected disk, Cha Hα 3, has the shortest period. If the interaction with the disk is responsible for the braking, the results from Eislöffel & Scholz (2001) indicate that brown dwarf inner disks have been dissipated at an age of 36 Myr. These limits for the time scale of disk dissipation for brown dwarfs are in agreement with that for T Tauri stars, which are known to dissolve their inner disks within

about the first 10 Myr (e.g. Calvet et al. 2000).

6.4 Outlook

In the presented work kinematic and rotational properties as well as the multiplicity fraction of a population of twelve very young brown dwarfs in the Cha I star forming region have been determined. The determined fundamental properties of these extremely young brown dwarfs have been applied to constrain the formation and early evolution of brown dwarfs.

Constantly, new brown dwarfs and brown dwarf candidates are discovered in star forming regions. For example, López Martí & Eislöffel (2001) found more than 50 new brown dwarf candidates in the Cha I star forming cloud. In addition, new brown dwarf candidates have been identified in the Lupus and CrA star forming regions (Comerón et al. 2002, Fernandéz & Comerón 2001). Also in Taurus, about a dozen brown dwarf candidates of spectral type M6–M9 are known (see Stelzer & Neuhäuser 2001 for a list). These discoveries enable us to determine fundamental properties for a much larger number of young brown dwarfs and in addition to compare the properties of brown dwarfs in different star forming regions.

Further observational exploration of the formation mechanism of brown dwarfs is one of the main topics in brown dwarf research. Additional tests of the ejection-scenario for the formation of brown dwarfs should include an extension of the presented kinematic study carried out for brown dwarfs in Cha I to the newly found brown dwarfs within this star forming cloud in order to achieve a better statistical basis. A determination of precise radial velocities for additional brown dwarfs with UVES at the VLT and comparison of their radial velocity dispersion with predictions from theoretical dynamical calculations are planned. Furthermore, kinematic studies should be carried out also for brown dwarfs in other star forming regions in order to compare the results with that one for Cha I. We will be able to examine three-dimensional velocities in a few years, when proper motions will be available for the studied brown dwarfs in Cha I. It is planned to re-observe them with a high-resolution infrared detector ($\sim$100 to $\sim$200 milli arc sec pixel scale), for example with ISAAC at the VLT. An additional test of the ejection-scenario is the check for a *halo* of ejected brown dwarfs around Cha I and other star forming clouds and young clusters.

A further constraint of the substellar angular momentum evolution is also much-needed. The rotation rates determined in this work for ages of a few million years should be completed by additional measurements of rotation rates for a large sample of young brown dwarfs at various ages. Furthermore, this will allow a statistical treatment of rotation rates and activity indicators. Photometric monitoring campaigns of newly detected brown dwarfs in Cha I, Lupus and Taurus

at small (1.5 m) to medium size telescopes (2 m–2.5 m) will provide the necessary data to determine rotational periods for a statistically significant number of young brown dwarfs.

For objects where significant radial velocity variations have been detected (two very low-mass T Tauri stars and one brown dwarf candidate), follow-up observations are planned in order to clarify the nature of the detected variations. Furthermore, follow-up deep imaging for example with CONICA/NAOS at the VLT of Cha Hα 2 will allow the confirmation or rejection of the object as a brown dwarf binary. Last but not least, the search for companions to brown dwarfs by means of radial velocity and direct imaging surveys should be continued despite the finding that the multiplicity rate for the Cha I brown dwarfs is apparently rather low, since multiple systems provide the unique possibility to constrain brown dwarf masses and therefore valuable constraints for theoretical evolutionary models.

Appendix

The observing log for UVES observations of brown dwarfs and very low-mass stars is given on the following two pages. It lists all individual exposures and radial velocities. This is a more detailed listing of the radial velocities than given in Sect. 3 (Table 3.1 and 3.2) since for several objects the radial velocity given in Table 3.1 and 3.2 for one night is a mean value based on two consecutive single spectra. This procedure allows a solid estimation of the error. The individual values are given here (Table 6.1 and 6.2).

Table 6.1: **Observing log: UVES spectroscopy of brown dwarfs and very low-mass stars in Cha I.** Given are the date of the observation, heliocentric Julian day (HJD) at the middle of the exposure, the exposure time and the radial velocity RV for each spectrum.

Object	Date	HJD	Exposure [s]	RV [km s^{-1}]
Cha Hα 1	2000 Apr 04	2451638.56395	2x1650	16.167
	2000 Apr 24	2451658.57346	2x1650	16.648
Cha Hα 2	2000 Apr 04	2451638.59431	1x1029	16.015
	2000 Apr 24	2451658.60407	1x1029	16.282
Cha Hα 3	2000 Apr 04	2451639.49340	1x899	14.357
	2000 Apr 24	2451658.61991	1x899	14.758
Cha Hα 4	2000 Mar 14	2451617.72337	1x2200	15.176
	2000 Mar 14	2451617.74954	1x2200	14.642
	2000 Mar 24	2451627.79079	1x2200	14.732
	2000 Mar 24	2451627.81697	1x2200	14.999
	2000 Mar 31	2451635.51085	1x2200	14.773
	2000 Apr 23	2451658.50840	1x2200	14.941
	2000 Apr 23	2451658.53460	1x2200	14.875
	2000 May 22	2451687.49289	1x2200	14.774
	2000 May 23	2451687.51900	1x2200	14.885
	2002 Jan 17	2452291.73197	2x1100	14.761
	2002 Jan 17	2452291.75976	2x1100	15.614
	2002 Jan 17	2452291.79010	2x1100	14.661
	2002 Jan 17	2452291.81794	2x1100	15.260
	2002 Jan 17	2452291.84586	2x1100	14.450
	2002 Jan 18	2452292.81113	2x1100	14.669
	2002 Jan 18	2452292.83902	2x1100	14.839
	2002 Jan 24	2452298.69149	2x1100	14.575
	2002 Jan 24	2452298.71931	2x1100	14.694
	2002 Feb 02	2452307.70591	2x1100	15.338
	2002 Feb 02	2452307.73367	2x1100	14.790
	2002 Feb 04	2452309.72831	2x1100	14.821
	2002 Feb 04	2452309.75613	2x1100	14.820
	2002 Feb 13	2452318.70523	2x1100	14.939
	2002 Feb 13	2452318.73306	2x1100	15.031
Cha Hα 5	2000 Apr 05	2451639.51485	1x800	15.499
	2000 Apr 24	2451658.63522	1x800	15.446
Cha Hα 6	2000 Apr 05	2451639.58967	1x1029	16.093
	2000 Apr 24	2451658.65099	1x1029	16.652

Table 6.2: **Observing log: UVES spectroscopy of brown dwarfs and very low-mass stars in Cha I.** Given are the date of the observation, heliocentric Julian day (HJD) at the middle of the exposure, the exposure time and the radial velocity RV for each spectrum.

Object	Date	HJD	Exposure [s]	RV [km s^{-1}]
Cha Hα 7	2000 Apr 05	2451639.55225	2x2150	16.513
	2000 Apr 24	2451658.68756	2x2150	17.664
Cha Hα 8	2000 Apr 05	2451639.61095	1x1599	14.787
	2000 Apr 24	2451658.72597	1x1600	14.935
Cha Hα 12	2000 Apr 05	2451639.63487	1x1599	15.021
	2000 Apr 25	2451659.59469	1x1600	13.905
B 34	2000 Mar 13	2451616.82387	1x1350	15.730
	2000 Mar 13	2451616.84023	1x1350	15.859
	2000 Mar 25	2451628.61377	1x2700	15.746
	2000 Mar 31	2451634.54665	1x1350	15.687
	2000 Mar 31	2451634.56298	1x1350	15.810
	2000 Apr 23	2451657.52652	1x1350	15.591
	2000 Apr 23	2451657.54287	1x1350	15.743
	2000 May 21	2451686.50566	1x1350	15.720
	2000 May 22	2451686.52202	1x1350	15.908
CHXR 74	2000 Mar 13	2451616.78332	1x600	15.313
	2000 Mar 13	2451616.79097	1x600	15.439
	2000 Mar 31	2451634.51710	1x600	14.537
	2000 Mar 31	2451634.52473	1x600	14.460
	2000 Apr 22	2451656.50861	1x600	15.048
	2000 Apr 22	2451656.51633	1x600	14.660
	2000 May 21	2451686.47878	1x600	14.320
	2000 May 21	2451686.48644	1x600	14.232
Sz 23	2000 Mar 14	2451617.68093	2x1350	14.652
	2000 Mar 25	2451628.66914	2x1350	15.926
	2000 Mar 31	2451634.58325	1x1350	15.656
	2000 Mar 31	2451634.59958	1x1350	15.472
	2000 Apr 22	2451657.48819	1x1350	14.575
	2000 Apr 22	2451657.50452	1x1350	14.905
	2000 May 20	2451685.47992	1x1350	15.288
	2000 May 20	2451685.49632	1x1350	15.178

References

Ackerman, A.S. Marley M.S. 2001, ApJ 556, 872

Allard F., Hauschildt P.H., Baraffe I., Chabrier G. 1996, ApJ 465, L123

Allard F., Hauschildt P.H., Alexander D.R., Starrfield S. 1997 ARA&A 35, 137

Apai D., Pascucci I., Henning Th. et al. 2002, AJ 573, L115

Bailer-Jones C.A.L., Mundt R. 1999, A&A 348, 800

Bailer-Jones C.A.L., Mundt R. 2001, A&A 367, 218

Balthasar H., Thiele U., Wöhl H. 1982, A&A 114, 357

Baraffe I., Chabrier G., Allard F., Hauschildt P.H. 1995, ApJL 446, 35

Baraffe I., Chabrier G., Allard F., Hauschildt P.H. 1997, A&A 327, 1054

Baraffe I., Chabrier G., Allard F., Hauschildt P.H. 1998, A&A 337, 403

Baraffe I., Chabrier G., Allard F., Hauschildt P.H. 2002, A&A 382, 563

Basri G., Marcy G.W. 1995, AJ 109, 762

Basri G., Marcy G.W. 1997, 'Early Hints on the Substellar Mass Function'. In: *AIP Conf. Proc. 393, Star Formation, Near and Far*, ed. by S. Holt, L.G. Mundy, New York, p.228

Basri G., Martín E.L. 1999, ApJ 118, 2460

Basri G. 2000, ARA&A 38, 485

Basri G., Mohanty S., Allard F. et al. 2000, ApJ 538, 363

Bate M.R., Bonnell I.A., Bromm V. 2002, MNRAS 332, L65

Bejár V.J.S., Zapatero Osorio M.R., Rebolo R. 1999, ApJ 521, 671

Berger E. 2002, ApJ 572, 503

Bessel M.S., Brett M.J. 1988, PASP 100, 1134

Bildsten L., Brown E.F., Matzner C.D. Ushomirsky G. 1997, ApJ 482, 442

Bodenheimer P. 1985 'Evolution of the giant planets'. In: *Protostars and Planets II*, ed. by D.C. Black, M.S. Matthews, Univ. of Arizona Press, Tucson, p. 393

Böhm-Vitense E. 1958, Zeitschrift für Astrophysik, Vol. 46, p.108

Boss A.P. 1997, Science 276, 1836

Boss A.P. 1998, AJ 503, 923

Boss A.P. 2001, ApJ 563, 367

Bouvier J. 1990, AJ 99, 946

Bouvier J., Cabrit S., Fernández M., Martín E.L., Matthews J.M. 1993, A&A, 272, 176

Burgasser A.J., Kirkpatrick J.D., Brown M.E. et al. 1999, AJ 522, L65

Burgasser A.J., Kirkpatrick J.D., Reid I.N., Liebert J. Gizis J.E., Brown M.E. 2000a, AJ 120, 473

Burgasser A.J., Kirkpatrick J.., Cutri R.M. et al. 2000b, ApJ, 531, L57

Burgasser A.J., Kirkpatrick J.D., Brown M.E. et al. 2002, ApJ 564, 421

Burrows A., Liebert J. 1993, Rev. Mod. Phys. 65, 301

Burrows A., Marley M., Hubbard W.B. et al. 1997 ApJ 491, 856

Burrows A., Sharp C.M. 1999, ApJ 512, 843

Burrows A., Hubbard W.B., Lunine J.I., Liebert J. 2001, Rev. Mod. Phys. 73, 3

Caccin B., Cavallini F., Ceppatelli G., Righini A., Sambuco A.M. 1985, A&A 149, 357

Chabrier G., Baraffe I., Plez B. 1996, ApJ 459, L91

Chabrier G., Baraffe I. 1997, A&A 327, 1039

Chabrier G., Baraffe I. 2000, ARA&A 38, 337

Chabrier G., Baraffe I., Allard F., Hauschildt P.H. 2000 ApJ, 542, 464

Calvet N., Hartmann L., Strom S.E. 2000, 'Evolution of Disk Accretion', In: *Protostars and Planets IV*, ed. by Mannings V., Boss A.P., Russell S.S., Univ. of Arizona Press, Tucson, p. 377

Charbonneau D., Brown T.M., Latham D.W., Mayor M. 2000, ApJ 529, L45

Clarke F.J., Tinney C.G., Covey K.R. 2002, MNRAS 332, 361

Close L.M., Potter D., Brandner W. et al. 2002a, ApJ 566, 1095

Close L.M., Siegler N., Potter D., Brandner W., Liebert J. 2002b, ApJ 567, L53

Comerón F., Rieke G.H., Neuhäuser R. 1999, A&A 343, 477

Comerón F., Neuhäuser R., Kaas A.A. 2000, A&A 359, 269

Comerón F. et al. 2002, in prep.

Covino E., Alcalá J.M, Allain S. et al. 1997, A&A 328, 187

Cumming A., Marcy G.W., Butler R.P. 1999, ApJ 526, 890

D'Antona F., Mazzitelli I. 1985, ApJ 296, 502

D'Antona F., Mazzitelli I. 1994, ApJS 90, 467

D'Antona F., Mazzitelli I. 1997, Mem. Soc. Astron. Ital. 68, 807

DeCampli W.M., Cameron A.G.W. 1979, Icarus 38, 367

Dekker H., D'Odorico S., Kaufer A., Delabre B., Kotzlowski H. 2000, 'Design, construction, and performance of UVES, the echelle spectrograph for the UT2 Kueyen Telescope at the ESO Paranal Observatory'. In: SPIE Vol. 4008, p. 534, ed. by M.Iye, A.Moorwood

Delfosse X., Tinney C.G., Forveille T. et al. 1997, A&A 327, L25

Delfosse X., Forveille T., Perrier C., Mayor M. 1998a, A&A 331, 581

Delfosse X., Forveille T., Mayor M. et al. 1998b, A&A 338, L67

Delgado-Donate E.J., Clarke C.J., Bate M.R. 2002, 'The Ejection of Brown Dwarfs from Unstable Multiples'. In: *Brown dwarfs. Proceedings of IAU Colloquium No. 211*, held in Hawai'i, USA, May 20–24 2002, ed. by Martín E., in press

Dubath P., Reipurth B., Mayor M. 1996, A&A 308, 107

Durisen R.H., Sterzik M.F., Pickett B.K. 2001, A&A 371, 952

Durney B.R., De Young D.S., Roxburgh I.W. 1993, SoPh 145, 207

Dworetsky M.M. 1983, MNRAS 203, 917

Eislöffel J., Scholz A. 2001, 'Rotation and Atmospheres of Brown Dwarfs'. In: *Origins of stars and planets: The VLT view*, ESO workshop, Garching, Germany, April 24-27, 2001, in press

Els S.G., Sterzik M.F., Marchis F. et al. 2001, A&A 370, L1

Fegley B., Lodders K. 1996, ApJ 472, l37

Feigelson E.D., Broos P., Gaffney J.A. et al. 2002, ApJ in press, astro-ph/0203316

Fernández M., Comerón F. 2001, A&A, 380, 264

Fleming T.A., Giampapa M.S., Schmitt J.H.M.M., Bookbinder J.A. 1993, ApJ 410, 387

Garmire G., Feigelson E.D., Broos P. et al. 2000, ApJ 120, 1426

Gelino C.R., Marley M.S. Holtzmann J.A., Ackermann A.S., Lodders K. 2002, ApJ 577, in press, astro-ph/0205305

Ghez A.M., Neugebauer G., Matthews K. 1993, AJ 106, 2005

Ghez A.M., McCarthy D.W., Patience J.L., Beck T.L. 1997, ApJ 481, 378

Giampapa M. S., Rosner R., Kashyap V., Fleming T. A., Schmitt J. H. M. M., Bookbinder J. A. 1996, ApJ 463, 707

Gizis J.E., Monet D.G., Reid I.N. et al. 2000, AJ 120, 1085

Gizis J.E., Kirkpatrick J.D., Burgasser A. et al. 2001, ApJ 551, L163

Guenther E.W., Joergens V., Neuhäuser R. et al. 2000, 'A spectroscopic and photometric survey for pre-main sequence binaries'. In: *Birth and Evolution of Binary Stars*, IAU Symposium No. 200, Potsdam, Germany, April 10–15, ed. by B. Reipurth, H. Zinnecker (ASP Conference Series, in press)

Guenther E.W., Neuhäuser R., Huélamo N., Brandner W., Alves J. 2001, A&A 365, 514

Guenther E.W., Wuchterl G. 2002, 'Searching for planets of brown dwarfs', In: *Brown dwarfs. Proceedings of IAU Colloquium No. 211*, held in Hawai'i, USA, May 20–24 2002, ed. by Martín E., in press

Halbwachs J.L., Arenou F., Mayor M., Udry S., Queloz D. 2000, A&A 355, 581

Hawley S.L., Covey K.R., Knapp G.R. et al. 2002, AJ 123, 3409

Imanishi K., Tsujimoto M., Koyama K. 2001, ApJ 563, 361

Joergens V., Guenther E., Neuhäuser R. et al. 2001 'Multiplicity of young brown dwarfs in Cha I'. In: *Origins of stars and planets: The VLT view*, ESO workshop, Garching, Germany, April 24-27, 2001, in press, astro-ph/0106185

Joergens V., Guenther E. 2001, A&A 379, L9

Joergens V., Fernandéz M., Neuhäuser R. 2002, A&A subm.

Jorissen A., Mayor M., Udry S. 2001, A&A 379, 992

Kenworthy M., Hofmann K.-H., Close L. et al. 2001, ApJ 554, L67

Kirkpatrick J.D., Reid I.N., Liebert J. et al. 1999a, ApJ 519, 802

Kirkpatrick J.D., Allard F., Bida T. et al. 1999b, ApJ 519, 834

Kirkpatrick J.D., Reid I.N., Liebert J. et al. 2000, AJ 120, 447

Kirkpatrick J.D., Dahn C.C., Monet D.G. et al. 2001, AJ 121, 3235

Koerner D.W., Kirkpatrick J.D., McElwain M.W., Bonaventura N.R. 1999, ApJ 526, L25

Köhler R., Kunkel M., Leinert Ch., Zinnecker H. 2000, A&A 356, 541

Kraft R.P. 1967, ApJ 150, 551

Kumar S. 1962, AJ 67, 579

Kumar S. 1963, ApJ 137, 1121

Lane B.F., Zapatero Osorio M.R., Britton M.C., Martín E.L., Kulkarni S.R. 2001, ApJ 560, 390

Latham D.W., Stefanik R.P., Mazeh T., Mayor M., Burki G. 1989, Nature 339, 38

Lowrance P.J., McCarthy C., Becklin E.E. et al. 1999 ApJ 512, L69

Lowrance P.J., Schneider G., Kirkpatrick J.P. et al. 2000, ApJ 541, 390

Leggett S.K., Allard F., Berriman G., Dahn C.C., Hauschildt P.H. 1996, ApJS 104, 117

Leggett S.K., Allard F., Hauschildt P.H. 1998, ApJ 509, 836

Leggett S.K., Toomey D.W., Geballe T.R., Brown R.H. 1999 ApJ 517, L139

Leggett S.K., Golimowski D.A., Fan X. et al. 2002, ApJ, 564, 452

Leinert Ch., Zinnecker H., Weitzel N. et al. 1993, A&A 278, 129

Liebert J., Kirkpatrick J.D., Reid I.N., Fisher M.D. 1999, ApJ 519, 345

Lin D.N.C., Papaloizou J.C.B., Terquem C., Bryden G., Ida S. 'Orbital evolution and planet-star tidal interaction'. In: *Protostars and Planets IV*, ed. by Mannings V., Boss A.P., Russell S.S., Univ. of Arizona Press, Tucson, p.1111

Liu M.C., Fischer D.A., Graham J.R. et al. 2002, ApJ 571, 519

López Martí B., Eislöffel J. 2001, 'WFI Survey of Brown Dwarfs in the Chamaeleon I Cloud'. In: *Proceeding of the Joint European and National Meeting JENAM 2001 of the European Astronomical Society and the Astronomische Gesellschaft*, held in Munich, Germany, September 10-15, 2001, AGM, 18, P30

Luhman K.L. 1999, ApJ 525, 466

Marchal L. 2002, 'Multiplicity statistic of brown dwarfs and very low mass stars'. In: *Brown dwarfs. Proceedings of IAU Colloquium No. 211*, held in Hawai'i, USA, May 20–24 2002, ed. by Martín E., in press

Marcy G.W., Butler R.P. 1998, ARA&A, 36, 57

Marcy G.W., Cochran W.D., Mayor M. 2000, 'Extrasolar planets around main-sequence stars'. In: *Protostars and Planets IV*, ed. by Mannings V., Boss A.P., Russell S.S., Univ. of Arizona Press, Tucson, p. 1285

Marilli E., Catalano S., Trigilio C. 1986, A&A 167, 297

Martín E.L., Basri G., Delfosse X., Forveille T. 1997, A&A 327, L29

Martín E.L., Brandner W., Basri G. 1999, Science 283, 1718

Martín E.L., Brandner W., Bouvier J. et al. 2000a ApJ 543, 299

Martín E.L., Koresko C.D., Kulkarni S.R., Lane B.F., Wizinowich P.L. 2000b, ApJ 529, L37

Martín E.L., Zapatero Osorio M. R., Lehto H.J. 2001, ApJ 557, 822

Mayor M., Queloz D. 1995, Nature 378, 355

Mayor M., Queloz D., Udry S. 1998a, 'Mass Function and Orbital Distributions of Substellar Companions'. In: *Brown Dwarfs and Extrasolar Planets*, ed. by R. Rebolo, E.L. Martín, M.R. Zapatero Osorio, San Francisco, p.140

Mayor M., Udry S., Queloz D. 1998b, 'The Mass Function Below the Substellar Limit'. In: *ASP Conf. Ser. 154, Tenth Cambridge Workshop on Cool Stars, Stellar Systems, and the Sun*, ed. by R. Donahue, J. Bookbinder, San Francisco, p.77

Mermilliod J.C. 1981, A&A 97, 235

Meyer F., Meyer-Hofmeister E. 1999, A&A 341, 23

Mizuno A., Hayakawa T., Tachihara K. et al. 1999, PASJ 51, 859

Moffat A.F.J. 1969, A&A 3, 455

Mohanty S., Basri G., Shu F., Allard F., Chabrier G. 2002, ApJ 571, 469

Mokler F., Stelzer B. 2002, A&A, in press

Muench A.A., Alves J., Lada C.J., Lada E.A. 2001, ApJ 558, L51

Nakajima T., Oppenheimer B.R., Kulkarni S.R. et al. 1995, Nature 378, 463

Natta A., Testi L. 2001, A&A 376, L22

Neuhäuser R., Sterzik M.F., Schmitt J.H.M.M., Wichmann R., Krautter J. 1995, A&A 297, 391

Neuhäuser R., Comerón F. 1998, Science 282, 83

Neuhäuser R., Comerón F. 1999, A&A 350, 612

Neuhäuser R., Briceño C., Comerón F. et al. 1999, A&A 343, 883

Neuhäuser R., Guenther E.W., Brandner W. et al. 2000, A&A 360, L39

Neuhäuser R., Brandner W., Alves J., Joergens V., Comerón F. 2002a, A&A 384, 999

Neuhäuser R., Brandner W., Guenther E. 2002b, 'VLT spectra of the companion candidate Cha Hα 5/cc1'. In: *Brown dwarfs. Proceedings of IAU Colloquium No. 211*, held in Hawai'i, USA, May 20–24 2002, ed. by Martín E., in press

Noyes R.W., Hartmann L.W., Baliunas S.L., Duncan D.K., Vaughan A.H. 1984, ApJ 279, 763

Oppenheimer B.R., Kulkarni S.R., Matthews K., Nakajima T. 1995 Science 270, 1478

Persi P., Marenzi A.R., Olofsson G. et al. 2000, A&A, 357, 219

Pickett B.K., Durisen R.H., Cassen P., Mejia A.C. 2000, ApJ 540, L95

Potter D., Martín E.L., Cushing M.C. et al. 2002, ApJ 567, L133

Preibisch T., Zinnecker H. 2001, AJ 122, 866

Preibisch T., Zinnecker H. 2002, AJ 123, 1613

Randich S. 1997, Mem. Soc. Astron. Ital. 68, 971

Rädler K.-H., Wiedemann E., Meinel R., Brandenburg A., Tuominen, I. 1990, A&A 239, 413

Rebolo R., Martín E.L., Magazzú A. 1992, ApJ 389, L83

Rebolo R., Zapatero Osorio M.R., Martín E.L. 1995, Nature 377, 129

Rebolo R., Zapatero-Osorio M.R., Madruga S. et al. 1998, Science 282, 1309

Reid I.N., Gizis J.E. 1997a, AJ 113, 2246

Reid I.N., Gizis J.E. 1997b, AJ 114, 1992

Reid I.N., Kirkpatrick J.D., Gizis J.E., Liebert J. 1999a, ApJ 527, 105

Reid I.N., Kirkpatrick J.D., Liebert J. et al. 1999b, ApJ 521, 613

Reid I.N., Gizis J.E., Kirkpatrick J.D., Koerner D.W. 2001, ApJ 121, 489

Reipurth B., Clarke C. 2001, ApJ 122, 432

Rieke G.H., Lebofsky M.J. 1985, ApJ 288, 618

Rutledge R.E., Basri G., Martín E.L., Bildsten L. 2000, ApJ 538, L141

Rutten R.G.M. 1986, A&A 159, 291

Saumon D. 1994, 'A comparative study of hydrogen equations of state', In: *The equation of state in astrophysics. Proceedings of IAU Colloquium No. 147*, held in Saint-Malo, France, 14-18 June 1993, Cambridge: Cambridge University Press, ed. by G. Chabrier and E. Schatzman, Evry, p.306

Saumon D., Chabrier G., van Horn H.M. 1995, ApJS 99, 713

Saumon D., Hubbard W.B., Burrows A. et al. 1996, ApJ 460, 993

Shu F.H., Adams F.C., Lizano S. 1987, ARA&A 25, 23

Spiegel E.A., Weiss N.O. 1980, Nature 287, 616

Spiegel E.A., Zahn J.-P. 1992, A&A 265, 106

Stauffer J.R., Hamilton D., Probst R. 1994a, AJ 108, 155

Stauffer J.R., Caillault J.-P., Gagne M., Prosser C.F., Hartmann L.W. 1994b, ApJS 91, 625

Stelzer B., Neuhäuser R. 2001, A&A 377, 538

Sterzik M.F., Durisen R.H. 1995, A&A 304, L9

Sterzik M.F., Durisen R.H. 1998, A&A 339, 95

Sterzik M.F., Durisen R.H. 1999, 'Binary Properties in Dynamically Decaying Few-Body Clusters'. In: *Proc. Star Formation*, ed. by T. Nakamoto (Nobeyama Radio Obs.), p.387

Sterzik M., Durisen R. 2002, 'Brown dwarf companion frequencies and dynamical interactions'. In: *Brown dwarfs. Proceedings of IAU Colloquium No. 211*, held in Hawai'i, USA, May 20–24 2002, ed. by Martín E., in press

Tarter J. 1975, PhD thesis, University of California at Berkeley

Terndrup D.M., Krishnamurthi A., Pinsonneault M.H., Stauffer J.R. 1999, AJ 118, 1814

Tinney C.G., Reid I.N. 1998, MNRAS 301, 1031

Tinney C.G., Tolley A.J. 1999, MNRAS 304, 119

Torres G., Ribas I. 2002, ApJ 567, 1140

Tsuji T., Ohnaka K., Aoki W. 1996a, A&A 305, L1

Tsuji T., Ohnaka K., Aoki W., Nakajima T. 1996b, A&A 308, L29

Valtonen M., Mikkola S. 1991, ARA&A 29, 9

Ward W.R., Hahn J.M. 2000, 'Disk-planet interactions and the formation of planetary systems'. In: *Protostars and Planets IV*, ed. by Mannings V., Boss A.P., Russell S.S., Univ. of Arizona Press, Tucson, p.1135

White R.J., Ghez A.M., Reid I.N., Schulz G. 1999, ApJ 520, 811

Whitmore B., Heyer I., Casertano S. 1999, PASP 111, 1559

Wilking B.A., Greene T.P., Meyer M.R. 1999, AJ 117, 469

Wilson J.C., Kirkpatrick J.D., Gizis J.E. et al. ApJ 122, 1989

Wuchterl G. 2000, 'New Pre-MS Evolutionary Tracks and Planet Formation'. In: *ASP Conf. Ser. 223, Eleventh Cambridge Workshop on Cool Stars, Stellar Systems, and the Sun*, ed. by R.J.G. López, R. Rebolo, M.R. Zapatero Osorio, San Francisco, p.39

Wuchterl G., Guillot T., Lissauer J.J. 2000. 'Giant Planet Formation', In: *Protostars and Planets IV*, ed. by Mannings V., Boss A.P., Russell S.S., Univ. of Arizona Press, Tucson, p.1081

Wuchterl G. 2001, 'A Dialogue on Dynamical Pre-Main Sequence Tracks'. In:*Birth and Evolution of Binary Stars*, Proceedings of IAU Symposium No. 200 held 10-15 April, 2000, in Potsdam, Germany, ed. by B. Reipurth, H. Zinnecker, 2001, p. 492.

Wuchterl G., Klessen R.S. 2001 ApJ 560, L185

Wuchterl G., Tscharnuter, 2002, A&A subm.

Wuchterl G., 2002, 'The Collapse of Proto-Brown Dwarfs'. In: *Brown dwarfs. Proceedings of IAU Colloquium No. 211*, held in Hawai'i, USA, May 20–24 2002, ed. by Martín E., in press

Zapatero Osorio M.R., Béjar V.J.S., Rebolo R., Martín E.L., Basri G. 1999, ApJ 524, L115

Zapatero Osorio M.R., Bejar V.J.S., Martín E.L. et al. 2000, Science 290, 103

Zapatero Osorio M.R., Bejar V.J.S., Martín E.L., Barrado y Navascués D., Rebolo R. 2002a, ApJ 569, L99

Zapatero Osorio M.R., Bejar V.J.S., Pavlenko Ya. et al. 2002b, A&A 384, 937

Zapatero Osorio M.R., Bejar V.J.S., Martín E.L. et al. 2002c, ApJ in press, astro-ph/0206353

Zucker S., Mazeh T. 2001, ApJ 562, 1038

Abbreviations:

A&A	Astronomy and Astrophysics
ApJ	Astrophysical Journal
AJ	Astronomical Journal
Astron. Ges. Abstr. Ser.	Astronomische Gesellschaft Abstract Series
Mem. Soc. Astron. Ital.	Memorie della Societa Astronomia Italiana
PASP	Publications of the Astronomical Society of the Pacific
Rev. Mod. Phys.	Reviews of Modern Physics
SoPh	Solar Physics
SSRv	Space Science Reviews

Danksagung

Ich möchte mich herzlich bei Prof. Dr. Gregor Morfill bedanken für die Bereitschaft diese Arbeit zu vertreten und die positive Unterstützung meiner Forschungen und besonders für die Möglichkeit, an vielen nationalen und internationalen Konferenzen sowie Sommerschulen teilzunehmen.

Ganz besonders möchte ich mich bei Prof. Dr. Ralph Neuhäuser für die sehr gute Betreuung bedanken. Sein umfangreiches Wissen und seine vielen guten Ideen, seine kaum enden wollende Energie, wenn es um neue Projekte, Beobachtungsanträge, weitere Analysen und (inter)nationale Zusammenarbeiten geht, haben es mir ermöglicht mit einer Vielzahl von Teleskopen und Instrumenten zu beobachten, eine Vielzahl interessanter Menschen kennenzulernen und mit ihnen meine Arbeit zu besprechen. Dies alles hat die vorliegende Arbeit erst ermöglicht. Ich bin auch für die Ermutigung sehr dankbar, meine Ergebnisse und Ideen in vielen Seminaren und auf vielen Konferenzen vorzustellen und zu diskutieren.

Es ist ein besonderer Glücksfall, dass ich meine Arbeit in der Sternentstehungsgruppe am MPE schreiben konnte, die von Ralph Neuhäuser geleitet wird. Die dort herrschende offene, produktive, lebendige und freundschaftliche Atmosphäre hat meine Arbeit extrem positiv beeinflusst. Die Menschen in dieser Gruppe decken ein breites Spektrum an Wissensgebieten im Stern- und Planetenentstehungsbereich, sowie ein breites Wellenlängenspektrum von infrarot bis radio ab und man findet auf die allermeisten Fragen eine kompetente, nette Antwort.

Desweiteren haben viele Menschen im In- und Ausland meine Arbeit sehr bereichert. Im Speziellen gilt mein Dank:

Dr. Eike Guenther (TLS Tautenburg) für die fruchtbare Zusammenarbeit, besonders bei den spektroskopischen Beobachtungen, und für die fundierten Erläuterungen zur Auswertung von Echellespektren. Ich habe die ungezählten, sehr lehrreichen Gespräche über Sonnenaktivität, T Tauri Sterne, Braune Zwerge und über Beobachtungshandwerkszeug sehr geschätzt. Ich möchte mich ausserdem für die Software zur Berechnung der Grenzmassen für Begleiterkandidaten bedanken. Und besonders für die wiederholt in Anspruch genommene Gastfreundschaft an der TLS.

Dr. Matilde Fernandeź (IAA Granada) für die gute Zusammenarbeit, für viele Erklärungen zu photometrischen Beobachtungen und Auswertungen, für die Unterstützung bei umfangreichen Photometrie Kampagnen sowie für die Gastfreundschaft in Granada.

Dr. Günther Wuchterl, für interessante und sehr lehrreiche Gespräche über die theoretische Seite der Planeten-, Braunen Zwerg - und Sternentstehung - er ist eine echte Bereicherung für unsere eher beobachtungslastige Gruppe. Ausserdem bedanke ich mich für das Lesen von Teilen des Manuskripts.

Dr. Beate Stelzer, für die Gespräche über Aktivität von Braunen Zwerge, für viele Hilfestellungen bei kleineren oder grösseren Fragen sowie die nette Zimmernachbarschaft.

Dr. Fernando Comerón (ESO Garching) für viele interessante Gespräche über die von ihm gefundenen Braunen Zwerge in Cha I und Hilfestellungen bei der Durchführung von Beobachtungen.

Desweiteren danke ich Dr. Elvira Covino und Dr. Juan Alcalá (beide Capodimonte Observatory Napoli), Dr. Guillermo Torres und Dr. Scott Wolk (beide CfA Cambridge) und Joao Alves (ESO Garching) für die gute Zusammenarbeit.

Ein ganz besonderer Dank gilt Anne Baxter für den genialen Einsatz bei der Korrekturlesung! Vielen, vielen Dank, Anne!

Ich danke den Systemadministratoren Harald Baumgartner, Achim Bohnert und Joachim Paul, die hier am MPE einen unschätzbaren Support leisten.

Danken möchte ich auch dem Leiter des Wendelstein Observatoriums, Dr. Heinz Barwig, für die Zusammenarbeit und die Möglichkeit am Wendelstein zu beobachten.

Zudem bin ich den Nachtassistenten am Wendelstein, sowie der Support staff am Calar Alto Observatorium, an den ESO Teleskopen in La Silla und am Paranal sowie am CTIO Observatorium für die gute Unterstützung bei den Beobachtungen dankbar.

Ich danke meinen Eltern für Carepakete zur rechten Zeit und die guten Gedanken!!!

Ganz besonders herzlich danke ich Claudia für die geniale und unschätzbare Unterstützung! Du und Alfred habt mir unerwarteter Weise geholfen, im ganz normalen Wahnsinn des Wissenschaftsalltags das Lachen nicht zu verlernen.

Und schliesslich danke ich Veronika für ihre Liebe und Unterstützung.

Curriculum Vitae

Viki Joergens
* 20.6.1970 in Munich

Education:	**Abitur** (general qualification for university entrance), Nuremberg, Germany	May 1989
	Study of physics at the University of Regensburg degree with a grade of excellence	1998
	Diploma thesis at the **University Observatory Munich**, Subject: *Doppler tomography of the dwarf nova EX Dra* Supervisor: Dr. K.-H. Mantel, grade: excellence	1997-98
	PhD in Astrophysics at the **Max-Planck-Institute for Extraterrestrial Physics**	1999-today
	Michelson Interferometric Summer school, Berkeley, USA	Aug. 2000
	Saas-Fee advanced course on brown dwarfs and planets, Grimentz, Switzerland	April 2001
Professional experience:	**Supervision of an internship in physics** for medicine students at the University of Regensburg	1995-97
	University Observatory Munich, Scientific assistant	1998
	Max-Planck-Institute for Astrophysics, Garching Scientific assistant for Prof. H. Spruit, discovery of spiral structures in the dwarf nova EX Dra	1998-99
	Max-Planck-Institute for Extraterrestrial Physics, pre-doctoral work on photometric data of T Tauri stars	1999
Supervision of theses and internships	Supervision of the **diploma thesis** of M. Ammler, Subject: *Test of Pre-Main-Sequence tracks*	2001
	Supervision of a half-year mandatory **internship** of T. Spranger, Subject: *Photometry of T Tauri stars*	2001
	Participation in the supervision of the **diploma thesis** of C. Broeg, Subject: *Rotational periods of T Tauri Stars*	2002
Observational Experience	ESO Kuyen 8.2 m telescope (VLT) - UVES	
	ESO 3.6 m NTT - SofI	
	Calar Alto 3.5 m telescope - TWIN	
	ESO Danish 1.5 m telescope - DFOSC	
	Calar Alto 1.23 m telescope - CCD Camera	
	CTIO 90 cm telescope - CCD Camera	
	Wendelstein 80 cm telescope - CCD Camera	